Title
Microfluidic Microbial Fuel Cells for Microstructure Interrogations

Author
Parra, Erika Andrea

Publication Date
2010

Peer reviewed|Thesis/dissertation

Microfluidic Microbial Fuel Cells for Microstructure Interrogations

by

Erika Andrea Parra

A dissertation submitted in partial satisfaction of the
requirements for the degree of
Doctor of Philosophy

in

Engineering - Mechanical Engineering

in the

Graduate Division

of the

University of California, Berkeley

Committee in charge:

Professor Liwei Lin, Chair
Professor Carlos Fendandez-Pello
Professor John D. Coates

Fall 2010

Microfluidic Microbial Fuel Cells for Microstructure Interrogations

Abstract

Microfluidic Microbial Fuel Cells for Microstructure Interrogations

by

Erika Andrea Parra

Doctor of Philosophy in Engineering - Mechanical Engineering

University of California, Berkeley

Professor Liwei Lin, Chair

The breakdown of organic substances to retrieve energy is a naturally occurring process in nature. Catabolic microorganisms contain enzymes capable of accelerating the disintegration of simple sugars and alcohols to produce separated charge in the form of electrons and protons as byproducts that can be harvested extracellularly through an electrochemical cell to produce electrical energy directly. Bioelectrochemical energy is then an appealing green alternative to other power sources. However, a number of fundamental questions must be addressed if the technology is to become economically feasible. Power densities are low, hence the electron flow through the system: bacteria-electrode connectivity, the volumetric limit of catalyst loading, and the rate-limiting step in the system must be understood and optimized. This project investigated the miniaturization of microbial fuel cells to explore the scaling of the biocatalysis and generate a platform to study fundamental microstructure effects. Ultra-micro-electrodes for single cell studies were developed within a microfluidic configuration to quantify these issues and provide insight on the output capacity of microbial fuel cells as well as commercial feasibility as power sources for electronic devices.

Several devices were investigated in this work. The first prototype consisted of a gold array anode on a SiO_2 passivation layer that intended to imitate yet simplify the complexity of a 3D carbon structure on a 2D plane. Using *Geobacter sulfurreducens*, an organism believed to utilize direct electron transfer to electrodes, the 1 mm^2 electrode demonstrated a maximum current density of 1.4 μA and 120 nW of power after 10 days. In addition, the transient current-voltage responses were analyzed over the bacterial colonization period. The results indicated that over a 6-day period, the bacteria increased the capacitance of the cell 5-orders-of-magnitude and decreased the resistance by 3X over the bare electrode. Furthermore, over short experimental scales (hours), the RC constant was maintained but capacitance and resistance were inversely related. As the capacitance result coincides with expected biomass increase over the incubation period, it may be possible for an electrical spectroscopy (impedance) non-invasive technique to be developed to estimate biomass on the electrode. Similarly, the R and C relationship over short experimental scales could be explored further

to provide insight on biofilm morphology. Lastly, fluorescence and SEM microscopy were used to observe the biofilm development and demonstrated that, rather than growing at even density, the bacteria nucleated at points on the electrode, and dendritically divided, until joining to form the "dense" biofilm. In addition, viable microorganisms undergoing cell division were found dozens of microns from electrode surfaces without visible pili connections.

To investigate single-cell catalysis or microstructure effects, a sub-micro-liter microfluidic single-channel MFC with an embedded reference electrode and solid-state final electron acceptor was developed. The system allowed for parallel (16) working ultra-micro-electrodes and was microscopy compatible. With *Geobacter sulfurreducens*, the semiconducting ITO electrodes demonstrated forward bias behavior and suitability for anodic characterization. The first prototype demonstrated, with 179 cells on the electrode, a per cell contribution of 223 fA at +400 mV (vs. SHE). The second prototype with a 7 μm diameter electrode produced a current density of 3.9 pA/μm^2 (3.9 A/m^2) at +200 mV (vs. SHE) and a signal-to-noise ratio (SNR) of 4.9 when inoculated at a seeding density of 10^9 cells/mL. However, diluting the sample by 10x produced an SNR of 0.5, suggesting that obtaining single cell electron transfer rates to an electrode over short experimental time scales may not be possible with the system as tested. Nevertheless, the platform allows microstructure characterization and multiplexing within a single microfluidic chamber.

Acknowledgments

An old proverb states that "it takes a village to raise a child". Similarly, the completion of a dissertation is the culmination of the work of a personal and professional community.

First and foremost, I must thank Jorge and Maria Isabel, my parents, and my sister Monica for their continuous support throughout the years and their passion for education and science. Papito, tu dedicacion y talento por la ingenieria a sido una inspiracion para mi. Mamita, siempre te agredecere por haber creido en mi cuanto mas lo necesitaba. Hermanita, gracias por darme alas y escusa para conocer el mundo! Tambien debo agradecerle a Douglas M., mi esposo, por ser mi raiz y darme perspectiva durante los momentos intensos con su ejemplo y serenidad.

More directly, I want to thank Prof. Liwei Lin and Prof. John Coates for their mentorship and support both with academic and personal matters. In addition, Prof. Carlos Fernandez-Pello and Prof. Alice Agogino I would like to acknowledge for taking a personal interest in my success from the beginning of my graduate career.

Within the Lin Lab, I would like to thank everyone for their comradeship and support! Heather, Adrienne, and Shogo - thank you for being you! Brian, Qin, Armon, Yingqi, Ryan, Ryan, Kevin, Jiyoung, Kosuke, and more recently Alina and Rich - you guys have been instrumental in getting me through these years! Similarly, I would like to acknowledge the Coates lab members, and particularly Kelly, for taking me under their biological wing.

Suz, Sarah, Esther, Fabian, you guys are family! From speed soccer to 4am airport rides - thank you!

Lastly, I would like to acknowledge the CUES office and Beatriz Lopez-Flores for providing the scaffold through which Berkeley became my home.

List of Figures

List of Tables

Contents

Chapter 1

Introduction

1.1 Motivation

The surge of oil prices along with the concern for global warming aggravated by industrialization of developing nations has motivated the search for both short and long term energy alternatives to the currently available technology. Reports forecast that current technology will not satisfy the world demand as it is expected to more than double from 500 to 1200 EJ/a in the next 50 years [8]. Consequently, efficient and sustainable energy conversion is the focus of many research programs underway. In this dissertation, the phenomenon of harvesting energy from microbial metabolism is studied for it addresses both of these issues by generating electricity from fuels produced biologically from CO_2 as illustrated in Figure 1.1.

As with most energy cycles on earth, the energy that initiates this process comes as light from the sun assisting in the photosynthetic process in green plants or microorganisms that convert carbon dioxide (CO_2) and water (H_2O) into glucose and biomass as

$$6CO_2 + 6H_2O + \text{light} \rightarrow C_6H_{12}O_6 + 6O_2 \tag{1.1}$$

The glucose can then be converted by acetogenic bacteria or other microorganisms into non-fermentable organics like acetate [9] where, catabolic bacteria ingest it (1.2), retrieve energy from the fuel, and, as waste, produce separated charge that can be coupled with an electrochemical cell to produce electricity and water (1.3).

$$CH_3COOH + 2H_2O \rightarrow 2CO_2 + 8H^+ + 8e^- \tag{1.2}$$

$$2H^+ + 2e^- + \frac{1}{2}O_2 \rightarrow H_2O + \text{electricity} \tag{1.3}$$

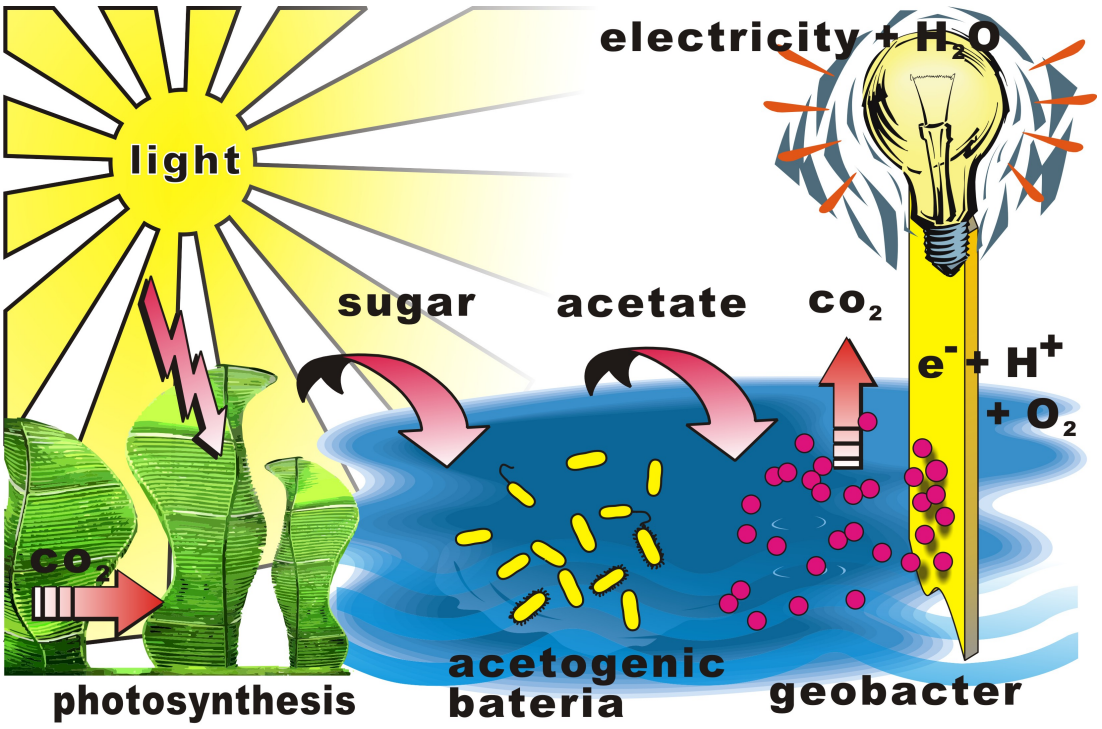

Figure 1.1: Motivation of the project is to learn about organic energy conversion. In nature, photosynthesis process in green plants converts carbon dioxide and water into glucose with the assistance of light. Next, microorganisms ferment glucose into acetate, and iron-reducing bacteria breakdown acetate to provide electrons that can be captured by machinery. The goal of this project is to learn from nature and apply engineering approaches to generate and extract energy from the natural processes through artificial systems.

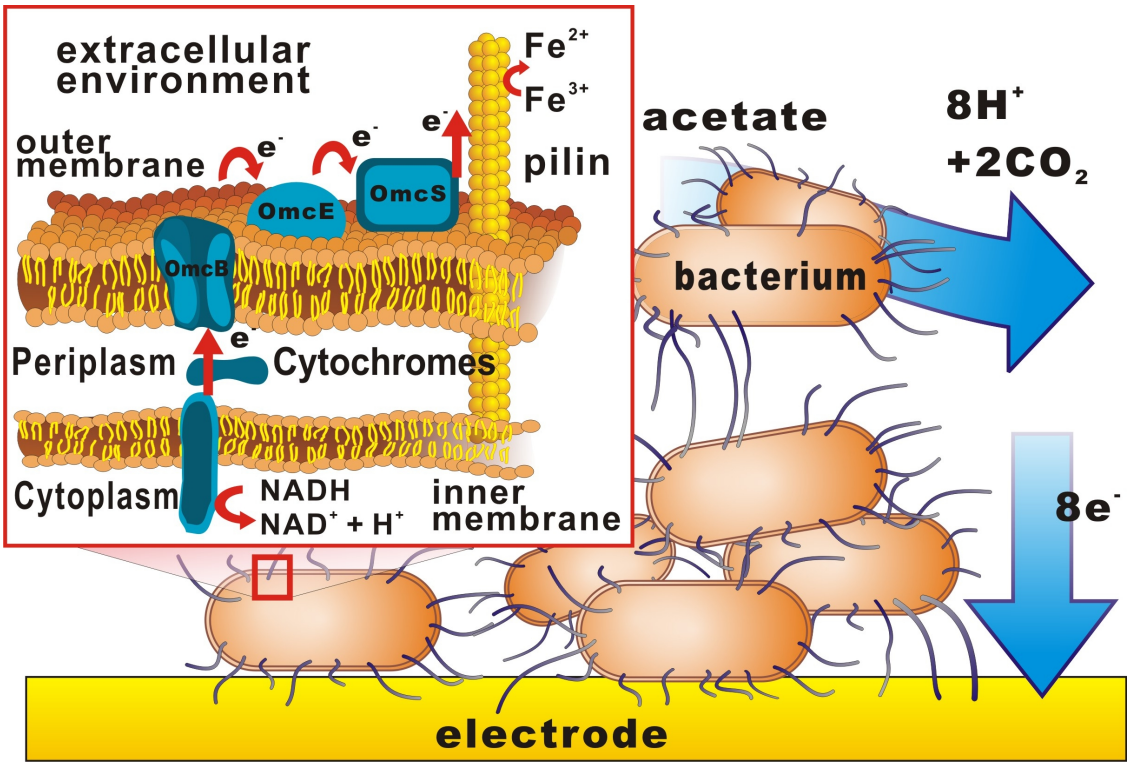

Figure 1.2: Cartoon of microbial mechanism that is exploited to scavenge energy from microorganisms. As shown, the bacteria *G. sulfurreducens* utilize acetate (vinegar) as a nutrient and generate carbon dioxide, protons, and electrons. The electrons are transferred from the cytoplasm through the membrane to the extracellular environment using mechanisms intrinsic to the microorganism (inset). The microorganisms also produce pili or "organic nanowires" believed to act as conduits for the electrons. When microorganisms are near to metallic substrates, electrons can transferred to produce direct current.

This process is sustainable provided that the energy scavenged from the microorganisms does not conflict with their metabolic processes. In this work, the iron reducing bacteria *G. sulfurreducens* was adopted because it is able to externalize electrons to its extracellular environment and thrive in highly anoxic environments, making it intrinsically compatible to the application. As illustrated in Figure 1.2, these bacteria are distinctive because they have evolved a mechanism to "breathe" out the electrons that result from their metabolism onto extra-cellular solids like insoluble iron [10]. The electrode of the fuel cell essentially substitutes the iron in this sustainable series. Therefore, collecting electricity from their metabolism is merely a detour of the natural energy flow through the ecosystem.

The biomass energy harvesting process that is studied, also known as a microbial fuel

cell (MFC), can be defined as an energy conversion mechanism that utilizes simple sugars or alcohols as the chemical energy source and uses living microorganisms as catalysts to break them down. Analogous to a hydrogen fuel cell, it can reduce oxygen to produce water. Because the device converts energy, its energy storage density is limited to that of the fuels in which the fuel "tank" can be infinitely large or infinitely refilled. Additionally, the device could be scaled to provide greater energy or stacked to increase potential. Unlike the hydrogen fuel cell, however, an MFC is highly efficient under ambient conditions and the fuel can be stored in liquid or solid forms.

1.2 Principles of Operation

Microbial electrochemical cells are scavengers of microbial metabolism. The microbial interactions with the electrode surfaces occur at the protein level or through metabolites and can be reductive or oxidative in nature. For simplicity, only microbial anodic electrochemical phenomena will be discussed hereafter as it is the focus of this work. Anodic reactions, by definition, occur when electrons are "absorbed" into the electrode. Hence these reactions occur when organic molecules are broken down by the microorganism into electrons and subjected to a potential gradient that causes them to drift to power a load. At the cathode, the (now) lower energy electrons are "released" to an electron acceptor through a cathodic reaction as illustrated by Figure 1.3.

In their simplest form, MFCs consist of two electrodes, an electron donor (metabolic nutrient) and an electron acceptor (oxygen for example), microorganisms that catalyze the reactions, an electrolyte that allows movement of the compounds within the system, and a circuit that allows electrons to transfer between the two electrodes. Sediment microbial fuel cells are examples of minimal systems as the electrodes need not be contained but rather interact with their environment.

The minimal microbial electrochemical system, however, is rarely utilized. In practicality, many additional components are incorporated to optimize the electrochemical reactions and/or as "sensors" for debugging and understanding the system. For example, to mitigate ionic transport losses, the anode and cathode are placed in close proximity, and the anodic and cathodic electrolytes optimized for conductivity and acidity, often resulting in dissimilar compositions. As a result, a semipermeable membrane (ie. Dupont's Nafion PEM) is employed as a half-cell barrier to prevent the solutions (and redox) from mixing. Figure 1.4 depicts a typical microbial electrochemical system.

Within the bioelectrochemical context, however, the electrolyte optimizations are somewhat limited because of the fragility of biological components. As the proteins or enzymes that catalyze the reactions can easily denaturate (loose structure that is fundamental for specificity), particularly if outside of the protection of the host cell and its cell membrane.

The external stresses capable of enzyme denaturation include strong acids or bases, concentrated inorganic salts, organic solvents, and heat. As a result, electrolytes in microbial electrochemical systems are limited to physiological media and ambient environmental conditions including temperature and pressure.

In regards to sensors, in electrochemistry the essential probe is the reference electrode that indicates the redox potential of the reacting components. Because redox is so fundamental and not widely understood, it will be explained more in the Theory Chapter. Research electrochemical systems can contain one to three or more reference electrodes and are typically located at the anode, cathode, and/or membrane.

1.3 Applications

The applications for biomass energy conversion are vast and span over many size scales. Ultimately, the cost of the materials and manufacturing required for sufficient performance will dictate which markets can be penetrated. Presented here are macro-scale applications currently pursued in the literature that span industries such as wastewater treatment, sediment or marine fuel cells for field electronics, and robotics. The novel miniature and microscale applications as they pertain to this work will be discussed in the Future Work Chapter.

1.3.1 Wastewater treatment

A literature search on microbial fuel cells quickly reveals that the majority of the engineering research effort in regards to these systems has concentrated around wastewater treatment. The costs to implement MFCs would be minimal at these sites since the infrastructure for biological treatment already exist as wastewater plants already utilize microbial digestion for the removal of organic compounds. In addition, since the electrochemical devices provide electrical power, the system's energy demands could be self-sustained and costs lowered as currently water treatment consumes 30 kWhr per person per year [11].

On the larger scale, MFCs have been investigated for wastewater treatment at brewery sites and wineries. As the high-strength wastewaters from industrial sources such as hospitals, paper mills, and breweries could power a biological fuel cell device as a supplemental power source [12]. The University of Queensland, Australia, has completed a prototype MFC with the Fosters Brewing Company. The 10 liter prototype design, converted the brewery waste water into carbon dioxide, clean water, and electricity. The plan is to expand the device and produce a 660 gallon version, which is expected to generate 2 kilowatts of power. In addition to power, they are interested in utilizing the MFC as a water purification device, as clean water is of utmost importance to Australia. Likewise, the Napa Wine Company has implemented similar prototypes utilizing the winery wastewater.

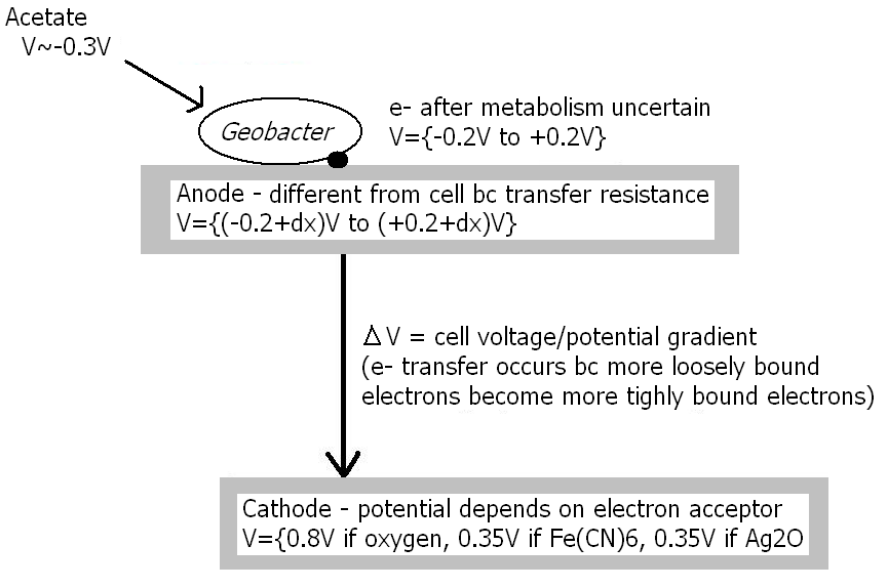

Figure 1.3: Electrical energy is harvested from microorganisms. The initial energy comes from acetate (redox of -0.3V vs. SHE) that serves as the bacteria's electron and carbon source. Next, electrons generated from their metabolism as waste are collected by an anode. The electrical potential of these electrons is dependent on many environmental factors but has empirically demonstrated between -0.2 to +0.2 V (vs.SHE). Lastly, the cathode interactions with oxidants (ie. dioxygen, ferricyanide) creates a voltage potential gradient across the electrodes that causes electrons to drift across an electrical circuit (load) and into the catholyte, completing the circuit.

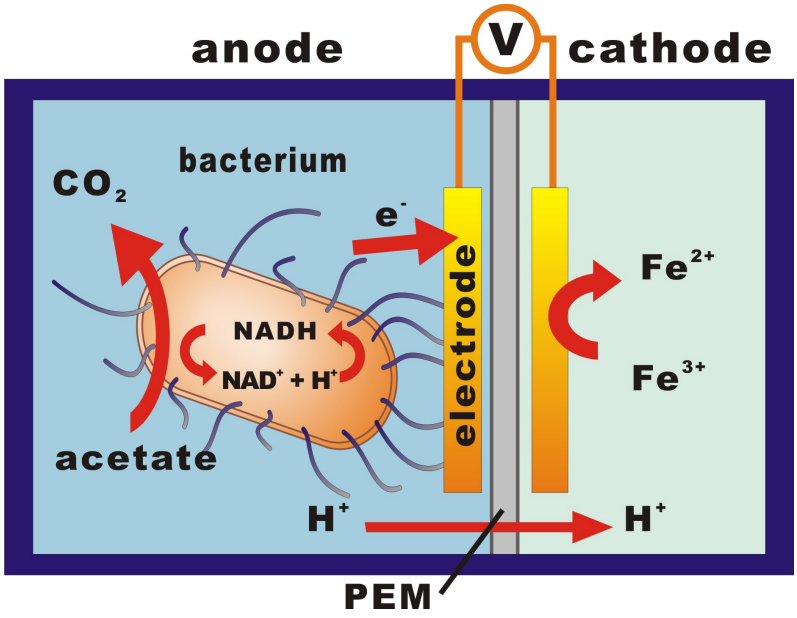

Figure 1.4: Schematic of typical microbial fuel cell. Microorganisms catalyze anodic reactions and "strip" electrons and protons from carbohydrates, such as acetate, to generate energy for their own metabolic processes. Carbon dioxide is also released in the process. The electrons from metabolism are transferred to an anode. The system utilizes two electrodes separated by a semipermeable polymer exchange membrane (PEM) that keeps anolyte and catholyte from mixing. Voltage potential is generated across the electrodes, and power is produced by the fuel cell.

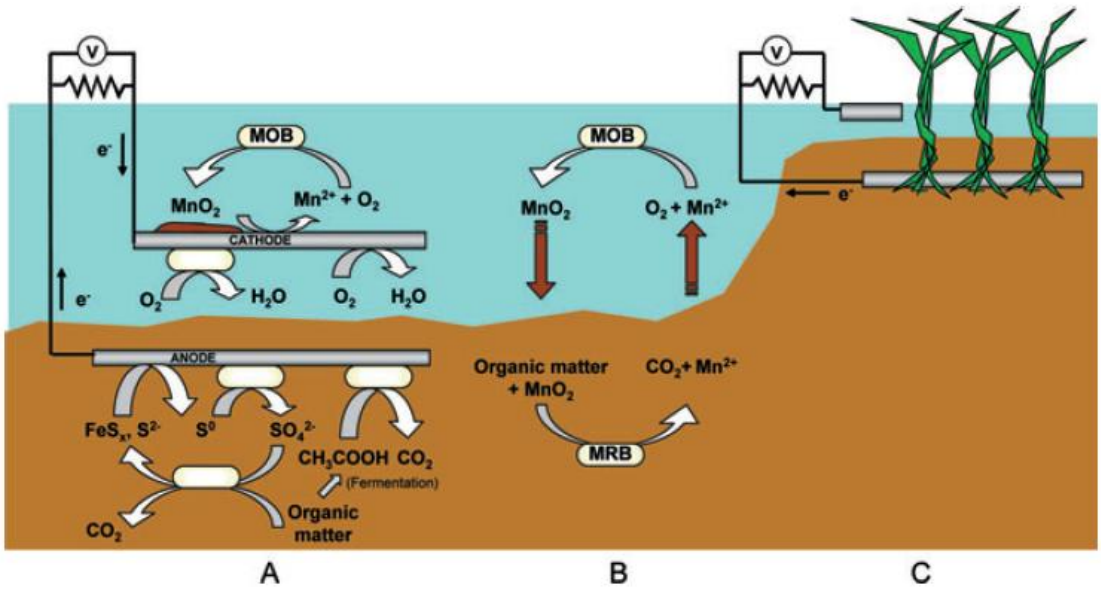

Figure 1.5: Sediment microbial fuel cells demonstrating marine (left) and soil (right) environment scavenging [1].

1.3.2 Sediment and Marine

Microbial fuel cells can also operate autonomously off the environment, as a redox gradient exists both in water and sediment columns. Typically, reduced species occur deep into the system and oxidized (aerobic) species near the surface. Sediment microbial fuel cells are devices that utilize this naturally occurring potential difference in the environment to scavenge electrical power. The concept has also found interest in low-power remote applications such as energy scavenging from rice field paddies and sediment scavenging for LED lighting [1]. As illustrated by Figure 1.5, the minimal system consists of two electrodes connected by a load, where one electrode is generally buried within the sediment, the second is left suspended in a different medium, and the natural phase barrier between the two forms the junction. Sediment fuel cells are characterized by very low voltage potentials, generally less than 300 mV, due to redox mixing and/or mass transport losses between the electrodes, but they are complete scavengers as they utilize electron donors naturally present in their environment.

1.3.3 Robotics

The consumer market space for microbial fuel cells lies within electronics, especially robotics and portable devices. A microbial cell could act as an artificial "stomach" that catabolizes the chemical energy and provides a man-made metabolism to supply power-hungry actuators, sensors, and processors. In comparison to methanol or ethanol fuel cells, acetate and simple sugars have the advantage over alcohols in that these are ubiquitous, renewable, and non-flammable. Thus far, microbial metabolism has been studied as a power source for artificial muscles, artificial gills, and RC devices [13, 14, 15]. However, greater power densities are required of current MFC designs to be able to compete with current power technology and approach realistic commercialization.

1.3.4 Bioimplantable Devices and Sensors

At the small scale, microbial fuel cells find their application in the biomedical industry and as environmental sensors. Chiao, Lin, and Lam first envisioned the concept where an MFC replaces the battery that powers bioimplantable devices [16, 17, 18]. Glucose from the blood plasma fuels the system and microorganisms catalyze the reactions to obtain electrical energy. Likewise, miniature scale laminar MFCs were developed as environmental sensors for wastewater treatment [19]. In this case, however, the devices' output is used to estimate the carbohydrate content in the bioreactor.

1.4 Dissertation Goals and Overview of Contributions

Within the context of microbial electrochemical processes, this dissertation specifically focused on the development of a microfabricated microbial fuel cell platform to investigate the microstructure effects of microbial catalysis, and the exploration miniaturization or scaling of systems for further fundamental understanding of the microbial fuel cell devices. The goal has been to explore the extreme small scale of the systems through micro- and ultra-micro-electrochemistry while providing environmental controllability through microfluidics. In addition to increasing the resolution of the experiments, we demonstrated that miniaturization shortens the experimental time scale or improves the "agility" of the system, aiding with kinetic characterizations and temporal resolution of the applied perturbations. Hence, this dissertation discusses characterization of microbial anodic process from the bottom up. In addition, this work is the first to explore microbial interactions with ITO, a semiconductor, as a material for collecting the metabolic current and to demonstrate compatibility (no reverse bias effects).

1.4.1 Microstructure effects

The fundamental thrust of this dissertation consisted on the development of a microfabricated bioelectrochemical cell with an imbedded reference electrode for single cell studies. The microfluidic system developed was designed to be microscopy compatible and hence allows transmitted and fluorescence signatures to be monitored in real-time, opening a whole realm of experiments that couple electrochemistry, photochemistry, and microbiology. The scale of the microfluidic system also allows increased controllability of the experiments, as compared to macro-scale reactors, by resolving temporal and spacial nutrient gradients, biocatalyst loading, and viability. Hence, the inoculum can be dissected to understand its microstructure characteristics, and topics such as bio-catalyst kinetic variability and adaptation to environmental stresses studied. Specifically, through its electrical output, the system was designed to answer questions such as:

1. What are the different species average metabolic rate? What species produces greater current and with higher coulombic efficiency?

2. What is the variability within a species? How do the kinetics change with nutrient concentration and electrode redox? How does catalysis change over time?

3. How much mass and energy is lost due to cell division?

4. What is the metabolic time scale? How fast are nutrients processed?

5. How does surface energy affect the reactions? What surface modifications enhance performance?

And although this is not a comprehensive list, it is one that begins to ask questions about the system from the cell level. As electrical output from a fuel cell is the compound signal of millions of microscopic phenomena, understanding the heterogeneity and involved factors is fundamental to improving its performance. Hence this dissertation provides insight on miniaturization of MFCs and the resulting advantages.

1.4.2 Parameter Scaling

As was mentioned earlier and is discussed in Chapter 2, a literature survey reveals that electrical performance of microbial fuel cells has a strong dependance on scale. In fact, miniature MFCs consistently outperform large systems. However, the justification for this trend is yet to be resolved. Through inspection of the scaling factors, the advantages of miniaturization are theoretically explored in the second section of Chapter 2, which discusses the

background theory. Meanwhile, these advantages are experimentally investigated in Chapter 3: Micro-Electrode MFC. Specifically, miniaturization provides a reduced experimental time scale that can be utilized to better understand time-dependent effects of the system. Hence, electrical signals' transients are analyzed for insights on the system's state at the time of testing. In addition, the steady-state electrical performance of micro-electrode MFCs and biofilm growth patterns are also discussed.

1.5 Organization

This dissertation has been divided into five chapters. The first two consist of the introduction and provide the literature survey and theoretical background for the work. Chapters 3 and 4 provide the experimental results that include design, fabrication, and characterization of miniature devices, and biological results. And Chapter 5 discusses future directions. Specifically,

Chapter 1 introduces the principles of microbial fuel cells and envisioned applications.

Chapter 2 discusses the background of this work. The first section is a literature review that aims to motivate the simplification and miniaturization of MFC devices, particularly for fundamental studies. In addition, a second section provides theoretical concepts in fuel cells, electrochemistry, and micro- and ultra-electrochemistry, as well as biological effects on these phenomena.

Chapter 3 presents the micro-electrode microbial fuel cell that explores microbial interactions through microscopy and electrochemical spectroscopy. As depicted by Fig. 1.6, the anode was micro-patterned and a fuel cell built through meso-scale components.

Chapter 4 delivers the microfluidic ultra-micro-electrode device capable of single-cell bioelectrochemical characterization. As shown by Fig. 1.7, the single-channel device arrayed working electrodes and utilized a solid-state chemistry for counter and reference electrode.

Chapter 5 concludes the dissertation by presenting many capabilities of the platform developed that could be explored in future studies. In addition, the chapter includes future directions and applications of micro-scale and MEMS bioelectrochemical systems.

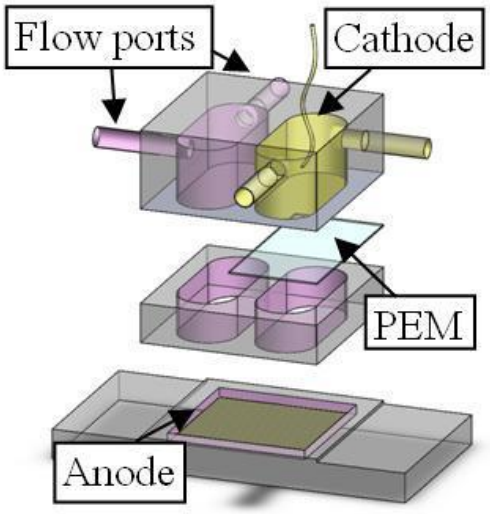

Figure 1.6: Schematic of MEMS electrode microbial fuel cell developed presented in Chapter 3. The micro-electrode increased spacial and temporal resolution of fundamental studies. However, the system did not allow real-time monitoring of biomass and large size (1 mm^2) provided a largely heterogeneous signal.

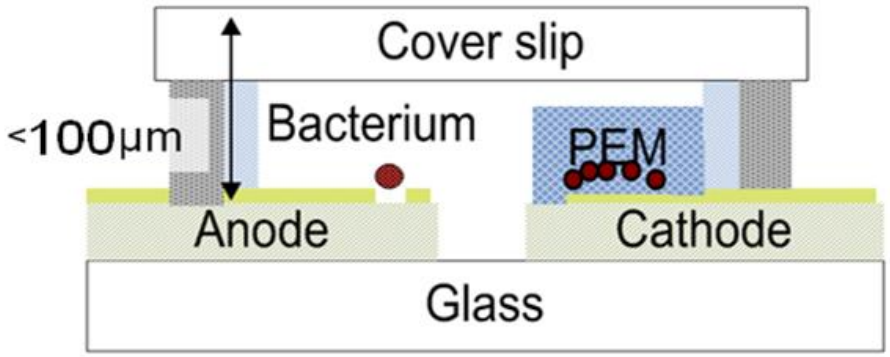

Figure 1.7: Side-view schematic of the second generation single-channel ultra-micro-electrode microfluidic microbial fuel cell presented in Chapter 4. All electrodes lay within the same plane. The cathode and reference electrodes are solid state and buried beneath a casted Nafion membrane. The system permitted biomass loading estimation, and the 50 μm electrode area mitigated heterogeneity.

Chapter 2

Background

Despite the environmental benefits that microbial electrochemical energy offers, these systems remain from becoming a disruptive technology for they currently cannot compete with energy conversion devices already available. Being an upstream technology, many fundamental questions remain to be answered, power densities are low, costs are high, and policy remains an unknown.

Although there have been many recent *microbiological* successes that illuminate electron transfer paths and membrane protein function, a solid understanding of cellular performance and system requirements at the microorganism level are still to be characterized. Understanding the complexity of the heterogeneous phenomena is non-trivial, as the output of the electrochemical cells is actually the added contribution of a large number of microorganisms (systems typically consist of 10^9 cells/cm^3) individual high impedance direct current sources working in parallel to add to the signal. The complex behavior is not only limited to the *chemical* effects such as temperature and electron donor distributions within the system, but also *temporally* as microorganisms' viability, quantity (cell division), and community composition (species ratio and spatial distribution) in the system changes, and *microstructure* effects as microorganisms themselves are also able to adapt to their surroundings under environmental stresses and modify their environment.

It is often difficult or impossible to deconvolute these factors and objectively compare microorganisms or systems' performance side-by-side in the literature; however, an independent understanding of all the previously mentioned effects is necessary in order to yield predictive capabilities. As a result, this Chapter attempts to emphasize the grand scope of current research efforts to motivate simplification of system architectures via miniaturization as a method for improving experimental controllability for *microbiological* characterizations and electrode material and microstructure optimizations.

2.1 Literature Review

2.1.1 Scale and Electrode Structures

The basic elements of the microbial electrochemical system consist of two electrodes, a semi-permeable medium that allows charged species diffusion between the electrodes, and a circuit that allows electrons to flow to power the load. However, the architecture of the system, or geometrical arrangement of the components, as well as the relative size of each, and the material microscopic composition greatly affect the electrical behavior. Although the MFC community is aware of these geometrical dependencies, few studies have attended these issues. In particular, the electrode scaling effects on MFC electrical performance has remained largely unaddressed in the literature as current and power densities are often normalized to a projected electrode area and, making the invalid assumption of a linear relationship, extrapolated to a different scale. This scaling issue is further aggravated by the strong temporal dependency of electrical performance on biocatalyst loading as bacterial coverage may not be homogeneous on the electrode surfaces. Consequently, comparing the electrical performance of the systems side-by-side is difficult and improvements often disputed. This section overviews the literature addressing these issues. Specifically, structural variations in the systems such as scale, and electrode macro-geometry and microstructure are discussed as they motivate the work in this dissertation.

System Scale

A survey of the MFC literature produced publications reporting on plethora of system sizes. Current MFC research ranges over 7 orders of magnitude from the μL to 10,000 L, and the power density results are very dependent on scale as miniature systems repeatedly outperform full-scale devices. However, the scientific foundation of this dependency remains unexplained and largely disregarded as studies repeatedly present their results in a scale different from the experimental. Dewan et al. provided a literature survey on this trend, and also verified through experimentation, that the power density of systems is not scaling linearly with system size but rather with the logarithm of electrode area, as illustrated by Figure 2.1 [20]. Hence, miniaturization intrinsically provides a favorable scaling factor and an opportunity to determine the optimum conditions for electrical performance. However, although various miniature studies have been published, to date these have yet to focus on this optimality but rather on demonstrating systems for particular applications. Nevertheless, these have begun the exploration of MFC behavior at the miniature scale.

Specifically, a handful of research groups have demonstrated devices in the μL scale for various objectives such as power generation, high-throughput screening, and protein-electrode surface interactions. From our research group, Chiao and Lam presented the first miniature system that consisted of a 1 cm^2 micromachined device using *Saccharomyces*

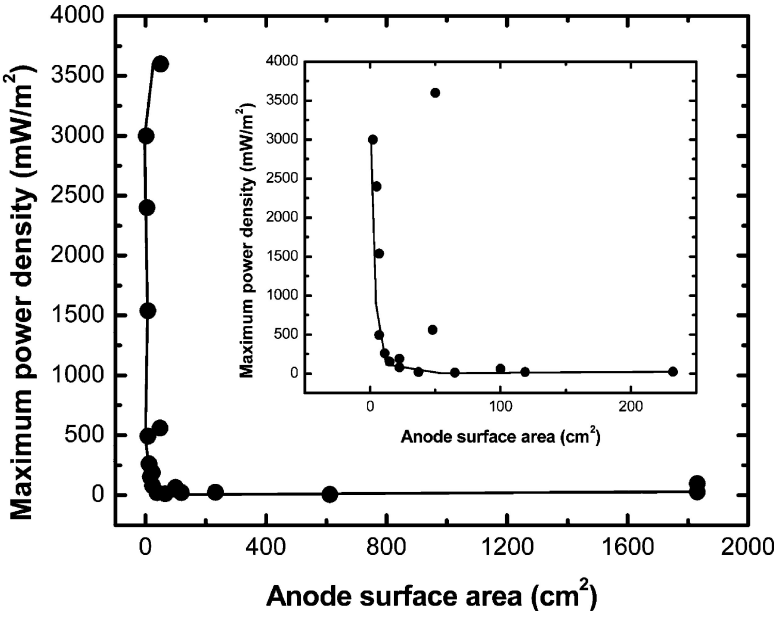

Figure 2.1: Relationship between power density and anode surface area in MFCs. Taken from Dewan and Lewandowski (2008).

cerevisiae and methylene blue as mediator to produce 2.3 nW/cm^2 [17]. This work was continued by Siu and Chiao who increased the specific anode surface area by patterning microfabricated pillars 8 μm tall and at 40 μm spacing within a 1.2 cm^2 gold electrode in PDMS. Their mediated MFC used *Saccharomyces cerevisiae* and human plasma and provided 401 nW/cm^2 [17]. At the miniature end of the spectrum, Qiang and Morse reported a 5.5 μL MFC utilizing a gold anode and carbon cloth cathode that supplied 15 W/m^3 with *Shewanella oneidensis* [21]. Using a similar architecture, Han reported on an array of graphite cloth electrodes on gold 7 mm in diameter within a batch-MFC configuration for high-throughput screening of consortia [22]. Lastly, more fundamentally, Crittenden and Sumner reported on a 10 μL system that compared glassy carbon disk electrodes to SAM monolayer molecules on gold. The study investigated the effects of SAM chain length and headgroup using *Shewanella oneidensis* [23]. Hence, in summary, several micro- to millimeter MFC systems that demonstrate an electrical output have been produced; however, most of these miniaturized systems have not taken advantage of the scaling characteristics nor the environmental controllability that they provide to fundamentally illuminate biocatalytic phenomena.

Electrode Macrostructure

Taking from hydrogen fuel cell components, many off-the-shelf carbon materials have been adopted as MFC electrodes because of their accessibility and low cost. However, these materials are typically characterized by either complex 3-dimensional structures or large surface areas (in the case of blocks) that provide microstructure uncertainty. This section summarizes these commercially available materials that have been utilized in MFC studies.

The literature is dominated by carbon felt and carbon paper electrodes due to their high specific surface area (1,000-2,500 m^2/g), simple implementation, and availability. These materials consist fiber "bundles", where each fiber is 5-7 microns in diameter, that are weaved or tangled together to create a conductive macroscopic substrate. Although, as materials these do increase specific surface area, the actual available surface to the microorganisms is difficult to accurately estimate. Even with manufacturer specifications, not all the area is available to the microorganisms as much of the area is internal to the bundle and the ratio changes with hydration conditions.

Carbon aerogels (CAs) have also been explored as MFC electrodes [24]. CAs are extremely porous materials with high specific area (up to 2500 m^2/g and low density 0.5 g/cm^3). As these can be made conductive, they are appealing as electrode substrates. However, CAs nanoporosity makes much of the electrode area unavailable to micrometer sized microorganisms. Likewise, hydration of these structures causes a structural change that typically causes contraction and degradation.

Generally utilized for *microbiological* characterization, graphite blocks, and more recently, evaporated gold electrodes, have served as planar electrode surfaces [25, 26]. Although estimating specific area is less involved than with complex 3D structures, macroscopic planar substrates are not immune to uncertainty as surface roughness effects can easily double the apparent surface area. Likewise, as it is explained in the next section, the microstructural properties of the material can affect electron transfer to the electrodes and same-scale electrode-to-electrode performance.

Less common as MFC electrode materials are carbon nanotubes (CNTs) [24]. However, as electrodes in MFCs serve as inert low-impedance current collectors, CNTs have tremendous potential as electrodes due to the their superior conductivity, low volume uptake (diameters range 1-30nm and extend to millimeters in length), and their ability to be imbedded and localized within larger structures. Vulpe et al. demonstrated biofilm growth using a wastewater inoculum on multi-wall CNTs [24]. However, limited literature exists that refers to their applicability.

Electrode Microstructure

In addition to the electrode geometrical structure, the microstructure and surface energy of the electrode material can also affect performance. This section discusses microstructure and surface-level manipulations to two materials already adopted by the MFC community in relation to microbial catalysis.

Intrinsic Material Microstructure - ie. Graphite

Graphite is a prominent carbon electrode material that consists of stacked graphene sheets held together by Van der Waals forces. Although much less geometrically complex that carbon cloth or carbon paper, macroscopic graphite structures can vary in crystallographic orientation and defect density, and these greatly affect their surface properties. Pyrolytic carbon, that consists of covalently bonded graphine sheets, is typically used instead of graphite as its conduction properties are less anisotropic. However, as-manufactured pyrolytic carbon samples are non-ideal as graphene is the favored cleavage plane, and graphene is highly non-polar and unlikely to interact with cytochromes for electron transfer [2]. As Hitchens and others have proposed, edge planes and vacancy sites that have greater surface energy are able to better mediate electron interactions with the environment as illustrated in Figure 2.2. As a result, some MFC graphite electrodes are treated with ammonia or HNO_3 as a means to oxidize the surface and increase cytochrome-electrode interactions, a treatment that has demonstrated a 3X improvement in electrical performance [27].

Surface Modifications and Self-Assembled-Monolayers

A successful electrode must accomplish two objectives. First, the electrode's surface must be such that it produces favorable orientation of the protein for electron transfer, as illustrated by Figure 2.2. And, secondly, the surface must equally allow absorption and desorption of the proteins as to not become electrochemically poisoned. However, proteins routinely irreversibly bind to metal surfaces, hence surface promoters in the form of self-assembled-monolayers (SAMs) are often used to probe the electrochemical properties of cytochromes.

Within the MFC context, Crittenden et al. investigated the effects of surface modifications on electrical output using *Shewanella putrefaciens* using SAMs [23]. Their results indicated that gold modified with a carboxylic acid headgroup produced significantly more current than the glassy carbon anodes. However, current collection decreased significantly when the acid-terminated SAM was replaced with a chain extended by five methylene units and almost completely suppressed when the SAM was replaced with one with an identical chain length but terminated with a methyl headgroup. In contrast, they reported that bare gold electrodes only exhibited a capacitive discharge within their six-hour experimental time frame.

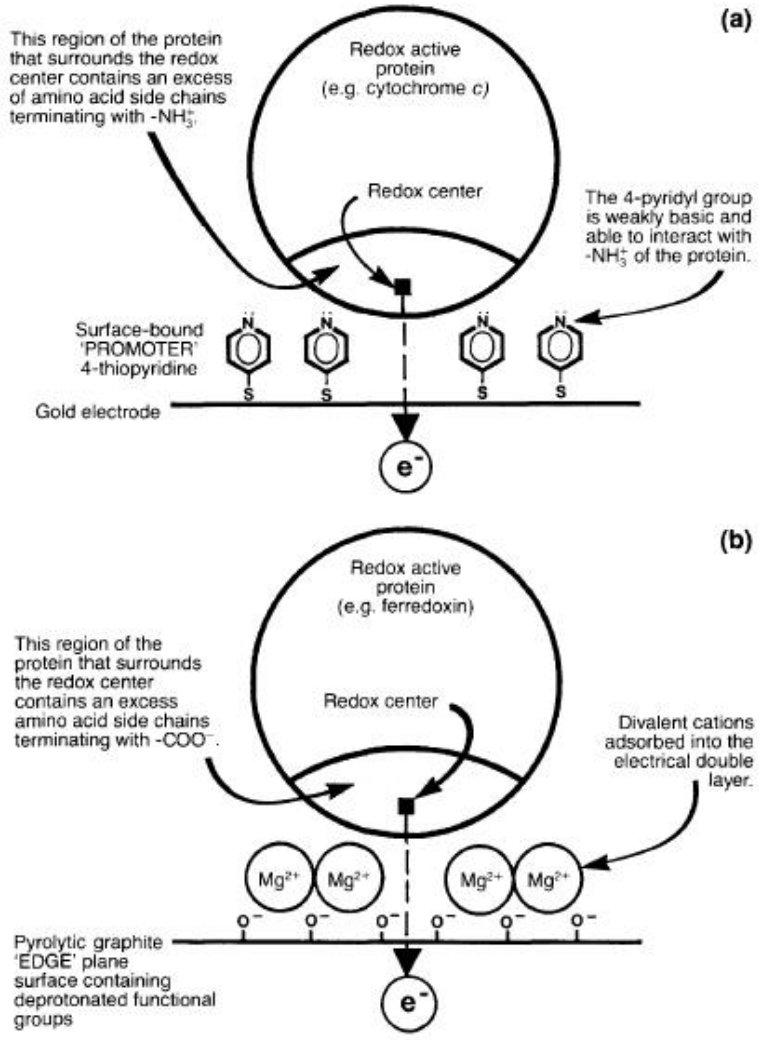

Figure 2.2: Generalized schemes for obtaining direct electron transfer between redox proteins and electrodes. The electrode in (a) has been modified by a promoter that modifies the surface to adsorb weakly basic pyridyl groups that interact with the positively charged interaction domains of proteins causing the redox centers to come close enough to the surface for electrons to tunnel to the electrode. The scheme for direct electron transfer shown in (b) indicates the possible role of multivalent cations in promoting stable attractive interactions between redox proteins with "negatively" charged interaction domains and the deprotonated surface of pyrolytic graphite [2].

However, other studies have reported dissimilar results indicating that direct electron transfer from microorganisms can be achieved on metal electrodes (Au, Ag, etc) without surface modifications [2]. Lovley et al. have reported that *G. sulfurreducens* provides comparable current densities to gold or carbon electrodes [25]. Hence, material compatibility may be specific to microorganism and/or electron transfer paths. If, for example, "protein nanowires" serve as electrical conduits from the membrane cytochromes, their specific orientation relative to the electrode may not be important provided that these are not adsorbed.

As bioelectrochemical phenomena is a surface effect, surface microstructure and modifications are expected to play an important role; however, this space is to-date largely unexplored. SAMs remain a possibility as there is extensive work by Whitesides that concerns the attachment and long term viability of cells on SAMs [28, 29].

In addition to SAMs, though, many other treatments can be applied to electrodes to modify their surface properties. Conductive polymers such as polyaniline, for example, have been demonstrated by Shroder [30]. Similarly, redox mediators such as AQDS and methylene blue have been either covalently bonded to electrodes or suspended within a conductive polymer matrix to modify the system's electrochemical properties [31, 32] . Nevertheless, the enhancement of microorganism-electrode interactions through surface modifications remains uncultivated, as many surface treatments have yet to be demonstrated. In this case, the miniaturization of electrodes could demystify the catalytic performance of microorganisms through high-throughput and highly-controlled characterization of to surface effects.

2.1.2 Chemical

In addition to geometrical variability, the chemical composition of the system also affects the electrical results. The literature refers to a vast array of chemical effects. For simplicity, this section overviews the most prominent *physio-chemical* and *bio-chemical* factors that have been studied.

Physio-chemical

Like inorganic fuel cells, system conditions affect the kinetics in the device. These include the acidity at the electrodes, the conductivity of the electrolyte, and temperature of the system among others.

Acidity

As with inorganic electrochemical systems, the acidic or basic nature of the system greatly affects its performance. Ideally, anodic reactions should be basic to favor proton generation and cathodic reactions acidic to favor oxygen reduction. Diverging from this causes a drop in

voltage across the cell. However, the acidity within the microbial fuel cell is limited to that accepted by the microorganisms, as species have a physiological preferred pH. Significant deviations can cause metabolic rate loss or perhaps even viability. He and Mansfeld investigated the effects of acidity on electrical power with a mixed bacteria culture and determined that performance was optimum at a bulk pH of 8-10 and dropped to 10% of maximum by a pH of 5 for their system [33].

Ionic conductivity

The effect of electrolyte ionic conductivity on the electrical performance of the microbial electrochemical cells has also been studied. As with other PEM fuel cells, it is generally advantageous to increase the charged species concentration to mitigate electrode-to-electrode transport losses. However, microorganisms must maintain a specific osmotic pressure across the plasma membrane, and, therefore, have limits to the salinity of the media. Logan et al. explored both the effects of ionic strength and electrode-to-electrode spacing and experimentally determined that at a moderate ionic strength (100 mM), power output is nearly proportional to electrode-to-electrode spacing [34]. And increasing the ionic strength of the media to 400 mM provides the best results. However, the electrolyte conductivity is limited to that of the physiologically tolerated by the bacteria. As a result, the anode-to-cathode distance should be minimized to mitigate the transport losses in the cell. However, placing the electrodes in close proximity also requires that a semi-permeable proton transporting membrane be utilized to prevent microorganism (and redox) mixing at the electrodes. As PEM membranes are expensive to deploy in large-scale systems (at \$200 per ft^2), many research groups have adopted membraneless architectures that instead utilize centimeter electrode-to-electrode spacing. However, the modification inevitably causes electrical power loss due to increased ohmic losses [35].

Biochemical

In addition to *physio-chemical* effects, *bio-chemical* factors greatly affect performance. Many metabolic pathways and mechanisms for electron externalization are found in nature that are well suited for different applications. Broadly speaking, *biochemical* research could be divided into pure culture and consortia studies. Within the pure culture studies, the literature is dominated by *G. sulfurreducens* and *S. onedeises*. These organisms are similar in that both are gram-negative bacteria, have an abundance of cytochromes on the outer membrane, can utilize solid oxides as terminal electron acceptors, and produce "pili" appendages believed to participate in extracellular electron transfer [36]. The microorganisms offer unique attributes in regards to metabolic pathways and oxygen tolerance [37, 38, 39, 40, 41]. However, a plethora of other species, many yet to be identified, can also interact with electrodes through metabolic processes.

Temperature also affects the performance of electrochemical cells. As all chemical reactions are governed by the Arrhenius equation, increasing temperature increases reaction rates. However, electrochemical cell temperature optimizations are limited as microorganisms can operate only within a physiologically tolerated temperature range. As investigated by Liu and Logan, temperature can provide roughly a 10% improvement in power density within a same culture [34]. However, greater effects may stem by utilizing thermophilic vs. mesophilic microorganisms as is being investigated by Wrighton and Coates and other groups [42, 43].

2.2 Electrochemical Theory

Electrochemistry is the field that studies spontaneous chemical reactions that utilize electrodes as intermediates. In other words, two electrodes "mediate" electron transfer between reacting compounds. The purpose could be to generate electrical energy, produce a compound, detect a species, or modify an electrode surface (electroplating) among others. However, the process rarely occurs just between two molecules, except for molecular sensors, and is highly heterogeneous as a result. Microstructure effects such as catalyst distribution couple with system complexities such as reactant concentration gradients to create highly convoluted systems that can be difficult to predict repeatedly. The complexity is further increased in biological catalysis, as this work studies, as microorganisms can divide, physiologically change, and manipulate their environment. As a result, our focus consisted on deconvoluting the system by utilizing micro- and ultra-micro-electrochemistry within microfluidics to assume homogeneity of the biocatalysis.

Due to the intrinsic interdisciplinary nature of bioelectrochemical systems, experience on a plethora of fields is required to understand the underlying mechanisms. This section covers theoretical and practical background on electrochemistry, microbiology, and miniaturization as they relate to this work. Within the first section, electrochemistry generalities, and fuel cells as power sources are introduced. The second section explains ultra-micro-electrochemical scaling and its advantages. The last section discusses the microbiological aspects of the system. Specifically, metabolism and catalytic qualities of the model microorganism, *Geobacter sulfurreducens*, are introduced.

2.2.1 Electrochemistry & Fuel Cells

For simplicity, this work only studies anodic microbial catalysis for electrical energy production. In other words, microorganisms breakdown organic fuels and produce electrons that are captured through a fuel cell to produce electricity. Since electrical power is the desired outcome, maximizing the electron transfer rate without sacrificing cell potential is

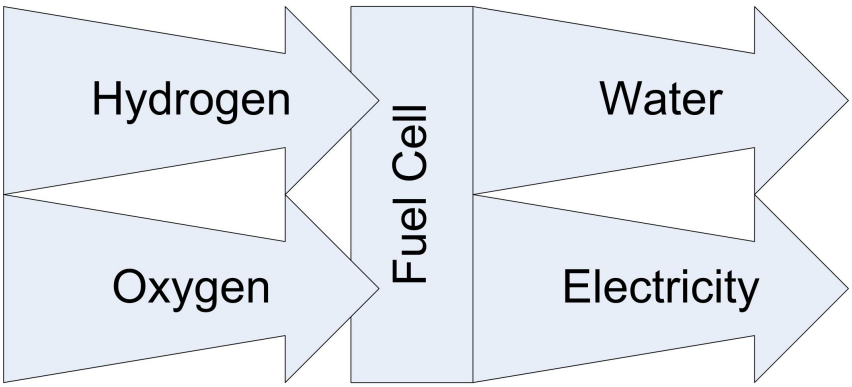

Figure 2.3: Plant schematic showing the inputs and outputs of an electrochemical cell.

the goal. As electrochemical cells are energy conversion devices, the maximum energy that can be attained is that which is added to the system as reactants. However, losses are inherent in the conversion and increase as more power is required of the system. In this section, proton exchange membrane (PEM) fuel cell performance, utilizing hydrogen/Pt as an analog for AcOH/*Geobacter* for simplicity, is explained.

General Electrochemistry and Redox

As was first introduced in Chapter 1, fuel cells are electrochemical cells where power is the desired product. In a nutshell, these devices are chemical factories that convert chemical energy and produce electrons from spontaneous chemical reactions that are mediated through electrodes. The system uses a fuel (electron donor) whose electrons are at high energy, passes the electrons through the load, and finally rests the electrons on a species where they are more tightly bounded to the atom's nucleus (electron acceptor). Hence, the maximum energy that can be captured by the system is the difference of the energy of these electrons as they convert from the electron donor to the electron acceptor (or sink). In the case of a hydrogen fuel cell, to use as an example, hydrogen gas is the electron donor and oxygen the electron acceptor. Water and electricity are the products, as illustrated in the Figure 2.1 below.

In electrochemistry, the convention is to separate the overall reaction into two half cell reactions, each for the electron donor and electron acceptor at each of the electrodes, to allow comparison between the vast array of reactions that could be coupled. Continuing using the hydrogen fuel cell as an example, the overall cell reaction consists of

$$\mathrm{H_2} + \frac{1}{2}\mathrm{O_2} \rightarrow \mathrm{H_2O} \tag{2.1}$$

However, by spatially separating the reactants and forcing the electrons to be mediated through electrodes, the overall cell reaction can be divided into two half cell reactions. Where at the anode

$$H_2 \rightarrow 2H^+ + 2e^- \tag{2.2}$$

and at the cathode

$$\frac{1}{2}O_2 + 2H^+ + 2e^- \rightarrow H_2O \tag{2.3}$$

Similarly to the potential energy released from the elevation change of mass in a gravitational field, the maximum energy that can be captured from an electrochemical process consists of the electron potential drop of the electron between the electron donor and electron acceptor, which is also the voltage potential difference between the two half cells. Much like with gravitational potential, it is difficult to assign an "absolute zero" to compare the energy of each species to. Instead, the convention is to refer to a "sea level" or an agreed "zero" of electron energy, where $V = 0$V, that has been defined as the potential of hydrogen at 1 atm under acidic conditions. The standard hydrogen electrode (abbreviated SHE), also called normal hydrogen electrode (NHE), is a redox electrode which forms the basis of the thermodynamic scale of oxidation-reduction potentials.

However, the maximum electron energy change, or that predicted by the enthalpy of formation (chemical energy) of the reacting compounds, is never truly captured. As illustrated by the polarization or iV performance schematic in Figure 2.4, a number of losses occur in the system due to entropy increasing (free energy), potential mixing, reaction energy barriers (activation), electrolyte ionic resistance, and mass transport losses. These are elaborated upon in the next sections: Thermodynamics and Kinetics of electrochemical reactions.

Thermodynamics & Cell Voltage

Building from microscopic phenomena, thermodynamics is a field that relates energy transfer between heat (molecular vibration), work (force acting through a distance), and internal (chemical bond) energy with temperature, volume, and pressure changes. Likewise, for electrochemical phenomena, that of electron and voltage potential, relations can also be described.

The maximum theoretically energy that can be acquired from a reacting system is the difference in the enthalpy of formation, ΔH, of the products to the reactants. However, this neglects the fact that entropy is perturbed in a reacting system. Taking this into consideration, the energy that is actually obtainable in an isothermal and isobaric system such as an electrochemical cell is described by the Gibbs free energy, ΔG, as

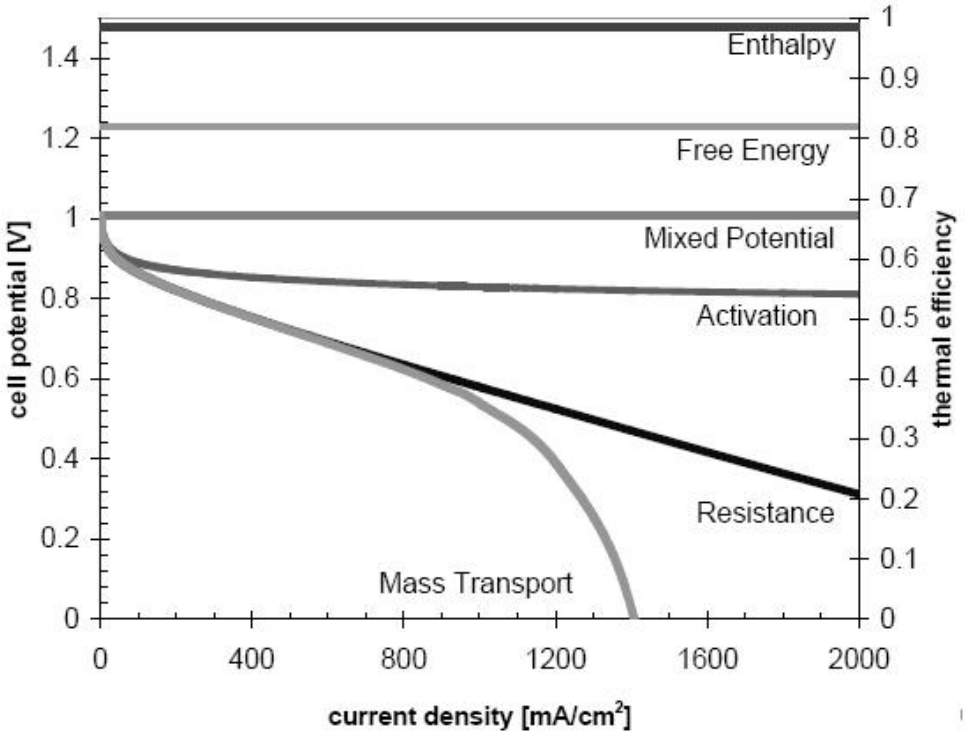

Figure 2.4: Polarization schematic of typical hydrogen fuel cell performance depicting cell voltage drops due to common thermodynamic, kinetic, and mass transport losses.

$$dG = dH - TdS \tag{2.4}$$

This predicts the energy that is released by converting the reactants into the products. Next, utilizing the second law of thermodynamics or energy conservation, that relates the system to its surroundings

$$dE = 0 \rightarrow dU = TdS - dW = TdS - (pdV + dW_{elec}) \tag{2.5}$$

Combining the previous two relations, and assuming that electrochemical cells are isothermal and isobaric,

$$dG = -dW_{elec} \tag{2.6}$$

hence

$$W_{elec} = -\Delta g_{rxn} \text{in molar terms} = E_0 nF \tag{2.7}$$

where,
E_0 = thermodynamically reversible voltage from the Gibbs free energy
n = the number of electrons transferred in the reaction
F = Faraday's constant (96485.3 C/mol e-)

So that the theoretical Voltage:

$$E_0 = \Delta G_{rxn}/nF \tag{2.8}$$

However, the cell voltage also depends on operating conditions such as temperature and species partial pressure of the system. The Nearst relation displays the more detailed relationship

$$E_{Nearst} = E_0 + \frac{RT}{2F} \ln \frac{P_{H_2} P_{O_2}^{1/2}}{P_{H_2O}} \tag{2.9}$$

where,
R = the universal gas constant (8.314 J/mol-K)
T = temperature (K)
P_i = partial pressure of species i

Here the theoretical efficiency of the system can be defined as η_{rev}. Table 2.1 summaries the theoretical voltage and efficiency that is expected of a H_2/O_2 fuel cell at various temperatures.

$$\eta_{rev} = \Delta G/\Delta H = E_{rev}/E_{theo} \tag{2.10}$$

Table 2.1: Temperature and phase factors on hydrogen fuel cell theoretical efficiency, η_{rev}, and V.

$H_2 + {}^1/_2O_2 \rightarrow H_2O$ 1 bar reactant pressure (standard conditions)						
Temp	**product H_2O phase**	**ΔH_{rxn} (kJ/mol)**	**ΔG_{rxn} (kJ/mol)**	**η theoretical**	**E_{tn} (V)**	**E_{rev} (V)**
25°C	LHV (vapor)	-241.8	-228.6	94.5%	1.253	1.185
	HHV (liquid)	-286	- 237.3	83%	1.482	1.229
80°C	LHV	-242.3	-226.2	93.3%	1.256	1.172
	HHV	-283.8	-233.7	82.3%	1.471	1.212
130°C	LHV	-242.8	-223.9	92.2%	1.258	1.160
	HHV	-282.1	-230.4	81.7%	1.462	1.195

Kinetics & Power Generalities

In the previous section, the theoretical and reversible cell voltages were computed from the energy of reactants and products, or end points, of the system. However, kinetics or reaction rates are also important. As a fuel cell is an electrochemical cell intended to power electronics, the ideal output is constant reversible voltage at any current density. This sort of performance is impossible, however, as it would require the system to deliver infinite power ($P = IV$) and zero internal resistance ($R = V/I$). This section describes the limitations in the system due to irreversible kinetic losses. These consist of mixed potential (fuel crossover), overvoltage (activation), ohmic (ionic), and fuel concentration (mass transport) losses, as illustrated by Figure 2.4. Hence the actual cell voltage is actually described by

$$V_{cell} = E_{Nearst} - i_{Rint} - \eta_{act} - \eta_{conc} (\eta \text{is the overpotential}) \tag{2.11}$$

where,
V_{cell} = real cell output voltage
E_{Nearst} = thermodynamic voltage from free energy
iR_{int} = ohmic loss due to ionic species transport, including mixed potential
η_{act} = activation loss due to sluggish reaction kinetics at electrode
η_{conc} = polarization due to insufficient supply of species for reactions

The kinetics of the system can be modeled as an electrical circuit, as shown in the Figure 2.5 below. In the case of a hydrogen fuel cell, to use as a related example, electrons are the negative carriers, and protons are the positive carriers. At the anode, the electron donor is broken into these charged species that must both transfer to the cathode to recombine

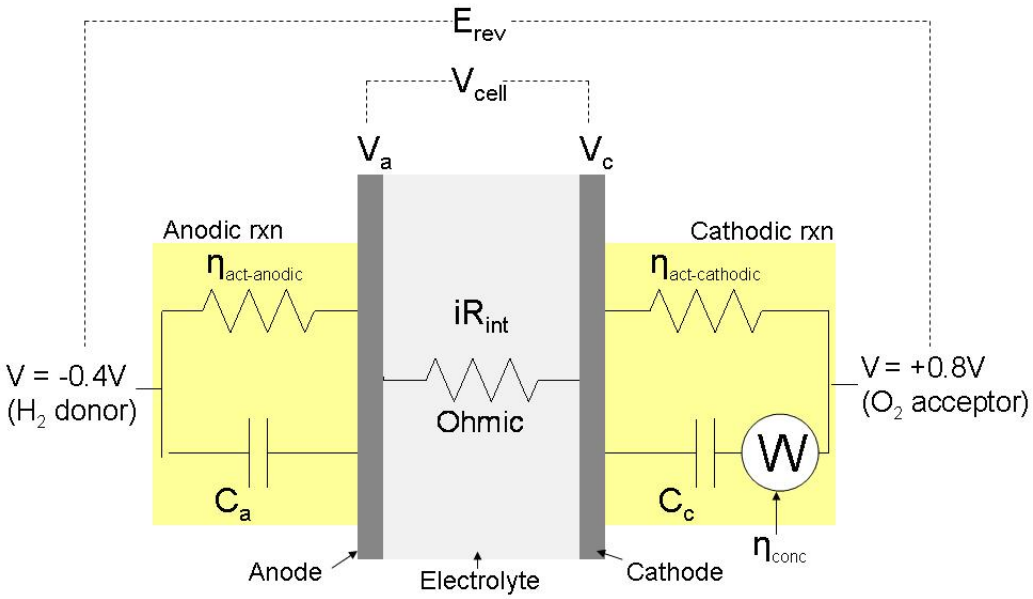

Figure 2.5: Model of hydrogen fuel cell kinetic losses including activation, ohmic, and mass transfer.

with the electron acceptor. Ideally, both charged species would travel instantly and simultaneously between electrodes; however, this is highly unlikely if not impossible and losses accrue. The electrode reactions are both faradaic (resistive) and capacitive, and hence affect the electrical potential of the electrons as they are transferred through the system. The electrolyte generates a kinetic lag that is linearly dependent on current. The objective is to keep the anode as negatively charged as possible (e^- saturated) while keeping the cathode as positively charged as possible (minimal e^- count) to maximize a potential differential between the electrodes. Since the system is an energy conversion device, it continuously consumes electron donor and acceptor and the reactions come to a halt when either reactant is exhausted.

Mixed potential

Mixed potential occurs from undesired reactant and electron crossover. As the electrolyte or polymer exchange semi-permeable membrane is imperfect at selecting species and as an electrical insulator. Consequently, it allows electron acceptor and donor to mix slightly allowing electrons to "short" or bypass the load. From this loss, an efficiency termed "faradaic" can be defined as the ratio of electrons or reactants that crossed over to short the reactions and did not travel through the load with respect to the number that were added as fuel, as Equation 2.12.

$$\eta_f = \frac{i}{i_f} \tag{2.12}$$

Activation

Activation losses stem from sluggish kinetics of the electrochemical half-reactions. As every chemical reaction must overcome an activation energy, some of the cell voltage is sacrificed to overcome the impediment. The losses are manifested as a large voltage drop that is particularly prominent at low current densities. The potential losses increase with current density and are described by the Butler-Volmer Equation 2.13

$$j = j_0 \left(exp\left(\frac{\alpha n F \eta}{RT}\right) - exp\left(\frac{(\alpha - 1) n F \eta}{RT}\right)\right) \tag{2.13}$$

where,
j = current density (A/cm^2)
j_o = exchange current density (A/cm^2)
n = number of electrons in reaction
F = Faraday's constant (96485.3 C/mol e-)
α = transfer coefficient
η_{act} = activation overvoltage (V)

The overpotential loss can be mitigated by increasing the exchange current density which is intimately related to the catalyst material and the reaction surface area available. The exchange current density (or exchange current) is defined as the equilibrium half-cell current that is transferred in and out of the electrode into the species at open circuit conditions. As each catalyst point allows electrons to be transferred through the electrode, each acts as individual high impedance current source with a characteristic activation energy. However, increasing the number of current sources lowers the "compound" activation impedance and activation overpotential. For this reason, electrochemical cells benefit from high catalyst loading and maximizing the number of triple phase boundaries (catalyst/electrode/electrolyte junctions).

In addition to faradaic currents, where charge transfer occurs at the electrode/electrolyte interface due to a redox reaction, non-faradaic or background currents occur due to capacitive effects. A distinction should be made, as non-faradaic currents are not due to chemical reactions but rather occur to equilibrate local charge imbalances at the electrode/electrolyte interface through the formation of an electric double layer (EDL). Because they do not require that an activation energy be overcome, but merely necessitate ionic species movement at a narrow distance from the electrode (about 2-30nm), they are characterized by very

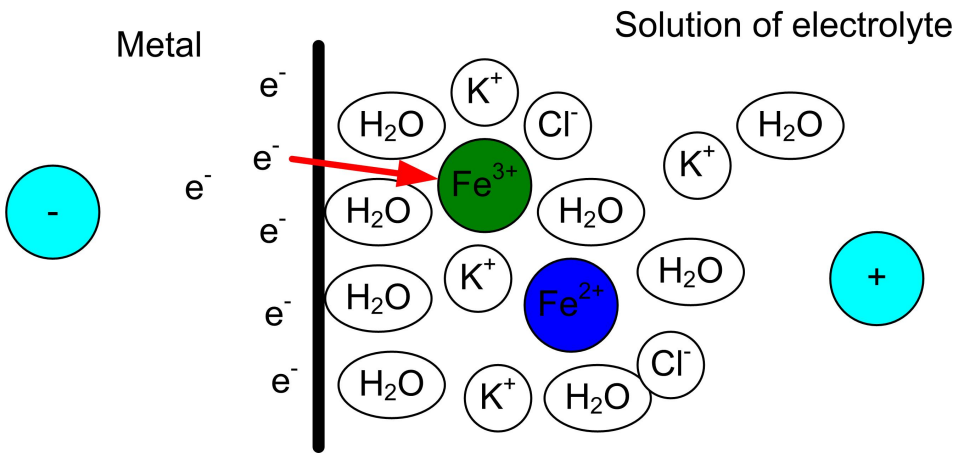

Figure 2.6: Faradaic currents defined by electrode/electrolyte charge transfer from redox reaction.

low impedances, quantifiable charge transfer, and reversibility (generally). The non-faradaic currents are modeled as a capacitor in parallel with the faradaic reaction resistance at each of the electrodes, as shown in Figure 2.5 above. The electrode capacitance is highly dependant on the true surface area of the electrode (roughness), as the EDL is conformal to the molecular geometry of the surface. Figures 2.6 and 2.7 illustrate faradaic and non-faradaic currents, respectively.

Ohmic Resistance

The ohmic or internal resistance in an electrochemical cell stems from the losses of conducting separated charge through the system. As shown in Figure 2.5 above, these losses are modeled as a linear resistance between the two electrodes, because they generally follow Ohms law ($R = V/I$). They occur due to material inefficiencies to transfer either protons through the electrolyte or electrons between the anodic-to-cathodic catalytic sites at each of the electrodes. In general, ionic electrolytes are more resistive than metals, with, as an example, salt water $\rho = 20$ Ωcm and gold $\rho = 2\text{x}10^{-6}$ Ωcm. However, ohmic resistance is an extrinsic property that is highly dependent on the geometry of the "conduction paths" of the separated charge, and it can hence be improved through design. Figure 2.8 below shows the geometrical relationship between intrinsic material resistivity and extrinsic system resistance.

And Equation 2.14 shows the mathematical relationship

$$R = \rho \frac{L}{HW} \tag{2.14}$$

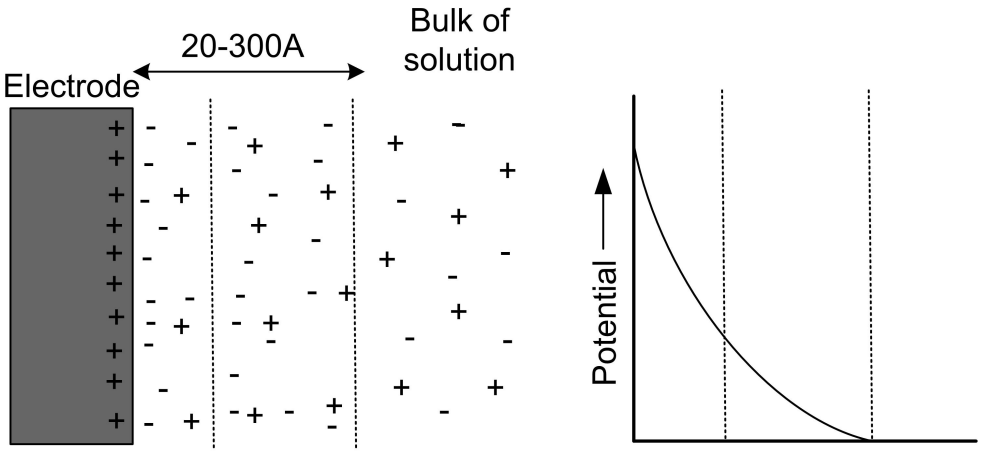

Figure 2.7: Non-faradaic (capacitive) currents occur due to rearrangement of species at electrode/electrolyte interface but where no redox reactions occur.

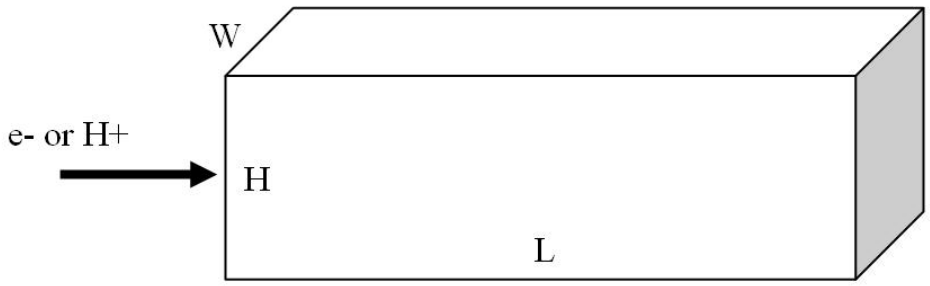

Figure 2.8: Geometrical relationship between bulk material resistivity, ρ, and intrinsic ohmic system resistance, R_{ohmic}.

where,

ρ = material resistivity (Ωcm)
L = species travel path length (cm)
W = species travel path cross section width (cm)
H = species travel path cross section height (cm)

Consequently, ohmic losses are minimized by large (cross sectional) surface area electrodes placed in close proximity. Physically, the protons and electrons are separated at the anode, must travel via their corresponding paths, and must both be simultaneously present at the cathode to recombine and reduce the oxidant. Hence, the ohmic resistance that is characteristic of the system is that of the slowest link, or $R_{int} = \max\{R_{e^-}, R_{H^+}\}$.

Concentration losses

Provided that the losses that were previously described do not dominate the system, at high current densities, the fuel or oxidant molecules can reach a point where they are consumed faster than they are supplied to the catalytic sites. Labeled as concentration polarization or concentration losses, these occur due to insufficient mass transport of the reactants to the electrodes. The concentration losses can be characterized by decreasing the resistance of the load until the electrochemical cell reaches a short circuit, as shown in Figure 2.5 above. The maximum cell electron transfer rate is labeled as the limiting current and is obtained when the voltage across the cell is zero. Physically, the drop in voltage (or power) occurs because significantly reducing the load's resistance allows electrons to "drift" faster from anode to cathode. However, since limited quantities of electron donor or electron acceptor exist, the system "stoichiometry" is perturbed. Consequently, charge equilibrates between the electrodes, and the voltage potential drops.

System efficiencies

Thus far in this Chapter, a number of efficiencies have been defined for electrochemical systems. Understanding that the maximum energy that can be obtained from a chemical reaction is the change in enthalpy of the system, losses due to entropy and irreversible kinetics were identified. However, two more efficiencies can be defined: utilization and auxiliary loads. Table 2.2 below summarizes all these relationships as well as the system overall efficiency.

Utilization

This efficiency refers to the "fuel" efficiency or rather the utilization of the electron donor for reactions in the electrochemical cell. As it is possible that in a flow-through system, reactants can be added, not utilized fully, and flushed out before they can react. Hence this

Table 2.2: Summary of electrochemical cell thermodynamic, irreversible, reactant, plant, and compound efficiencies.

Efficiency	Definition	Description
Reversible	$\eta_{rev} = \frac{\Delta G}{\Delta H} = \frac{E_{rev}}{E_{thermal}}$	Loss due to entropy increase
Voltage	$\eta_V = \frac{E}{E_{rev}}$	Activation and ohmic losses
Faradaic	$\eta_f = \frac{i}{i_f}$	Mixed potential and electron leakage
Utilization	$\eta_u = \frac{n_{reacted}}{n_{total}}$	Quantum electron efficiency
Auxiliary loads	$\eta_a = 1 - \frac{P_{PL}}{P_{total}}$	Energy for pumps and electrical systems
System efficiency	$\eta_{total} = \eta_{rev}\eta_V\eta_f\eta_u\eta_a$	Overall compound efficiency

efficiency, which is also described as the Coulombic efficiency, is defined as Equation 2.15 below.

$$\eta_i = \frac{\text{e- captured through circuit}}{\text{e- added as fuel}} \tag{2.15}$$

Auxiliary Loads

Lastly, since a true system will utilize power to run (ie. consume energy for mechanical pumps and electronic control), an efficiency that provides a gage for its "autonomy" is defined as Equation 2.16 below.

$$\eta_a = 1 - \frac{P_{PL}}{P_{total}} \tag{2.16}$$

2.2.2 Ultra-micro-electrochemistry (UME)

The basic concepts of electrochemistry and fuel cell theory were covered in the previous section. However, the behavior of an ultra-micro-electrode (UME), as it pertains to this work, differs significantly from that of macro-scale systems. UMEs are point-like electrodes ($r_0 < 100\mu$m) where the physiochemical properties scale in different ways, and, hence, yield capabilities that are not available through large-system testing. The scaling of UMEs offer two main advantages: faster temporal responsiveness (lower experimental time scale), τ_{cell}, and faradaic reaction preferential characterization, τ_{rxn}/τ_{cell}. As it is discussed in this section, and illustrated by Fig. 2.9, these largely stem from a reduced capacitance, C_d, and proportionally larger faradaic resistance, R_f, with respect to ohmic losses in the system. These have been adopted from [44, 45].

System time constant - τ_{cell}

The system electrical response time, or time to stabilize after perturbing the system, is expressed through the cell time constant, τ_{cell}, which is proportional to the electrolyte resistance and electrode capacitance.

$$\tau_{cell} = R_e C_d \tag{2.17}$$

In general terms, the electrolyte resistance, R_e, is dependent on ionic conductivity and electrode geometry, where t = thickness of the electrolyte (cm), r_0 = electrode radius (cm), and σ = electrolyte ionic conductivity (S/cm).

$$R_e = \frac{t}{4r_0^2\sigma} \tag{2.18}$$

However, since in ultra-micro-electrodes $r_0 \ll t$, the point electrode yields a hemispherical potential drop and $R_e \sim 1/r_0$.

$$R_e = \frac{t}{4r_0^2\sigma} \rightarrow R_e \approx \frac{1}{4r_0\sigma} \tag{2.19}$$

The electrode capacitance, C_d, stems from the electrical double layer (EDL) or the rearranging of the ionic carriers at the electrode-electrolyte interface and scales with r_0^2 as

$$C_d = C_d^0 \star \pi r_0^2 \tag{2.20}$$

where C_d^0 is the specific interfacial capacitance (F/cm^2). However, the EDL is conformal to the molecular geometry of the electrodes, which prevents straightforward normalization to electrode surface area in large systems. UMEs, on the other hand, offer the advantage that surface roughness can typically be somewhat controlled or at least characterized.

Hence, the system response or cell time constant, τ_{cell}, in UMEs scales linearly with r_0, as

$$\tau_{cell} = R_e C_d = \frac{\pi C_d^0 r_0}{4\sigma} \tag{2.21}$$

Faradaic relaxation - τ_f

Faradaic resistance, however, resistance for charge to be transferred from the reactant to the electrode scales inversely with true surface area, as

Table 2.3: Summary of ohmic, capacitive, and kinetic effects and UME scaling that demonstrate preferential isolation of faradaic reactions or *microbiological* factors from bioelectrochemical systems.

Parameter	Variable	Macro-electrode	UME
Electrolyte Resistance[1]	R_e	$R_e = \frac{t}{4r_0^2\sigma}$	$R_e = \frac{1}{4r_0\sigma}$
Electrode Capacitance[2]	C_d	$C_d = C_d^0 \star \pi r_0^2$	$C_d = C_d^0 \star \pi r_0^2$
System time constant[3]	τ_{cell}	$\tau_{cell} = R_e C_d = \frac{\pi t C_d^0}{4\sigma}$	$\tau_{cell} = R_e C_d = \frac{\pi C_d^0 r_0}{4\sigma}$
Faradaic resistance[4]	R_f	$R_f = \frac{R_f^0}{\pi r_0^2}$	$R_f = \frac{R_f^0}{\pi r_0^2}$
Faradaic relaxation[5]	τ_{rxn}	$\tau_{rxn} = R_f C_d = C_d^0 R_f^0$	$\tau_{rxn} = R_f C_d = C_d^0 R_f^0$
Time constant ratios[6]	$\frac{\tau_{rxn}}{\tau_{cell}}$	$\frac{\tau_{rxn}}{\tau_{cell}} = \frac{4R_f^0\sigma}{\pi t}$	$\frac{\tau_{rxn}}{\tau_{cell}} = \frac{4R_f^0\sigma}{\pi r_0}$

[1] Electrolyte resistance within microfluidic environment scales inversely with radius due to characteristic spacing as $r_0 << t$

[2] Capacitance scales as r_0^2 but is conformal to electrode molecular roughness

[3] Cell time constant refers to the speed at which system returns to steady state after an electrical perturbation and scales linearly with radius in UMEs

[4] Faradaic resistance refers to the kinetics of charge transfer through the electrode and scales inversely with surface area

[5] Faradaic relaxation time indicates the speed of the faradaic reaction and is independent of electrode geometry

[6] Ratio of faradaic relaxation time and cell time constant scales inversely with radius in UMEs indicating that the system responds rapidly and the faradaic reactions govern the system response.

$$R_f = \frac{R_f^0}{\pi r_0^2} \tag{2.22}$$

The system's response time, or relaxation time constant, with regard to faradaic reactions then can be estimated as

$$\tau_{rxn} = R_f C_d = C_d^0 R_f^0 \tag{2.23}$$

where R_f^0 is the specific faradaic resistance and C_d^0 is the specific capacitance. Hence the system's ability to respond and capture faradaic transfers can be expressed through the ratios of the faradaic relaxation time to the cell's time constant. For an UME, this relationship scales inversely with the radius of the electrode as Equation 2.24 below.

$$\frac{\tau_{rxn}}{\tau_{cell}} = \frac{4R_f^0\sigma}{\pi r_0} \tag{2.24}$$

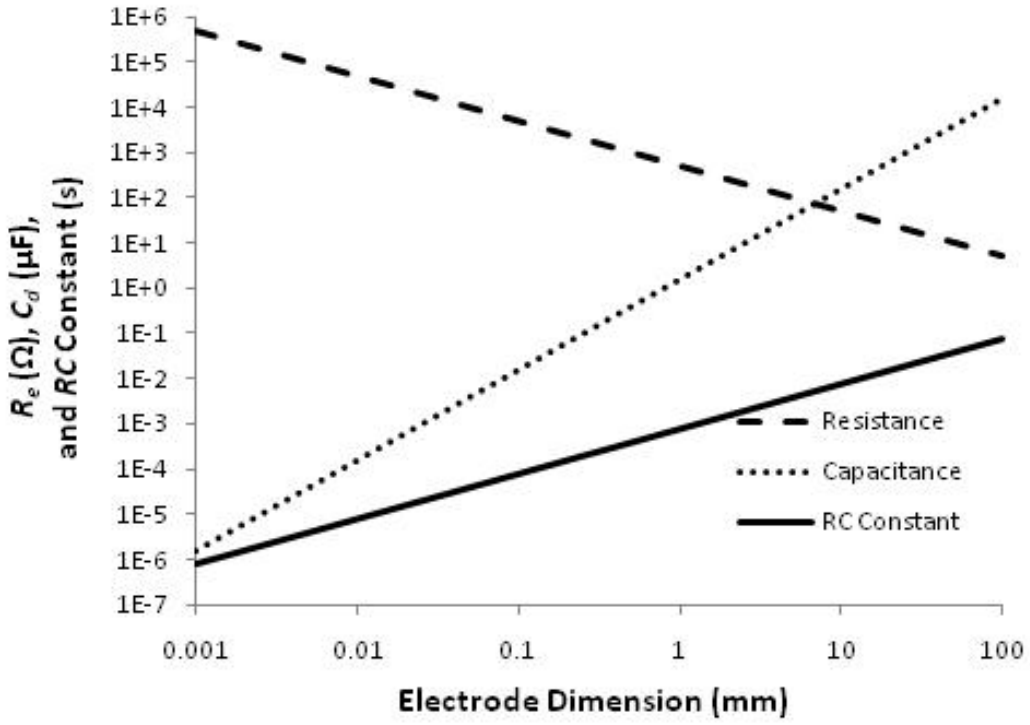

Figure 2.9: Scaling of the electrolyte resistance, electrode capacitance, and RC cell time constant as a function of microelectrode size. Typical double layer capacitance and basal media conductivity values ($C_d^0 = 50\ \mu\text{F/cm}^2$ and $\sigma = 5$ mS/cm) are used in this simulation. Decreasing microelectrode dimensions decreases the experimentally accessible time scale limits.

2.3 Bioelectrochemistry & *G. sulfurreducens*

The previous sections introduced the topics of electrochemistry, and power and efficiency of PEM fuel cells. In this section, the biological aspects of the system are discussed. For simplicity, this work focused on anodic bacterial reactions only, or utilizing whole living microorganisms to break down acetate into electrons and protons. In comparison to a hydrogen fuel cell, in the system the microorganisms "replace" the precious metal (platinum) catalyst and simple carbohydrates replace the hydrogen gas. Other aspects that differ from inorganic fuel cells are that the system must be kept in buffered aqueous solution at a certain salt concentration range (osmotic pressure) and within a biological temperature as the bacteria require. In addition, the system is temporally dynamic as the quantity of cells (biocatalyst loading) changes as well as the quality of their connectivity (contact resistance). Bacteria can also metabolically adapt (protein expression) and adjust their environment (deposit polyglycans) to environmental stresses.

At the anode, the microbes catalyze the break down of simple carbohydrates. The half reaction in the case of acetic acid oxidation is

$$CH_3COO^- + 4H_2O \rightarrow 8e^- + 2HCO_3^- + 9H^+ \tag{2.25}$$

In order to maximize the power of the system, the objective is to capture all the electrons from the fuel from the microorganisms at as high potential as possible and sustain the voltage as the electron flux (power) is ramped up. As the microorganisms require some energy for their own metabolic functions, not all of the potential from the acetic acid can be captured as is explained in the next section.

2.3.1 Metabolism and Redox

In inorganic PEM fuel cells, the maximum voltage potential of the system can be estimated from the free energy released by the electrochemical reaction of the reactants. The system is heterogeneous in microstructure, but homogeneous in regards to chemistry as there is (ideally) only one species to react if using a single fuel. However, in bioelectrochemical catalysis, the electron donor must be metabolized through a series of enzymatic reactions to breakdown the fuel and subsequently electrons are transferred to the electrode. As a result, the maximum anodic voltage that can be achieved is that at which the microorganisms metabolize the electron donor.

Traditionally, redox indicators (ie. methylene blue and neutral red) that are able to penetrate the cell membrane have been utilized as synthetic mediators to directly capture electrons from the metabolic enzymes and transport them to the electrode. However, mediators are highly oxidative to the cells, make electrons diffusion limited, and limit the anode

potential to that of the mediator's redox. Alternatively, microorganisms that have evolved mechanisms to intrinsically externalize waste electrons have been isolated and have shown to produce electricity sustainably.

Ideally, electrons should be captured at the exact enzymatic site where they have become "waste" within the metabolic pathway as to gain the most negative redox and provide the greatest potential differential with the electron acceptor. However, non-fermenting bacteria utilize the citric acid cycle to catalyze acetic acid into NADH, a process that occurs within the cytoplasm. Hence maximizing the metabolic redox requires external machinery to penetrate the cell membrane and risks viability. Alternatively, *G. sulfurreducens*, as Figure 2.10 illustrates, "shuffles" electrons through membrane-bound proteins out to the extracellular environment. The electron shuffling comes with an anode voltage cost as a potential drop occurs through the membrane electron transport chain. Furthermore, this method comes with an additional energy sacrifice to the microorganisms as protons must be pumped out instead of combining with soluble electron acceptors. Current research indicates at least two methods for electron externalization exist in nature: microbially produced metabolites that mediate, such as in *Shewanella oneidensis* [46], or through direct bacteria-electrode contact, such as in *Geobacter sulfurreducens* [10].

To elaborate on the thermodynamic losses incurred by metabolism, Figure 2.11 below, a redox tower, illustrates the electron voltage potentials that could be captured at the anode from these microorganisms. Acetic acid enters the cell at -0.28V (vs. SHE) and, in the case of *G. sulfurreducens*, the biocatalysts are able to thrive in a fumarate/succinate environment or reducing soluble electron acceptors at +0.03V (vs. SHE). Assuming that this potential corresponds to the metabolically ideal redox for electron acceptors, the organisms could provide a fuel cell voltage of +0.85V. However, as the electrons must be externalized to transfer onto electrodes, some of this energy is used (lost) in the shuffling of the electrons through membrane-bound cytochromes. Current research predicts that the last protein that interacts in this process is a c-type cytochrome that typically have a midpoint redox potential of +0.25V (vs. SHE), which would predict a cell voltage of +0.57V with oxygen as the electron sink. However, cyclic voltammograms of *G. sulfurreducens* immobilized on graphite electrodes have demonstrated absorbance at a mid-point potential of -0.17 V (vs.SHE) [10, 47]. Hence more intensive studies are still needed to clarify the potential characteristics.

Figure 2.12 depicts the dependence of anode potential on the physiology of the microorganisms. Metabolism (dotted line) affects the electrical performance in three ways. 1) The terminal protein in the electron transfer path for externalization governs the redox at which the electrons may be harvested from the cell. 2) The density of this terminal protein (cytochrome) determines the exchange current density that is intimately related with activation losses and resulting voltage. And 3) the metabolic rate of the cell must also be sufficient as to supply the terminal cytochromes with electrons and hence maintain the cells' membrane at a negative potential. Secondly, the bacteria-electrode transfer mechanisms (double line) also affect the system and provide a characteristic "contact" resistance, as is elaborated in

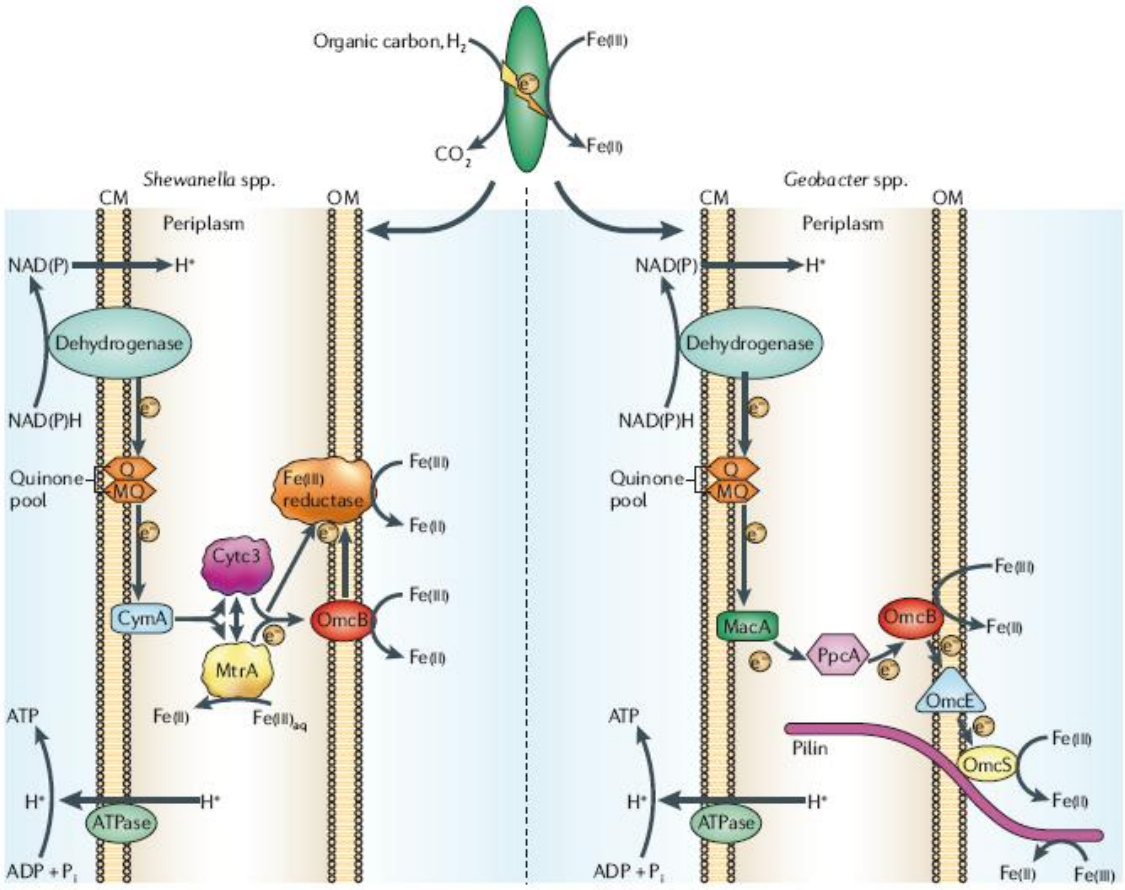

Figure 2.10: Models of electron externalization mechanisms in *Shewanella* and *Geobacter* species utilizing cytochrome network and pili "organic nanowires". From K.Weber and J.D.Coates [3]

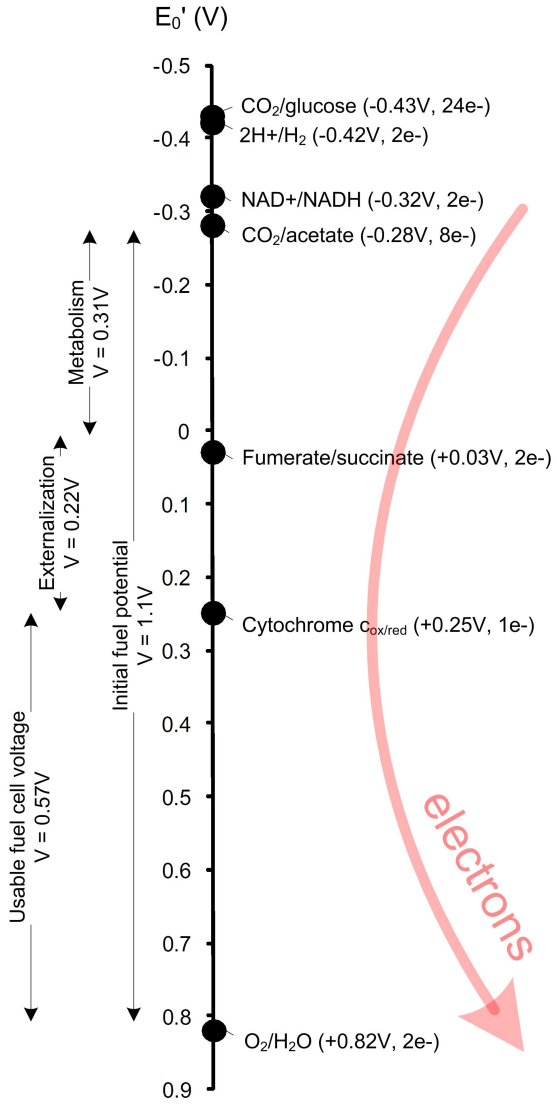

Figure 2.11: Simplified redox tower of electrons through *G. sulfurreducens* in bioelectrochemical systems. Initially, acetic acid is internalized at a redox of -0.28V (vs. SHE), and electrons loose energy as they progress through metabolism and externalization. Assuming c-type cytochrome with a midpoint redox potential of +0.25V (vs. SHE) as final protein in the electron transport chain, a fuel cell voltage of +0.57V can be predicted with oxygen as the final electron acceptor.

the next section.

Assuming the simplest model where the metabolic chain is a linear system and follows an ohmic response, a cell's lumped resistance could be defined as $R_{cell} = dV/di$. Hence, the *metabolic* or *faradaic resistance* can be estimated from the potential difference at which electrons enter and leave the cell and the respiration rate (electric current) through the cell. Figure 2.13 depicts the metabolic resistance model for one cell. To estimate the resistance, the voltage drop and electron rate (metabolism) across the cell are needed.

The potential drop of the electrons between acetate and the c-type cytochromes, as was discussed in the previous section, can be estimated as +0.53 V. Likewise, *G. sulfurreducens* metabolic rate has been characterized in bulk and can be obtained from the literature. One study measured the specific respiration rate using acetate as the limiting nutrient and Fe(III)-citrate in excess as the electron acceptor [48]. As Fe(III)-citrate is soluble but is reduced at the periplasm, this arrangement somewhat simulates respiration rate onto the extracellular environment and has resulted in a maximum of $0.15\frac{\text{mmol e}^-}{\text{mg}_{\text{dw}}\text{h}}$ at the highest cell growth rate of 0.08 h^{-1}. Assuming that microorganisms are 0.5 μm^3 in volume, essentially water, and 10% protein, a current of 200 fA/cell can be estimated at electron donor saturated conditions from this bulk experiment. Moreover, this value has been roughly validated by Nealson et al. who have characterized a metabolic rate of 200 fA/cell for *Shewanella oneidensis* on an electrode utilizing stained cell counting techniques [5]. Assuming these values as the metabolic rate per bacterium, the per cell metabolic resistance to externalize electrons can be estimated by Equation 2.26.

$$R_{cellmetabolic} = \frac{V}{i} = \frac{0.53\text{V}}{200\text{fA}} = 2.7\text{T}\Omega \tag{2.26}$$

Although this is an oversimplification of the actual system, it provides a first order-of-magnitude impedance and scope on the cumulative current contribution of the bacteria on the electrode. By comparison, the faradaic resistance of oxygen on platinum has been experimentally characterized as 6 G$\Omega\mu$m for micrometer sized structures [6], or the equivalent of 3 GΩ for the space occupied by a rod-sized bacterium. Consequently, assuming all other parameters are equal, microbial catalysis provides 3-orders-of-magnitude more sluggish kinetics than oxygen on platinum.

2.3.2 Electron transfer to electrode

The previous section discussed the resistance due to metabolism and electron externalization. As microorganisms must catalyze organic fuel into separated charge, a *metabolic resistance* was defined as a lumped parameter to account for diffusion between enzymes and their specific activity. However, that model did not account for the transfer or "contact"

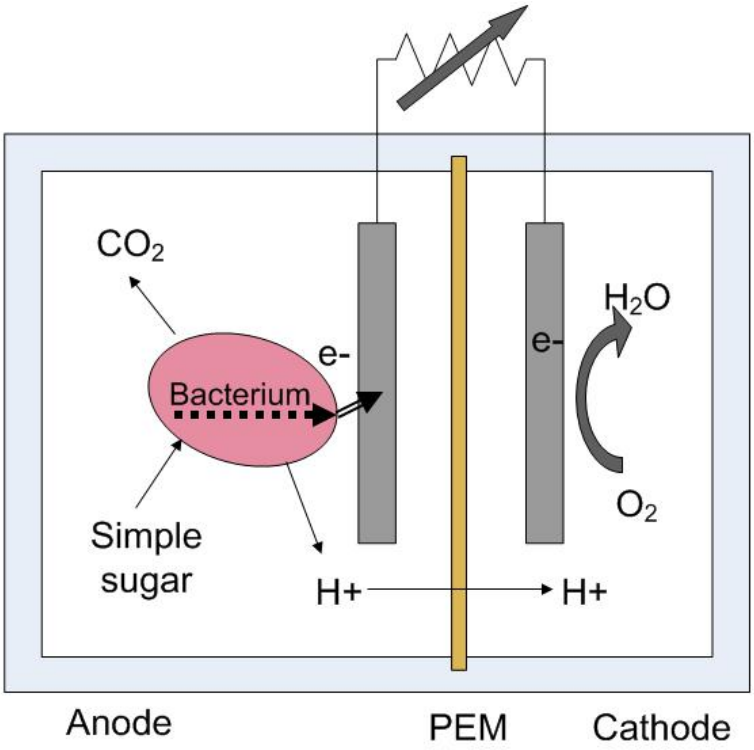

Figure 2.12: Anodic voltage depends on biocatalyst physiology. Microorganisms' metabolic chain as well as electron externalization mechanism affects anode potential. Step A: Metabolism (dotted line) affects the electrical performance in three ways. 1) The terminal protein in the electron transfer path for externalization governs the redox at which the electrons may be harvested from the cell. 2) The density of this terminal protein (cytochrome) determines the exchange current density that is intimately related with activation losses. 3) The metabolic rate of the cell must also be sufficient as to supply the terminal cytochromes with electrons and hence maintain the cells' membrane at a negative potential. Step B: Bacteria-Electrode Transfer Mechanisms (double line) also affects the system and provide a characteristic "contact" resistance. In the case of direct bacteria-electrode contact, such as in *G. sulfurreducens*, where protein nanowires are believed to act as electrical conduits, the electron transport is governed by the nanowires' material properties and the physical network density. In the species where metabolites transport the electrons to the electrode, the transfer resistance is affected in two ways. 1) The metabolite acts a mediator that will provide a maximum (lower) redox for the transfer. 2) The current density may be diffusion limited particularly if insufficient metabolite concentration is present to mediate the electrons.

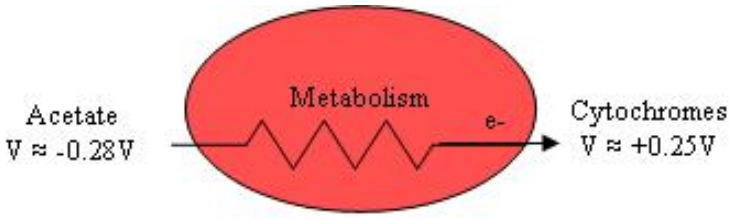

Figure 2.13: An ohmic model of $R = dV/di$ can be used to estimate a lumped metabolic resistance. Assuming a voltage drop of 0.53 V from the acetate fuel to c-type cytochromes in the membrane, and a metabolic rate of 200 fA/cell [4, 5], the resulting per cell faradaic resistance is 2.7 TΩ. Hence, the kinetics are estimated at 1000x slower than that of oxygen on platinum on a per micron area basis [6].

resistance to transfer the electrons to the electrode. As was first presented in Figure 2.12 and is presented in greater detail in Figure 2.14, microbial catalysis introduces two distinct resistances to replace the single *faradaic resistance* that was defined for inorganic systems. Hence, the *electron transfer resistance* is added in series to the *metabolic resistance* account for the electron transfer to the electrode. In addition, a more accurate model also includes a capacitance term, independent of the anode response, as the microorganisms have the capability to store charge within the electron transport chain and the membrane cytochromes. Similarly, as some of the energy and mass that is added as fuel is utilized for cell division, a grounded *biomass resistance* term should be included in the circuit to account for this loss.

In the case of direct bacteria-electrode contact, such as in *G. sulfurreducens*, where protein nanowires are believed to act as electrical conduits, the electron transport would be governed by the nanowires' material properties and the physical network density. In the species where metabolites transport the electrons to the electrode, the transfer resistance would be affected in two ways. 1) The metabolite acts a mediator that will provide a maximum (lower) redox for the transfer. 2) The current density may be diffusion limited particularly if insufficient metabolite concentration is present to mediate the electrons. Consequently, estimating the electron transfer resistance from the cell to the electrode is complicated. The ideal case would be for the electrons to be transported through a low-impedance 3-dimensional pili network that the bacteria self-generate and would not be lost through convection in the case of flow-through reactors. However, preliminary work on *G. sulfurreducens* that characterized the pili suggest semi-conductor behavior at best as a resistance of 150 MΩ through the 5 nm pili cross-section was measured using conductive-probe AFM [36]. However, fundamental understanding and characterization of bacteria-to-electrode electron transport mechanisms is still at its infancy, and we hope that with continued interest a low-resistance electron transfer mechanism can be either evolved or engineered.

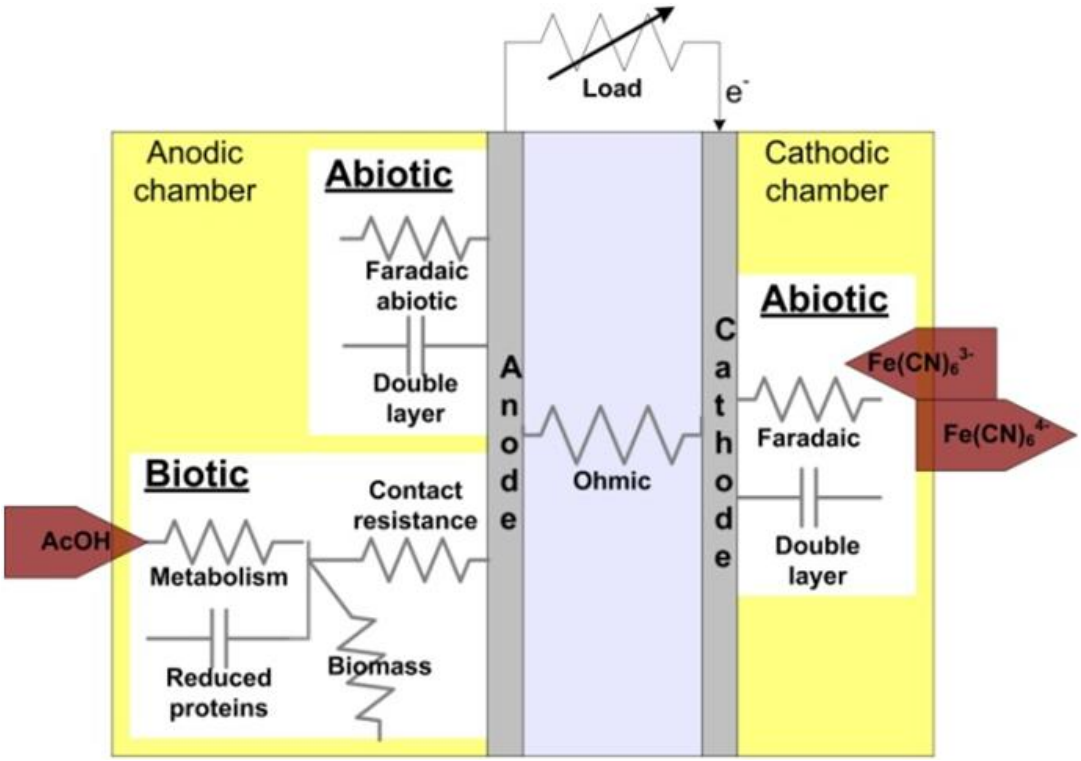

Figure 2.14: Model depicting kinetic transport within anodic microbial fuel cells. In addition, to the typical PEM fuel cell kinetics, the system also includes a metabolic overpotential, electron transfer resistance, and microorganism capacitance.

Chapter 3

Microfabricated MFC using *G. sulfurreducens*, an extracellular electron respiring bacteria

3.1 Introduction

Electricity scavenging from microbial metabolism is a phenomenon that has only been reasonably studied for about a decade, and, within this time, power densities have increased several orders of magnitude [12]. However, greater performance is expected as the system is just beginning to be understood. Further optimizations for power generation require identifying the important parameters within this multivariate system, but this task has proven difficult as the catalysis is biological and highly heterogeneous. For example, a slight change in a parameter (say a temperature change of 5^oC) causes prominent physiological changes in the system, which complicates the comparisons in various literature studies and it is hard to draw conclusive "lessons" from these investigations. Hence, many basic questions that are fundamental for optimization continue to remain unanswered.

At the most basic level, energy transfer is not fully understood, and the hypotheses that explain electron transfer mechanisms from the microorganism to the electrode are controversial. Broadly speaking, the transfer could occur through direct protein-electrode contact, a "nanowire" conduit, or mediating compounds. The specific mechanism is intrinsic to the microorganism, and multiple mechanisms may be possible for each species, as current evidence for *Shewanella odeneises* suggests. Naively speaking, it would be ideal for the microorganisms to self-generate a solid-state conductive electrical network that could sustain a dense and volumetrically thick biofilm. However, such a task is energetically expensive for the microorganisms and one could argue that the use of synthetic mediators maybe advantageous. From an engineering standpoint, this deficiency of fundamental understanding hinders the

engineering optimizations. In addition, improvements in performance are difficult to quantify experimentally as the catalysis is highly heterogeneous and great variability exists between systems. The miniaturization of microbial fuel cells and electrodes are investigated in this chapter to gain greater controllability of the biocatalysts and explore the scaling features. Specifically, microscale-electrodes provide the following advantages:

1. Mitigate heterogeneity - microorganisms utilized in bioelectrochemistry are roughly a micron in size. Hence, a cm^2 electrode can accommodate a fully-packed monolayer of 10^8 cells. Reducing the electrode area to 100 x 100 μm^2, for example, decreases the heterogeneity of the signal to that of 10^4 monolayer cells.

2. Entire electrode surface can be monitored concurrently and locally - as the signal is largely dependent on the biocatalyst loading (or bacteria quantity), the biofilm conformity to the electrode can be monitored and taken into account.

3. Parametric micro-geometry studies are possible - the electrode geometry can be studied parametrically down to the micron scale if micro-electrodes are fabricated using semiconductor processing techniques.

4. System response time is enhanced - as was discussed in the Theory Chapter, reducing the electrode size improves the RC constant and the system can reach steady state more rapidly, which allows transient outputs and steady state responses to be easier to identify. Hence, more characterization can occur within a specific time frame and improvements are more easily quantified.

5. Scaling has shown to improve performance - as Dewan el al. has demonstrated [20], the literature reveals that greater power densities are achieved in smaller systems. Parametric characterization of micro-electrodes could illuminate the scientific foundation for this phenomena as well as the optimum electrode size and shape.

6. Electrode microstructure effects can be characterized - performance enhancements from surface modifications have been difficult to confirm using macro-electrodes because of system-to-system biocatalyst loading fluctuations. Miniaturizing the electrodes, in this case, offers the advantage of biomass loading characterization along with the electrical signal.

In this chapter, these advantages are explored through micro-fabricated fuel cells. Using a micro-fabricated gold electrode, the electrical steady-state performance is studied [4], and the advantages of the scaling with respect to the reduced RC constant discussed (unpublished). Specifically, capacitance and resistance of the system are extracted from the transient electrical response and analyzed for a relationship with biocatalyst loading and biofilm discharge characteristics. In summary, the objective of this chapter is to explore the advantages of miniaturization and assist the development of non-invasive characterization techniques that promote understanding and troubleshooting of bioelectrochemical systems.

3.2 Device - Design and Fabrication

Micro-electrochemistry is a field that evolved within the last 20 years mainly from advances in fabrication at the micro-scale and instrumentation. Given that microfabrication provides features to the micrometer scale, we adopted this fabrication technique for the construction of micromachined MFC. In addition, semiconductor processes also provide controllability of planarity and surface roughness, which allows for more exact estimates of the surface area of the electrode. The first task here was to identify standard processes that could be utilized for the construction of MFCs for bioelectrochemical studies.

Graphite and carbon cloth are widely utilized in microbial fuel cells but are not standard materials used in micromachining processes. On the other hand, Lovely has demonstrated that *G. sulfurreducens* can also transfer electrons to elemental gold [10]. Furthermore, gold is inert and biocompatible such that it is chosen as the electrode material in this study.

In regards to the geometry of the electrode, a literature search provided little guidance on the specifics. In general, the electrode had to provide a sufficiently large current signal, or lower impedance than that of our data acquisition instrumentation. Hence, a micro-electrode of mm^2 surface area was chose for this initial study. In order to mitigate diffusion effects, various micro-electrodes were arranged to be at a distance, d, relatively large in comparison to the electrode characteristic size, r, and diffusion layers, Dt, so that

$$r << (Dt)^2 << d \tag{3.1}$$

where r is the electrode radius, $(Dt)^2$ is the characteristic diffusion distance, and d is the micro-electrode spacing. This would maintain a hemispherical diffusion profile at intermediate experimental values that would accentuate the bio-catalytic effects [44]. Consequently, the anode consisted of a micro-patterned electrode that was designated as 2 μm in width, the length of a single bacterium for single cell contact, arrayed at a 100 μm spacing (pitch), as shown in Fig. 3.1. The resulting geometry imitated a carbon cloth complexity within a 2D structure, but it also provided a known surface area. Moreover, the microelectrode array conformed to the bacteria and biofilm dimensions, as *G. sulfurreducens* biofilm has reached 40 μm in thickness [10]. The total gold surface area was 1 mm^2 and each chip's area was 50 mm^2.

The fabrication for the electrode consisted of a standard lift-off process. Figure 3.2 illustrates the single mask process, which started with the cleaning of a test p-type silicon wafer in a piranha bath. Next, the wafer was introduced into a furnace equipped for high temperature wet-oxide where a 1 μm SiO_2 film was grown. An HMDS adhesion layer was deposited in an oven and a 1 μm i-line resist layer was spun and soft baked. Using a mask-aligner, the micro-electrode array pattern was transferred onto the photoresist. The pattern was then developed and hard baked. Next, the wafer was submerged into a 10:1 BOH bath

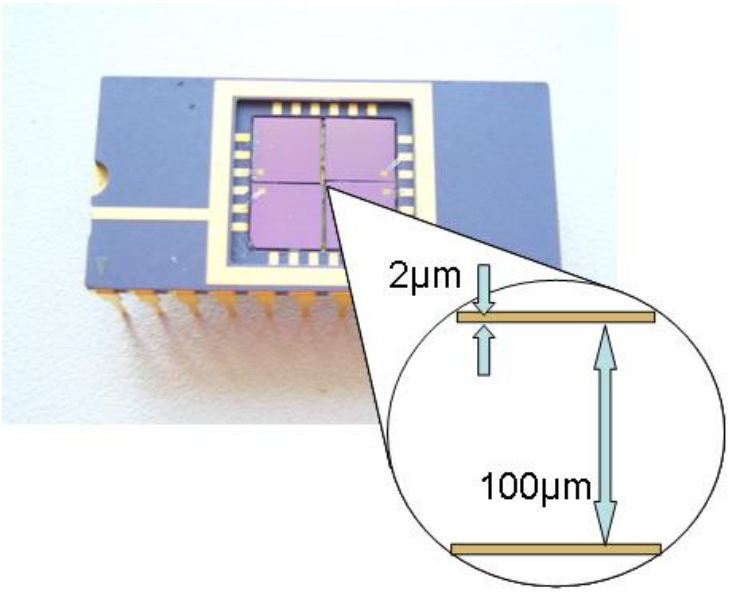

Figure 3.1: Micro-electrode array chip demonstrating the dimensions of the fabricated electrode. The design was to mitigate diffusion effects and planarize 3D cloth structures to provide a known surface area.

for 60 sec to delineate the array layer onto the SiO_2 to mitigate the protrusion and roughness of the surface due to the metal electrode. Subsequently, an Au thin film of 50 nm in thickness was deposited at a rate of 2nm/s using thermal evaporation. Lastly, the wafers were left in acetone overnight for lift-off and diced into 50 mm^2 chips.

The chips were then wire bonded into a chip carrier to insert into a breadboard. Wire bonds were passivated with silicone and the fuel cell assembly was attached to the exposed area. The electrochemical cell consisted of a two chamber flow-through configuration as shown in Fig. 3.3. The anodic chamber housed the bacteria in a 350 μL volume. The cathode consisted of a coiled gold wire with 100 mm^2 surface area immersed in 200 μL of catholyte. The two chambers were separated by a 50 mm^2 Nafion 212 membrane 50 μm in thickness. Additionally, a reference Ag/AgCl electrode was incorporated into the anolyte. Because anodic catalysis is of primary interest to this study, the cathodic reaction losses were mitigated by using potassium ferricyanide ($K_3[Fe(CN)_6]$) as an electron sink. The ferricyanide reduction to ferrocyanide has a midpoint redox of +0.36 V (vs. SHE) and proceeds as follows,

$$[\ Fe(CN)_6]^{3-} + e^- \leftrightarrow [Fe(CN)_6]^{4-} \tag{3.2}$$

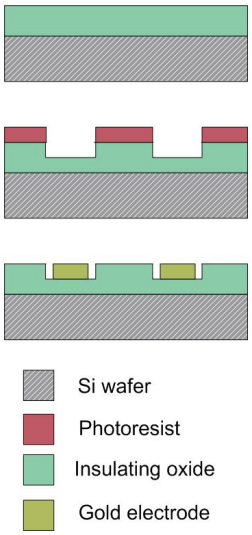

Figure 3.2: Electrode fabrication process. The process begins with a silicon wafer with insulating oxide on top. Photoresist is applied and patterned to define the electrodes with a lift off process.

where $1e^-$ is transferred in the reaction. The catholyte solution consisted of a 50 mM solution of potassium ferricyanide buffered at 7 pH, which was replenished with a fresh solution every 12 hours throughout the experiment.

3.3 Results, Analysis, and Discussion

In contrast to our previous work, this system does not require an electron mediator. The *Geobacter sulfurreducens* electrochemical cell generates electrical power by harnessing electrons from the bacterial metabolic breakdown of acetate. The bacteria retrieve energy from the fuel for biological maintenance functions or cell division, then release electrons as metabolic waste to be collected by an electrode as useful electrical energy. The mechanism is analogous to a standard fuel cell but *Geobacter* acts as the catalyst and acetate as the fuel, while the "organic nanowires" act as interfaces to the inorganic electrode, eliminating the need for an electron mediator.

In this section, all the results of the mm^2 arrayed electrode are presented and analyzed. Specifically, biofilm-level bacterial growth on the electrode is depicted through fluorescence microcopy. Through scanning electron microscopy, cells on the insulating oxide (off-electrode) and "protein nanowires" or electrical conduits were captured. In regards to electrical performance, polarization and power density curves that depict the steady state

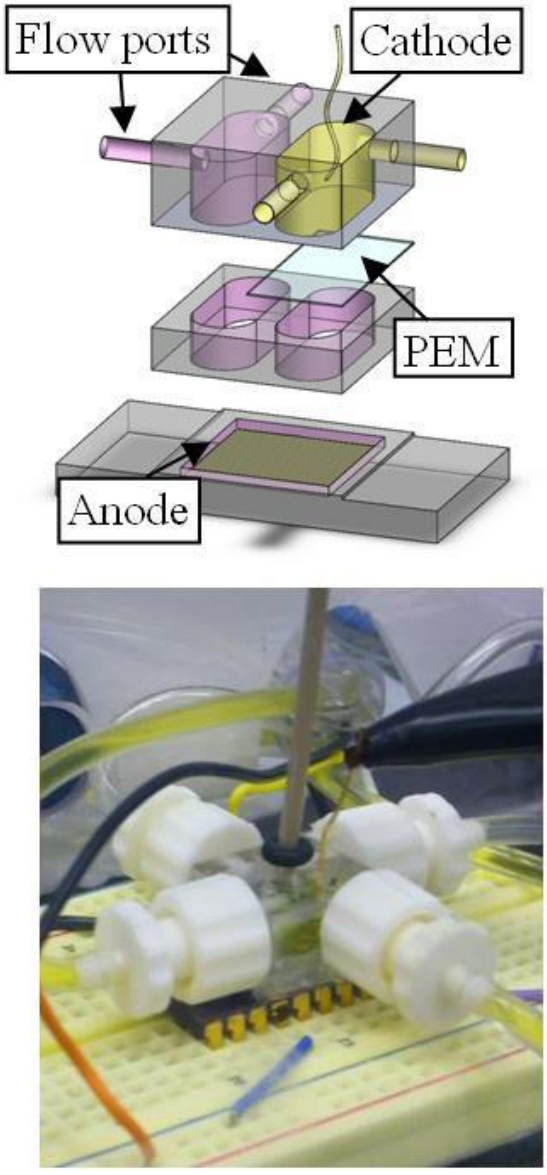

Figure 3.3: (a) Exploded view of the MEMS MFC. Anolyte and catholyte circulate through corresponding chambers separated by a Nafion membrane. (b) Fuel cell experimental setup using potassium ferricyanide as electron sink at cathode.

performance of the fuel cell were acquired over a 10 day biofilm growth period. The transient curves from the polarization experiment are then analyzed for capacitance and resistance over time.

3.3.1 Microscopy

Understanding the cell population on the electrode is a key advantage of micro-electrochemistry. As the electrical signal is intrinsically related to the biocatalyst loading, capturing information on the quantity of bacteria at the time that the electrical measurements are taken would provide additional information that could yield to more robust system-to-system comparisons. Hence both fluorescent and scanning electron micrographs were obtained throughout the experiments.

Biofilm-level Fluorescence

Figure 3.4 depicts the development of the bacterial biofilm over a 10 day period when cells are forced to respire on the electrode. The systems were initially inoculated with 350 μL of fully grown cells (originally 10^9 cells/mL), and the suspension was allowed to subsequently rest for 6 hours prior to injecting a solution of anaerobic media and 10 mM acetate. The electrical circuit was connected upon inoculation, and the anode was poised to the potential of the cathode (+0.3 to +0.5 V vs. SHE). The sequence shown is actually that of four distinct anodes, since the fluorescence staining technique used is destructive. Nevertheless, the sequence illustrates the biomass increase and biofilm growth pattern on the electrode. The live/dead stain consisted of SYTO BC (viable/green) and propidium iodide (dead/red).

Figure 3.4a shows the results one day after inoculation. At this time, no biofilm was observed. Cells in the form of a monodisperse monolayer appear to have settled on the surface. The density of cells on the electrode surface depends on the seeding density, and it increases with time as cells grow and divide. The electrode did not appear to preferentially draw cells to the gold metal as a significant population was found on the insulating oxide. During the first 24 hour incubation period, the bacteria may have completed 1-3 division cycles [48].

Figure 3.4b shows the growth results 3 days after the inoculation of cells. It was observed that *G. sulfurreducens* were nucleating and forming vertically elongated "clusters" at various locations on the metal. The biofilm clusters were not of equivalent height or volume but were distinguishable and prominently growing from a single connection point on the electrode. In general, the metal coverage was roughly 30% monolayer, 5% in clusters, and 65% of the electrode showed no biomass after 3 days.

Figure 3.4c depicts the biofilm after 6 days with continuous electron externalization. The characteristics were similar to the biofilm after 3 days of operation. However, as the cluster

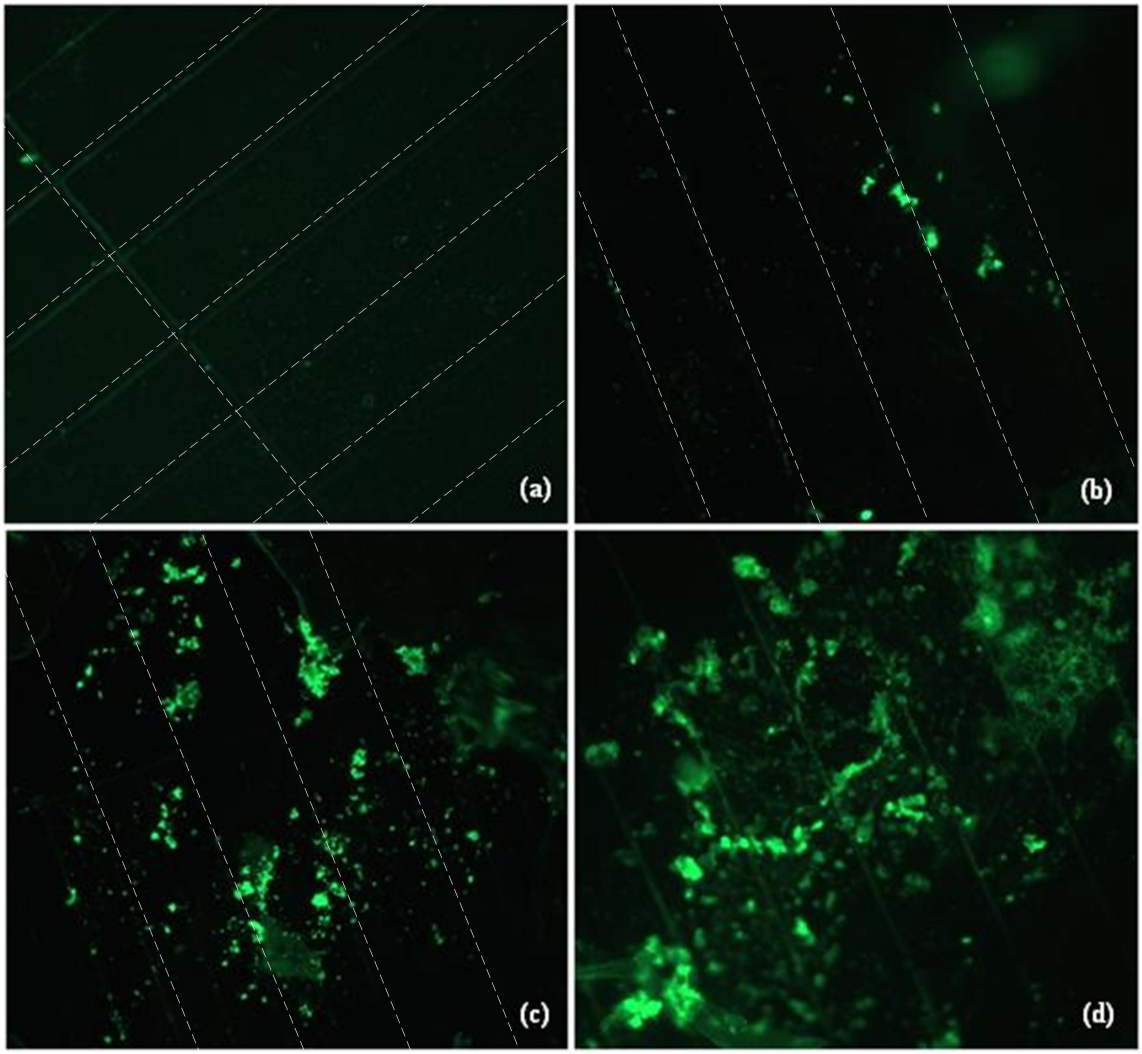

Figure 3.4: Live/dead representative fluorescence images of the biofilm as it develops over time. Images were acquired at (a) 1 day, (b) 3 days, (c) 6 days, and (d) 10 days after inoculation. The bacteria nucleate on metal electrode to grow vertical elongated clusters that overtime merge onto a continuous biofilm. Anode was continuously accepting electrons, and negligible non-viable cells were captured during the 10 day experiment. Dashed lines indicate gold electrode location.

density increased on the electrode, they appeared to join and engulf the insulating areas. The metal coverage is estimated at 70% in clusters, 20% monolayer, and 10% free of biomass. However, 20% of the insulating surface was also covered by a monolayer of cells, and the length of the clusters appeared to have reached 20-30 μm at this stage.

Figure 3.4d illustrates the biofilm growth after 10 days of fuel cell operation. At this point, the clusters have merged into a continuous biofilm and the overall cell density increased. Although there is greater coverage of the oxide, the biofilm is of uneven and thinner in this area of about 5-10 μm in thickness. The biofilms were estimated at 80% and 70% on the metal and insulating oxide, respectively.

Cell-level Scanning Electron Micrographs

In addition to performance, the viability of the bacterial catalysts during extracellular respiration is also of interest. SEM images in Fig. 3.5a illustrate bacterial growth patterns on gold electrodes and on insulating oxide. After six-days of respiration in the anodic chamber, bacteria populated more densely on the electrode area as the conductive surface probably facilitated the release of electrons from charged enzymes used in metabolism to promote the respiration process. Figure 3.5b shows that some cell division process was occurring on the insulating surface. Figure 3.5c depicts the intricate rooting of bacteria on an electrode. Bacteria grow multiple appendages that form interconnects to the electrode and other bacteria [36].

Implications

As these images suggest, *G. sulfurreducens* is able to survive and divide on microfabricated surfaces of gold and SiO_2. These microorganisms adapt well to the stress of being connected to an electrode for respiration and divide to develop a biofilm as long as nutrients (anaerobic media and acetate) are added to the anodic chamber. Although not shown, the limit to a fully developed biofilm appears to be around 40 μm in thickness [25]. The current hypothesis speculates that this occurs because electrons from microorganisms away from the electrode are unable to sufficiently "respire" on the electrode, or unable to remove waste electrons. This is the inverse of what limits the growth of a biofilm for non-electro-active species as microorganisms near the top of the biofilm thrive while those near the surface starve from insufficient nutrient diffusion. However, this phenomenon was not observed during this experiment as images were acquired over a 10 day period.

The electron microscopy images illustrate that significant solids, presumably biologically derived, were deposited on the gold electrodes during biofilm development using wild-type *Geobacter* as shown in Fig. 3.5c. The reason for the deposits is uncertain but they could have been acting as a passivation layer for the microorganisms to modify the system demands to

their own. If biologically derived, the solids matrix is a significant energy and mass sink that is unutilized for electricity. This effect has been addressed through evolutionary techniques as Lovley et al. has reported a microorganism derived from *Geobacter* to produce significantly less biomass and hence greater Coulombic efficiency [49].

3.3.2 Electrical Characteristics

The bacteria can produce a high potential upon inoculation of the anode due to reduced nature of the microorganisms. Fig. 3.6 depicts the most negative potential that was obtained upon inoculation of the cells at -0.25 V (vs. SHE), which is similar to results of previous studies that measured the cells' redox potential at -0.19 V (vs. SHE) [47]. However, in this case the cells were incubated in a test tube for two weeks prior to inoculation. If cells were harvested from the test tube culture within exponential growth as it is recommended, however, the anodic voltage typically reached roughly +0.25 V (vs. SHE) (not shown), or that of the midpoint redox of c-type cytochromes. Hence, anodic voltages can range between -0.25 to +0.25 V (vs. SHE) depending on the "bacteria's charge state" prior to measurement.

Next, after an initial "discharging" of the bacteria, the anodic redox reduces to +0.3 V to produce a V_{oc} of 100 mV against the potassium ferricyanide catholyte solution but increases over time as is illustrated by the polarization results shown in Fig. 3.7. After 10 days of respiration on the anode, V_{oc} values ranged from 550-600 mV and maintained a low standard deviation (roughly 1 mV) over 10 minute intervals.

Figure 3.7 shows the MFC polarization over time as the bacteria colonize the electrode surface. With increasing time and cell count on the electrode, the overpotential or connectivity losses are mitigated, and the open circuit voltage and current density increase. The maximum current obtained after 10 days of continuous operation, using acetate as nutrient and potassium ferricyanide as the catholyte, was 1.4 μA/1 mm^2. Figure 3.8 depicts the power obtained as a function of current after ten days of bacterial respiration. In this case, a maximum power of 0.12 μW/mm^2 occurs at 0.61 μA. By comparison, state-of-the-art hydrogen fuel cells are able to provide 10 mA/mm^2 at 0.7 V, or five-orders-of-magnitude greater power densities. Likewise, methanol fuel cells today provide in the 100 μW/mm^2 range or 1000 times greater power densities.

Figure 3.9 shows the micro-electrode temporal response to changing loads. This example was recorded 6 days after inoculation of the bacteria at a point where V_{oc} is roughly +0.2 V, and the polarization and power density derived from this data is depicted in Figs 3.7 and 3.8 as "Day 6". In each case, 90% of the V_{oc} was regained within minutes after removal of the load. The loads ranged from 1 MΩ to 940 Ω and provided a change in cell voltage, which was subsequently utilized to estimate the current transfer between electrodes. The cathodic curve illustrates the fast kinetics from the catholyte (ferricyanide) as its redox potential changed minimally throughout the experiment. It can also be observed that by the 5 kΩ load, the

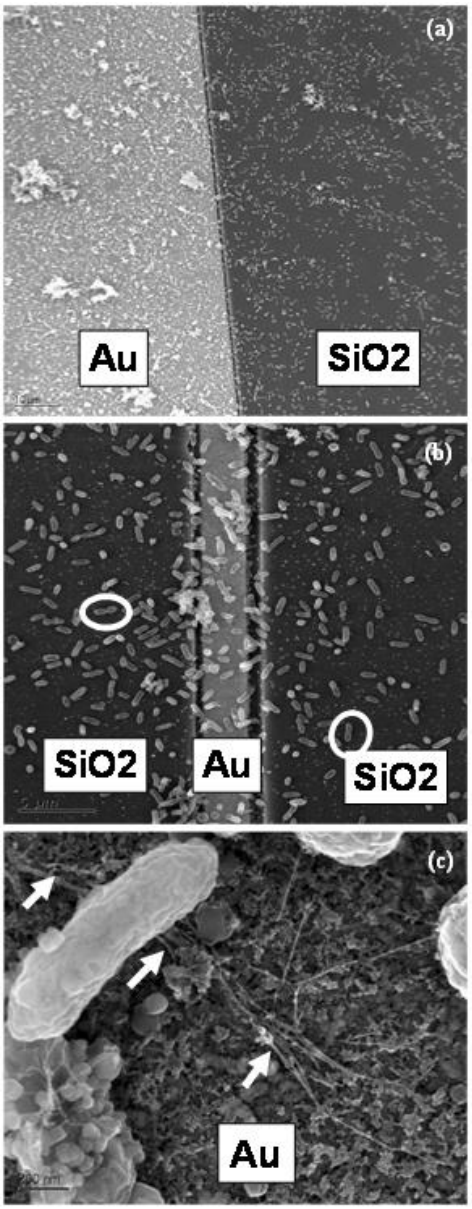

Figure 3.5: SEM images after 6-days of operation showing (a) greater growth of cells on gold electrode that insulating surface, (b) white circles illustrating cell division occurring on SiO_2 (oxide), and (c) bacteria illustrating significant appendages protruding into electrodes. Bacteria are roughly 300 nm in diameter and 2 μm long.

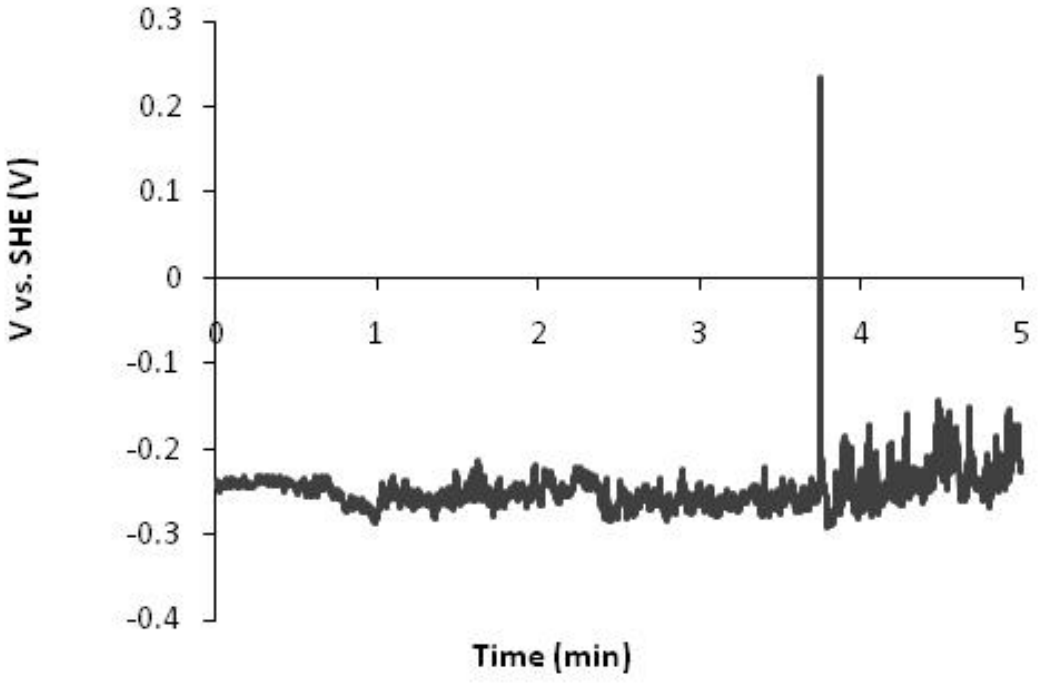

Figure 3.6: Anodic open circuit showing anodic potential of cells when harvested at a charged state. Cells manifested a -0.25 V (vs. SHE) when incubated in anaerobic conditions for two weeks prior to inoculation. When cells are harvested during exponential growth phase, however, anodic voltage typically ranges between +0.2 to +0.3 V (vs. SHE).

voltage difference between the electrodes drops to zero, or has short circuited, indicating that the anode has essentially been poised to the redox of the catholyte. Lastly, this transient behavior of voltage perturbations can be utilized to provide information on the state of the system by estimation of the RC constants, as will be explained in the following section.

3.3.3 Transient Electrical Behavior - RC Analysis

The previous section discussed the behavior of the system once it stabilizes. However, a great deal of information can also be gathered from the system's transient responses. Prior to the development of impedance spectroscopy, the RC characteristics of the system were extracted instead. The technique consists of perturbing the voltage potential via a poised electrode or by changing the load across the system and analyzing the transient current response. The analysis provides the resistance, R, capacitance, C, and RC constant, the last

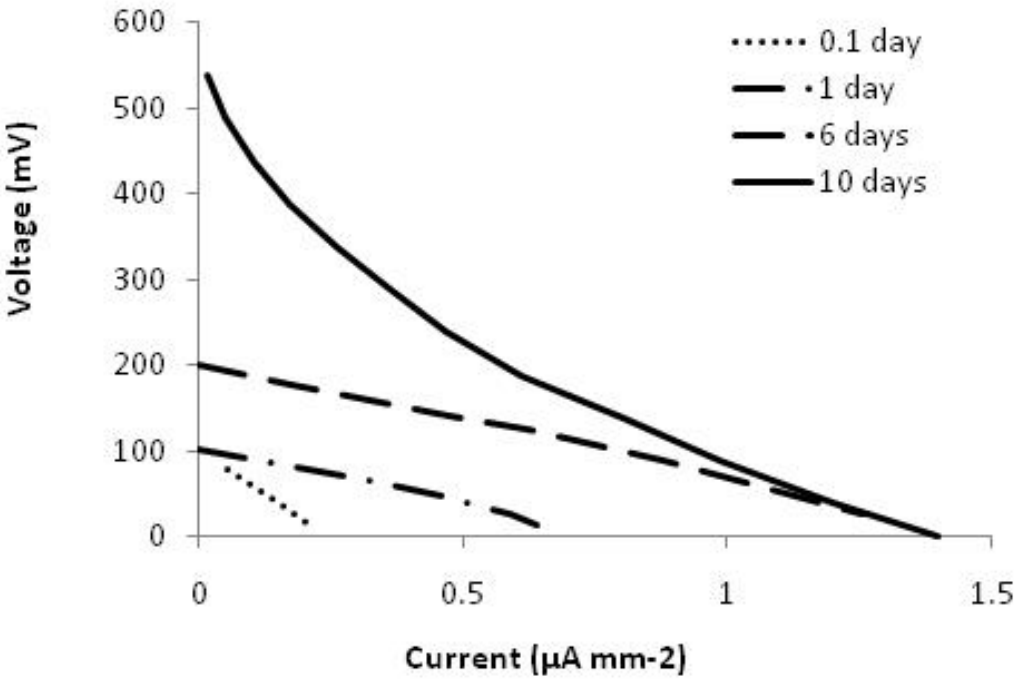

Figure 3.7: Polarization curves after 0.1, 1, 6, and 10 days, respectively, from the micropatterned microbial fuel cell. Note that $V_{oc,max}$ is roughly 630 mV with potassium ferricyanide.

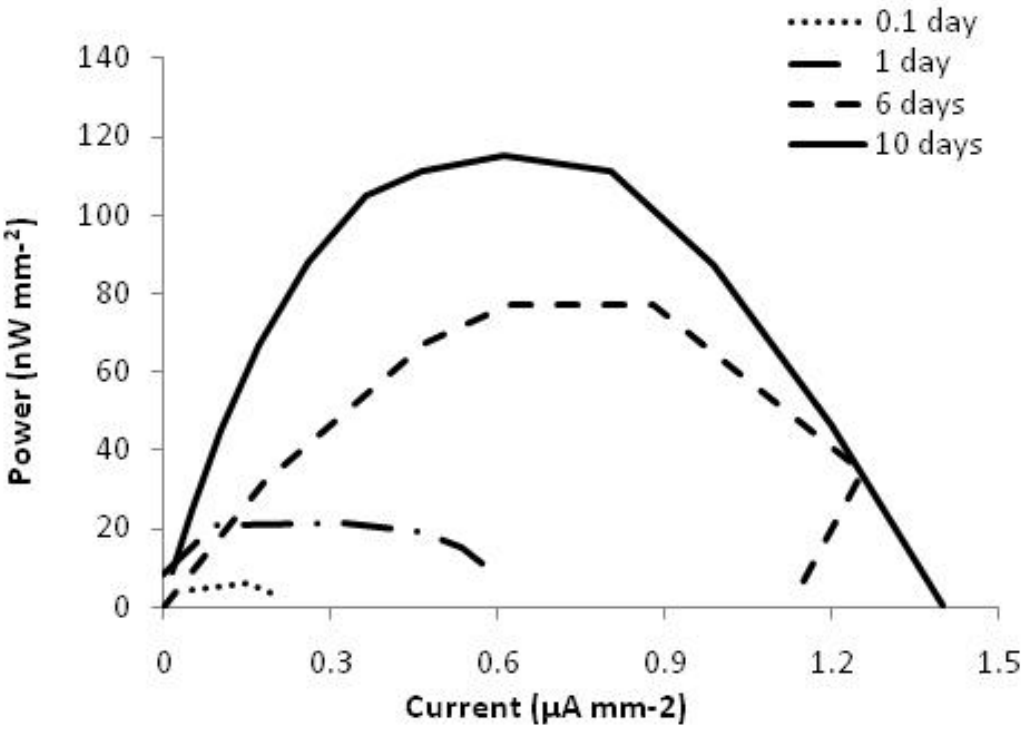

Figure 3.8: Power densities obtained at various loads during ten days of continuous bacterial respiration and growth on the electrode.

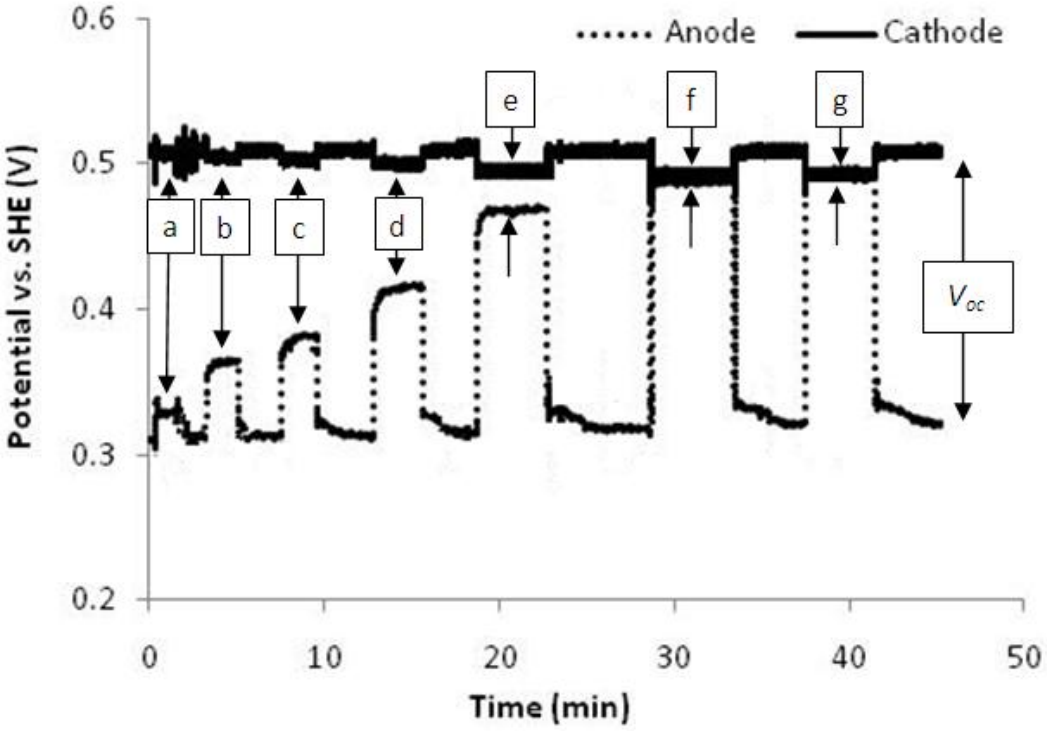

Figure 3.9: Microbial fuel cell electrical responses to different load resistors acquired from a fuel cell six days after inoculation that provided a V_{oc} (V_c - V_a) of +0.2 V, where the synthesized data is shown in Figs 3.7 and 3.8. Anodic and cathodic redox potentials for various loads were acquired against an Ag/AgCl reference electrode and are shown corrected to the SHE scale. The corresponding loads were (a) 1 MΩ, (b) 300 kΩ, (c) 200 kΩ, (d) 100 kΩ, (e) 22 kΩ, (f) 5 kΩ, (g) 940 Ω, and V_{oc} of 10^8 Ω (internal resistance of the DAQ utilized).

of which is defined as the time it takes the system to reach 36.8% (1/e) of the steady state signal.

Although the RC analysis is an elemental technique in electrical engineering, it is not one that has been applied to microbial fuel cells. However, this is surprising as it provides 2 fundamental parameters that could aid in the determination of the "state" (ie. biocatalyst loading, bacteria's level of adaptation, etc) of the system. First, the capacitance is bound to have a relationship with biomass, and, secondly, resistance must be related to the electron transfer paths (biofilm). As MFC output is highly dependent on these characteristics, such a non-invasive technique would prove to be very useful diagnostic tool.

Extraction of RC characteristics

Figure 3.9 illustrates that upon a perturbation in the load, the system responds by exponentially decaying a signal into a steady state response. Assuming an ideal voltage source and resistor, the Ohm's law can be extended to explain the relationship through the following

$$I(t) = \frac{\Delta V}{R} exp \frac{-t}{RC} \tag{3.3}$$

As illustrated by Fig. 3.10, which displays the converted response of Fig. 3.9d into current (100 kΩ response), the voltage potential disturbance across the electrodes causes the electric double layer (capacitance) to restructure and provides a sharp but decaying current peak. The data can subsequently be analyzed through a simple logarithmic manipulation to extract R and RC, the intercept and the slope respectively, characteristic of the system through the following equation.

$$lnI = ln\frac{\Delta V}{R} - \frac{t}{RC} \tag{3.4}$$

Figure 3.11 summarizes the results of this analysis, and the average and standard deviation of two systems' RC constants for 6 days. The abiotic system (control) resulted in an $RC = 100$ ms that provides a 100x slower response than the analytical model estimate for a millimeter-sized electrode shown in Fig. 2.9. This could be explained by the high internal impedance of the electrode due to the elongated features or imprecise assumptions in the model. However, once the microorganisms are added, the RC response changes considerably. The system's RC reaches to 16.7 sec upon inoculation, 0.5 sec after 24 hours, 10.7 sec at 3 days, and 140.5 sec at 6 days. This effect is the manifestation of slow kinetics in the system, which will be elaborated upon in the following section.

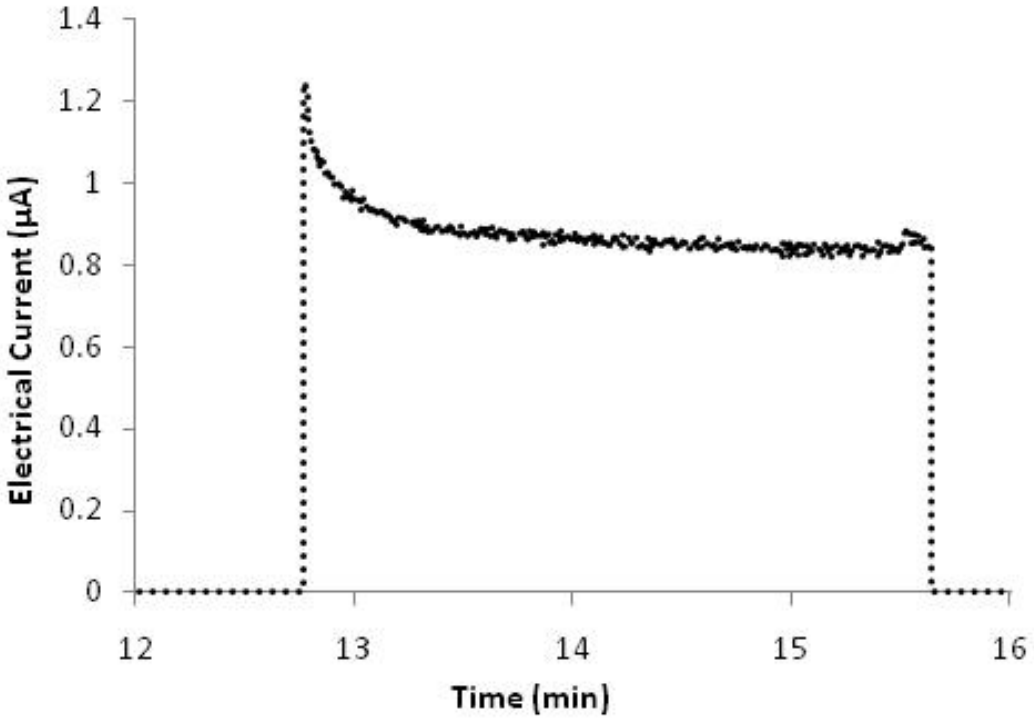

Figure 3.10: Transient electrical current obtained from 100 kΩ resistor data in Fig. 3.9d above. Behavior is analyzed to extract resistance and capacitance snapshots of the system at the time of testing.

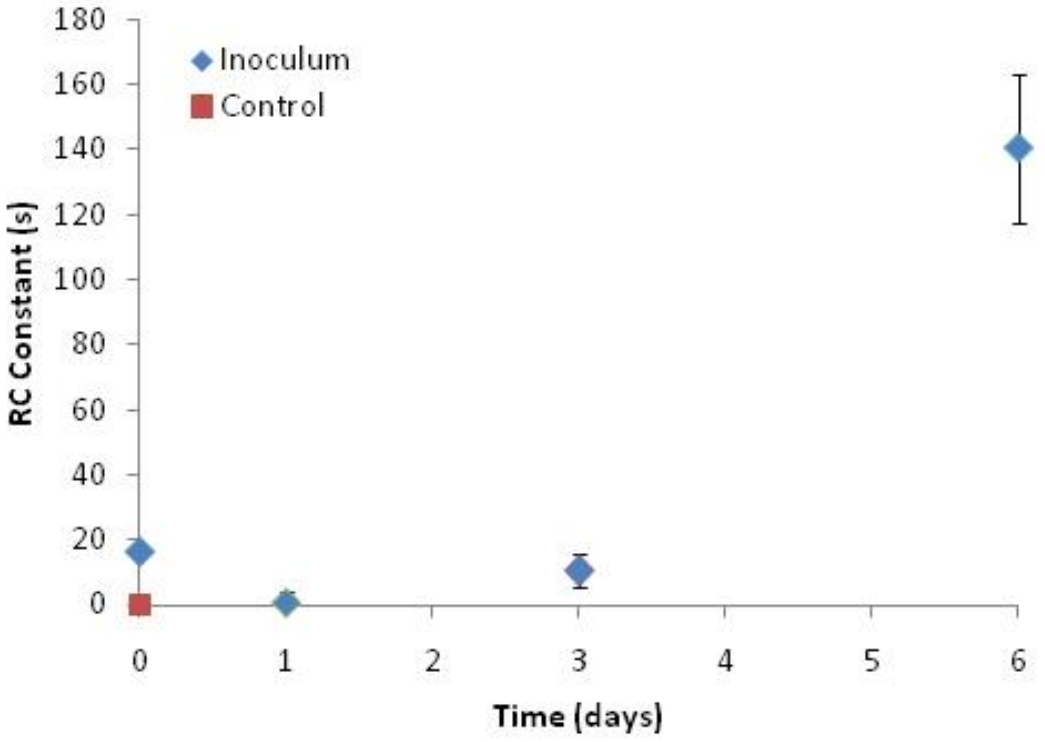

Figure 3.11: RC constants obtained for the system over time. Abiotic system's RC is estimated at 100 ms. However, addition of the cells increases the delay to steady state. The RC estimate for *G. sulfurreducens* 6 days after inoculation is 140.5 sec.

Resistance

Various research groups have proposed the idea of using impedance characterization to estimate the mammalian cell count on an electrode [50, 51]. The notion is founded on the impedance increase that occurs when cells lay on the electrode surface, as the cells effectively decrease the area that is available for faradaic reactions (electrode-electrolyte active exchanges). This behavior is also seen with cells of *G. sulfurreducens* but only briefly. As Fig. 3.12 illustrates, as compared with the resistance values of the abiotic controls (R = 3.55 MΩ/mm^2, SD = 1.22), *Geobacter* increased the system's resistance by a factor of 5.54x (R = 19.70 MΩ/mm^2, SD = 5.11) upon inoculation. However, contrary to the response using mammalian cells, the anode's resistance in the microbial fuel cells decreased over time, to 18% of the control after 6 days in our case, presumably because organisms attached and enhanced the kinetic processes. Hence, the resistance of the inert anode in the system is modified by the addition these bacteria. As is discussed next, however, the capacitance demonstrated a more distinctive and pronounced electrical behavior.

Capacitance

The capacitance of an electrode is a reversible (non-faradaic) characteristic that arises from the rearrangement of ions near its surface (less than 30 nm) due to a change in the electric field. The energy released is high power, but limited, and evident as a short-lived current peak that decays exponentially. Typically, the effect is highly dependent on true surface area, and abiotic electrodes portray an average specific capacitance of 50 μF/cm^2. However, MFCs exhibit significantly different behavior from that of abiotic systems. Specifically, the results indicate that the electrical signal is characterized by a strong damping-like effect, which is an attribute of a highly capacitive system.

The results of the abiotic control of the electrode without cells, as was expected, produced a low capacitance of 2.82 μF/cm^2. However, the average capacitance of the system quickly increased with addition of the cells by a factor of 30x upon inoculation over the control, 201x after 24 hours, and 12,823x after 6 days. Figure 3.13 depicts the 4-orders-of-magnitude capacitance increase of over the 6 day period.

As illustrated by Fig. 3.14, this capacitance followed a quadratic increase (R^2 = 0.99) over the 6 day period. Such a relationship correlates with the increase in biomass, as, during this start-up period, microorganisms duplicate through cell division to colonize the electrode surface. However, if the capacitance increase is due to biomass, it is not clear whether it would stem from the increased quantity of proteins available for redox reactions, or from the increased surface area produced by the biomass (serving as an extension of the electrode), or both. Nevertheless, bacterial time in the system is greatly affecting the capacitance of the system, and inferences can be formulated by making some assumptions.

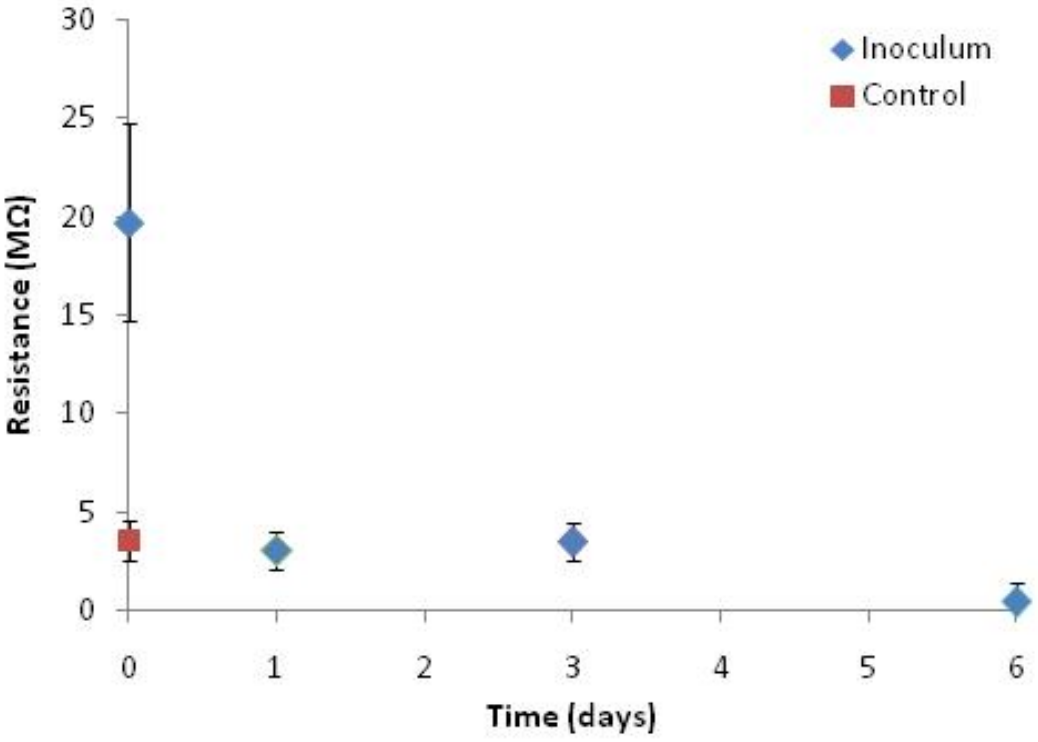

Figure 3.12: System resistance development over time. The microorganisms increase the system's resistance by 5x upon inoculation. However, the resistance decreases to 18% of the control level after 6 days suggesting that the bacteria and biofilm can enhance the catalytic process.

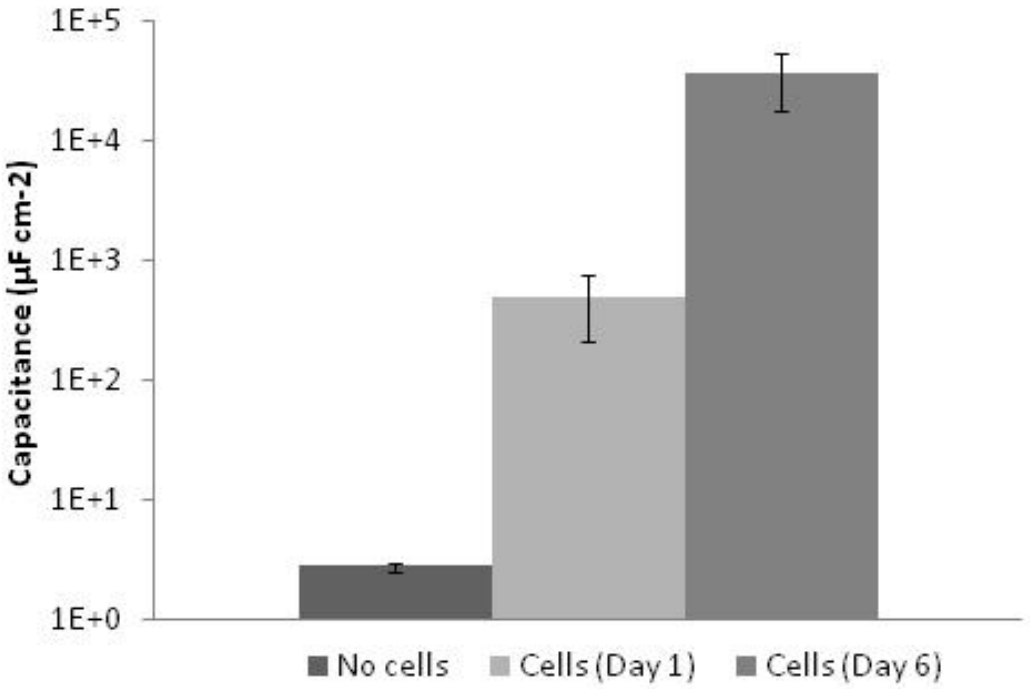

Figure 3.13: Capacitance of the system increases several orders of magnitude after the addition of the microorganisms. After 1 day, the bacteria acclimate to the electron externalization and begin attachment. After 6 days, capacitance increases by 63.5x over the day 1 value, which is the equivalent to 6 division cycles (26 = 64) and an average 20.0 hour doubling time for that period.

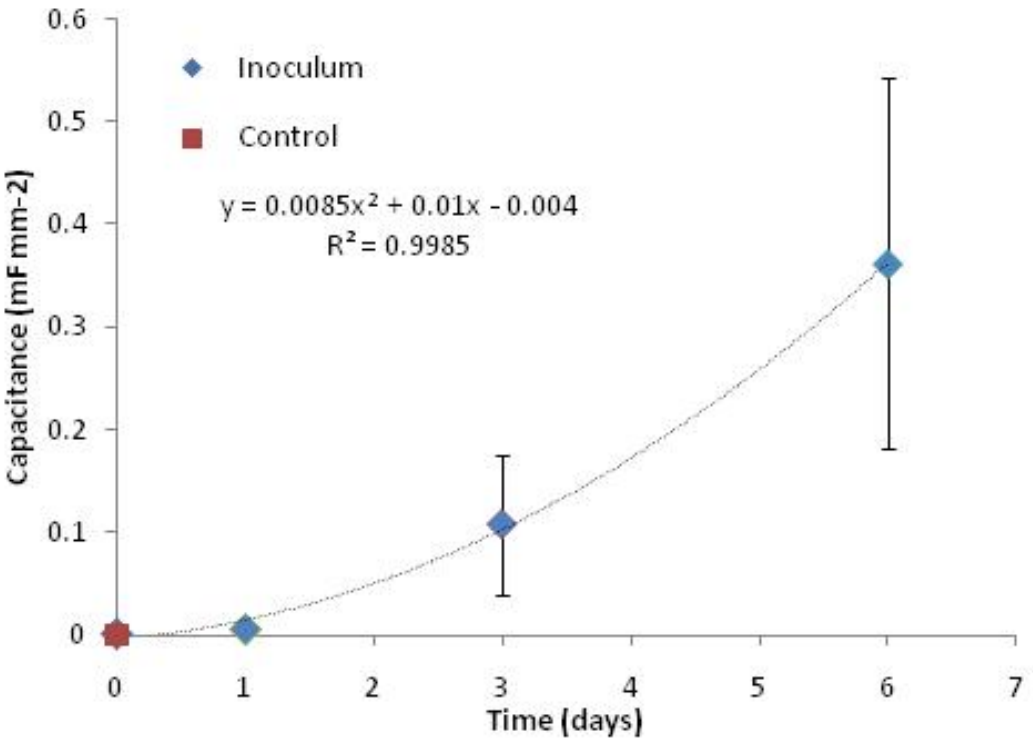

Figure 3.14: MFC capacitance is greatly affected by the addition and growth of cells on the anode. The system's average capacitance increased quadratically over 6 days and seems to correlate with biocatalyst division on the electrode.

Specifically, assuming that biomass and capacitance are proportionally related, the capacitance growth can be analyzed to estimate biomass doubling time. Table 3.1 summarizes the results. During the first interval, inoculation to Day 1, the capacitance showed 2.7 doubling cycles, which corresponds to a doubling time of 8.7 hours. For the next period consisting of the interval between Day 1 and 3, the capacitance completed 4.2 doubling cycles in 48 hours that correspond to a doubling time of 11.3 hours. Lastly, between Day 3 and 6, the capacitance doubled 1.7x in 72 hours indicating a doubling time of 41.2 hours.

These doubling times cannot be validated through the literature as no publications that discuss growth values on an electrode were found to compare. However, Esteve-N*úñ*ez and Lovley published 7.8 and 17.5 hour doubling times for *G. sulfurreducens* during exponential growth using fumarate and ferric citrate [48], respectively, suggesting that the values calculated from the capacitance could correlate with biomass increase. Provided that the culture is not under nutrient limited conditions, microorganisms are in exponential growth and adapting to the electrode during this period. Also, exponential growth, at least using

Table 3.1: Development of the system's capacitance over a 6 day period after adding *G. sulfurreducens*. With respect to the control, the anode's capacitance increased on average 30x after inoculation and 12,823x after 6 days. In addition, the capacitance is quadratic with time suggesting a relationship with cell division. Assuming that capacitance is proportional to cell count, the capacitance increase predicts an 8.7, 11.3, and 41.2 hour doubling time between the Day 0 & 1, Day 1 & 3, and the Day 3 & 6 data, respectively.

Time (days)	C_{avg} (μF/mm^2)	SD (μF/mm^2)	Doubling Cycles in Interval	Doubling Time (hrs)
No cells	0.03	0.00		
0	0.85	0.50		
1	5.68	3.35	2.7 in 24 hrs	8.7
3	107.46	68.67	4.2 in 48 hrs	11.3
6	361.23	180.15	1.7 in 36 hrs	41.2

fumarate as a soluble electron acceptor with *G. sulfurreducens*, ceases after roughly 48 hours, indicating that a doubling time decrease to 41 hours after 72 hours is plausible.

Within-System Capacitance Variability

The previous section suggested a relationship between the capacitance and the biomass increase of the system over several days. The bacteria's growth rate is showing proportionality with capacitance obtained from current interrupt experiments, and the results seem to agree with the suspended cells' empirical growth rates. However, Fig. 3.14 also illustrated that the MFCs' capacitance exhibited a considerable standard deviation. This section addresses the within-system transient behavior variability. Specifically, the results suggest that, over short time periods, the capacitance and resistance of the system are inversely related, while the RC constant is maintained, indicating that electrical spectroscopy could be utilized as a non-invasive probing technique.

To illustrate the within-system temporal RC variability, Figure 3.15 depicts the electric current from an MFC 6 days after inoculation. At this time, the anode is likely to be colonized by a bacterial biofilm 5-10 μm in thickness. Prior to testing, this system was left in open circuit conditions for 2 hours (140-142 hours), then "discharged" continuously for 2.5 hours, where the transient current characteristics were acquired at 142, 142.5, and 144 hours. The continuous decrease of the current indicates that the bacteria can discharge for over two hours before stabilizing the signal, and hence steady-state conditions are particularly difficult to establish in MFCs, even with a micro-electrode. From these curves, the resistance and capacitance were extracted as previously described.

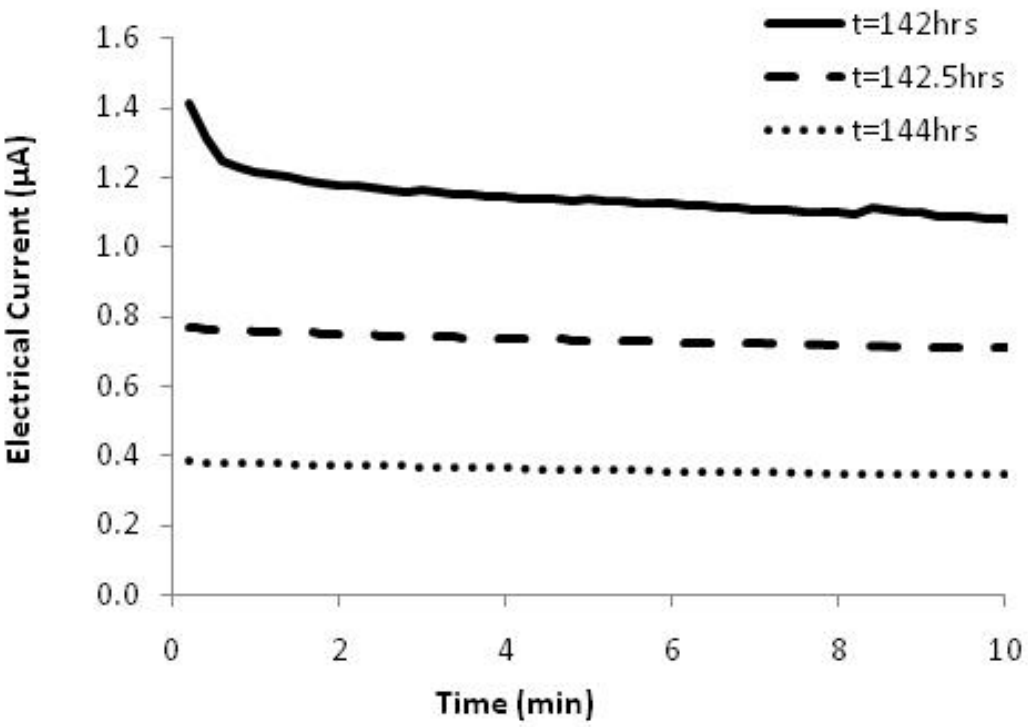

Figure 3.15: Electrical current of 10 minute intervals from a 2.5 hour period (6 days after inoculation) of continuous discharge superimposed to demonstrate output decrease over time. This behavior suggests that the system is discharging and steady state has not been reached.

Figure 3.16 shows the resulting transient RC characteristics. Within this period of continuous fuel cell operation, the resistance and capacitance of the system are inversely related. The capacitance of the anode decreases, while the resistance increases, but the RC constant remains stable. Using a material science model, the phenomenon can be explained by assuming that (1) the biofilm consists of a network of capacitive cells connected by resistive faradaic reactions (nanowires), and (2) the system is in a transient "discharging" state, where the bulk of the current signal is stemming from previously reduced proteins and not steady-state respiration. Specifically, the inversely related behavior between the capacitance and resistance is caused by the discharging of a developed but resistive biofilm. In this approach, during open circuit and prior to testing, the system is "charging" and increasing its capacitance. Upon closing of the circuit, cells that are in close proximity to the electrode provide the bulk of the current at a relatively low resistance. As time progresses and the electrons from the cells near the electrode are depleted, bacteria further away begin to be oxidized. The overall electron drainage from the biofilm decreases the system's capacitance. Meanwhile, the recruitment of cells further into the biofilm for electrons increases the perceived resistance. The trend terminates when the resistance and capacitance asymptote into a maximum and minimum value, respectively, reaching steady-state operation (not shown). Hence, the variability in capacitance within a system can be explained by understanding the "state" of the system at the time of testing, and the uncertainty mitigated by employing either the history of the system into the analysis or other more consistent parameters such as the RC constant as well.

3.4 Conclusion

In this Chapter, a micro-electrode microbial fuel cell using *Geobacter sulfurreducens* was demonstrated on a gold electrode. The system consisted of a thin array with a total surface area of 1 mm^2 that used an aqueous solution of potassium ferricyanide as a catholyte. The electrical output increased over time and provided a maximum of 1.4 $\mu A/mm^2$ and 120 nW/mm^2. Live/dead staining of anodes over time demonstrated a growing biofilm and its morphology. Although bacterial "clusters" preferentially grew on the electrode, a significant population also developed on the insulating oxide. Similarly, SEM images showed cell division on areas 10's of microns away from the electrode suggesting that a healthy metabolism occurs on non-conductive areas.

The microorganisms, undeniably, are excerpting a peculiar damping-like effect to perturbations in the signal that are manifesting as a strong capacitance that could be intimately related to biomass quantity on the electrode. However, it is unclear whether the capacitive nature is due to faradaic reactions from the "pre-charging" of metabolic proteins or from non-faradaic reactions caused by the biofilm is acting as an "extension" of the electrode. Although the presented analysis is a first level investigation of the actual system, it is still one that

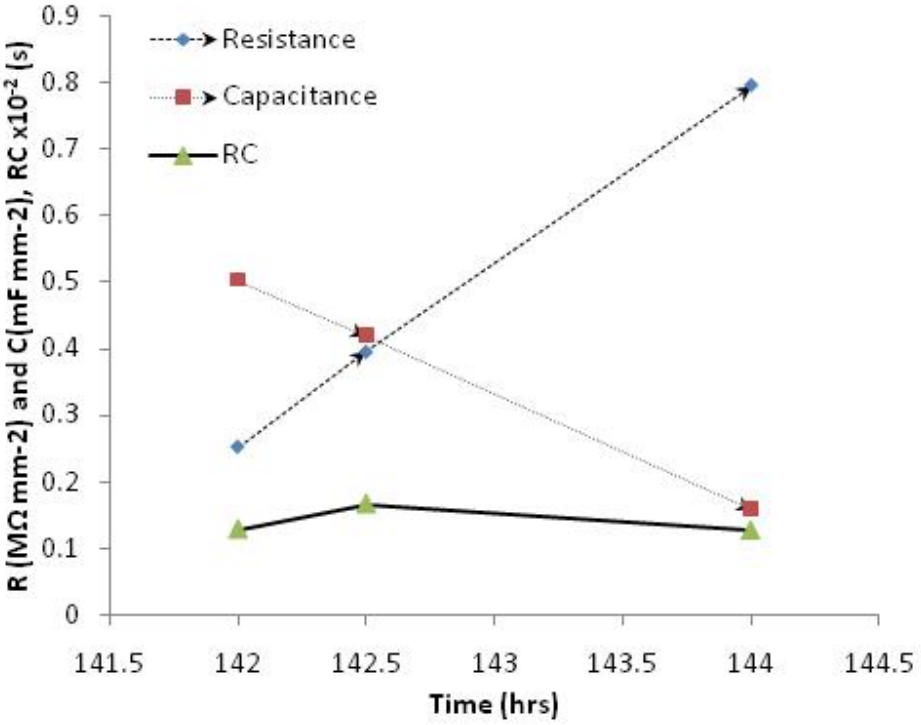

Figure 3.16: Resistance, R, capacitance, C, and RC values obtained from continuously running an electrode after 2 hours of open circuit conditions. They demonstrate the variability that stems from the "state" of the system at the time of testing and the inverse relationship between R and C. The RC constant maintains stable during discharge, however, suggesting that it could provide a more stable marker for characterization of biomass on microbial fuel cell anodes.

begins to probe into the "state" of the bacteria and biofilm through non-invasive impedance spectroscopy. This technique has been developed for mammalian cell studies to determine their quantity and location on an electrode. The notion is that cells affect the impedance characteristics of an electrode and by monitoring it, cell responses (through motility) and membrane morphology can be studied. Arguably, comprehending such transient phenomena could also illuminate important characteristics of microbial fuel cell systems that are yet to be understood, aid the development of troubleshooting tools, and potentially decrease fuel cell start-up time. Here, miniature electrodes aid the experimental time through low RC constants. However, thorough characterization of the system's capacitance with respect to biomass is still needed to determine the exact relationship and the extents of its significance.

Chapter 4

Microfluidic MFCs

4.1 Introduction

Intrinsic biocatalyst heterogeneity and architecture complexities make it difficult to optimize microbial fuel cells. Uncertainties in biocatalyst loading, their biocatalytic "state", as well as physiochemical gradients often result in complex electrical signals. This chapter aims to provide a platform that would decouple some of these effects to focus solely on the biological aspects of the biocatalysis. For this purpose, a microfluidic device with environmental controllability as well as high-resolution characterization was developed to analyze the important variables in the system and ultimately provide electrical predictability.

As was discussed in Chapter 2, a handful of small-scale microbial fuel cells have been demonstrated [17, 21, 22, 23] but none of them have focused on demystifying the heterogeneity of biocatalysis. Miniaturization provides a number of capabilities that are not available in macro-scale devices. Specifically, microfluidic systems offer real-time biocatalyst loading recognition, high-throughput and parallel experimentation, and controlled nutrient delivery. Hence, specific biocatalysis can be determined with statistical significance and at high temporal resolution. With such ability, topics such as microorganisms' kinetics (nutrient limited and redox effects) and physiological adaptations caused by electron externalization stress (gene expression) can be quantitatively determined. Understanding these characteristics also allows objective species-to-species assessments and provides a baseline for comparison for electrode surface modifications or architecture improvements.

In addition to benefiting fuel cell performance, micro-scale microbial fuel cells could also contribute to fundamental understanding of the microorganisms. Microfluidic experiments permit non-intrusive monitoring of the microorganisms' spatial behavior and fluorescent characteristics as well as the seamless inclusion of stimulating and/or sensing elements. Hence behavior due to chemotaxis, electrotaxis, and mineral interactions (phase and size) can be studied, even in tandem, to produce a synthetic micro-ecosystem on-a-chip. Similarly, the

microbes and biofilm can be electrically characterized through electrostatic and electrokinetic techniques [52]. The electrode microstructure can be micromolded to fit the microbe, or, through physical confinement, the microorganisms' and biofilms' shape and conductivity can be sculpted to fit a microreactor [53, 54]. In summary, the breath of questions and spectrum of experimental designs to answer them is endless at this scale.

Miniaturization provides the advantage of matching the scale of the device to that of the microorganisms. However, working at this scale also provides various challenges. Fundamentally, microorganism behavior may be cell density dependent and single-cell experiments, that isolate microorganisms from the inoculum, may alter the outcome of the results. This occurs because many species of bacteria use quorum sensing to coordinate their gene expression according to the local population density.

A more practical difficulty has been the bacteria placement within the microfluidic devices - as fabricating micro-structures for cell trapping or positioning has developed into a research topic in itself. Similarly, although research instrumentation has advanced tremendously, there is always concern on whether the signal that is to be measured will be detected. More specifically, the instrumentation used to acquire the signal must be sufficiently sensitive, and the phenomena studied must also provide a strong signal-to-noise ratio (SNR).

With single-cell amperiometric bioelectrochemical characterization coupled with microscopy as the capstone experiment in mind, this chapter discusses the miniaturization of a microbial fuel cell as a microfluidic platform. The system requirements are discussed first, followed by two of the several design iterations. The design, fabrication, characterization, and the results for each device are discussed.

4.2 General System Requirements

As microorganisms' physiology changes under environmental stresses, such as respiring onto an electrode, the first step in realizing the miniaturization experiments is to develop a platform that would promote the microorganisms to externalize electrons. Figure 4.1 illustrates schematic diagram for the system. In essence, the system consists of an anode, cathode, supporting electrolytes, and a junction that prevented these from mixing. However, microstructure effects or small population kinetics were of interest such that a micro- or ultra-micro-electrode had to be integrated. Lastly, the system also desired a reference electrode or redox probe that could poise the electrode at designated voltage potentials.

In addition to fuel cell components, the system had to support cell culturing requirements, where these were specific to the species. The microorganism that was utilized for these experiments was *G. sulfurreducens*, an anaerobe that has demonstrated growth in aerobic conditions for 24 hours [37]. However, *Geobacter* does not thrive in such an environment but rather prefers anaerobic settings. It thrives in conditions where acetate (vinegar) is the

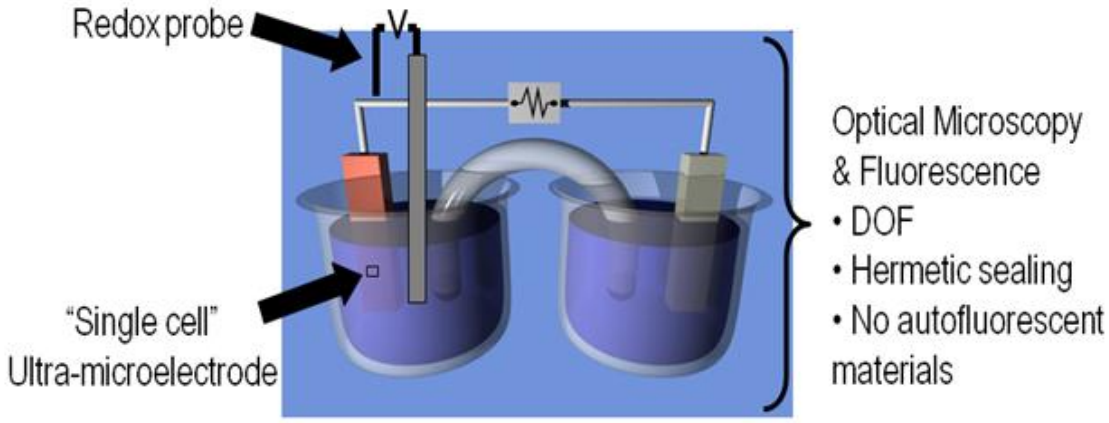

Figure 4.1: Schematic of the micro- microbial fuel cell required components. The system is based on reconfiguring a research MFC onto a microscopy compatible platform. In addition, ultra-micro-electrodes for microstructure (single-cell) metabolic studies and a redox probe have been included as key design features.

carbon and electron source and fumarate is the electron acceptor. *Geobacter* also grows in ethanol, hydrogen gas, and various other nutrients.

In addition to the microorganism preferring anaerobic environments, oxygen had to be eliminated from the system because dioxygen is also an electron acceptor that shorts the current away from the electrode. The dissolved oxygen content in fresh water under standard conditions is 9.1 mg/L or 55 μC/μL. It's particularly taxing in micro-scale systems as their surface to volume ratio (and gas diffusion) increases with decreasing size, producing great uncertainty in very low current experiments. Hence, the platform required a strategy to minimize oxygen content and diffusion into the anodic chamber.

As understanding the biocatalyst loading on the electrode required real-time visualization, the platform was designed to be microscopy compatible, including fluorescent capabilities. Hence, the system required high transmissivity in UV through the visible spectrum and the exclusion of auto-fluorescent materials. Furthermore, as high magnification was desired for single-cell visualization, the device had to conform to the working distance limitations set by the physics of the microscope's objectives. In addition to microscopy compatibility, the system also had to utilize materials that would not be toxic to the cells. The microfluidic and micro-total-analysis-systems (μTAS) fields have established a handful of widely available materials; however, these have yet to be confirmed as biocompatible with our model organism. Lastly, the system also had to provide a flow-through set-up for nutrient delivery and washing.

As was mentioned in the introduction, the fundamental sensing element in electrochem-

istry is the reference electrode. The ideal reference electrode has a stable, well-defined electrochemical potential that serves as the reference when applying a voltage to the working electrode. SCE, Ag/AgCl, $Cu/CuSO_4$ are common reference electrode chemistries for this application that are commercially available. However, the reference electrode must also provide a low impedance (less than 20kΩ) to prevent the potentiostat from becoming unstable. Because the level of sensing current would be low, as with single-cell studies, a high impedance reference electrode will cause phase shifts and excessive noise in the signal outputs. This is not an issue for macro-scale MFCs, but it becomes problematic in microfluidic cells. Specifically, the issue is that miniature systems provide minute aqueous electrical conduction paths (cross-sectional areas in μm^2), and basal media is rather resistive (σ = 5 mS/cm). Hence, the reference electrode must be within μm of the working electrode to maintain a low-impedance and the potentiostat's stability.

Many design iterations were attempted to fulfill these requirements. In this Chapter, two of the systems are presented to illustrate the challenges and contradictions, and the strategies applied to solve them. This first section presents System A: ultra-micro-electrode MFC where hundreds of cell's signal was simultaneously acquired. The later section provides System B: "single-cell" design.

4.3 System-A: Ultra-micro-electrode MFC

In a nutshell, the objective was to develop a microfluidic culturing chamber that forced the bacteria to utilize the electrode for respiration. The system was to provide controllability of the aqueous and redox environment while concurrently permitting microscopy techniques. Hence, a microbial fuel cell had to be redesigned to fit within a glass microscope configuration.

Most MFC systems consist of two electrodes suspended or embedded within two chambers that are separated by a Nafion PEM. Some designs have eliminated the polymer electrolyte junction by placing the electrodes centimeters apart [55]. Alternatively, others envisioned a laminar MFC that takes advantage of the diffusion barrier between two parallel flows as the junction (Buie, unpublished). However, none of these architectures satisfied our requirements as these would obstruct the pathway for optical microscopy, generate large ohmic resistances within the device, or require constant flow to prevent redox mixing. Consequently, the microfluidic MFC was redesigned in this chapter.

4.3.1 Device Design and Fabrication

Given that microscopy compatibility was a primary objective, the notion was to develop a system that would resemble the apparatus that were already designed for microscopes.

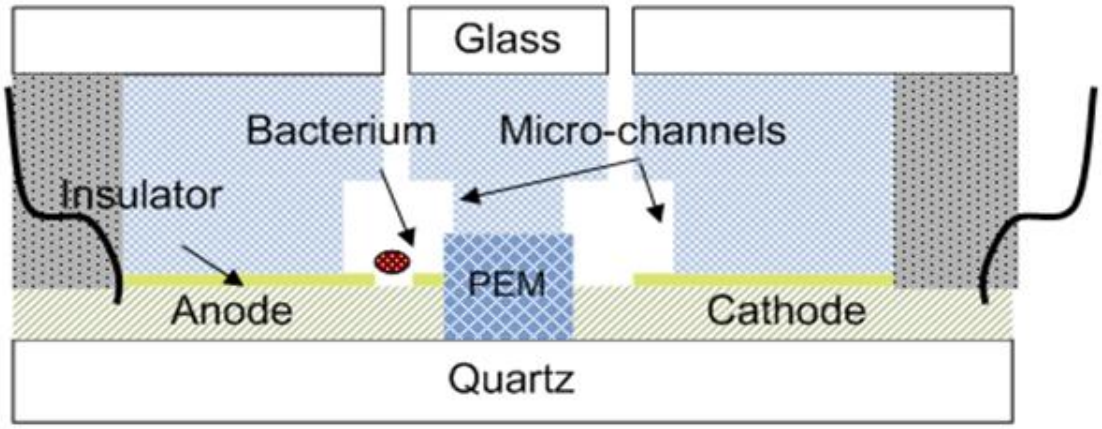

Figure 4.2: Side view schematic of the microfluidic microbial fuel cell. The system consisted of a planar configuration MFC where a single wafer was processed to define the electrodes. A subsequent SiO_2 deposition served as a passivation layer that limited the bacteria/electrode contact to small "active areas". The electrolyte junction consisted of a casted Nafion dispersion between the microchannels and electrode plane. Through a soft lithography process, PDMS was molded to form the microchannels. To mitigate oxygen diffusion, the device was capped with a glass cover.

However, to achieve micrometer scale features, these would have to be coupled with microfabrication. As microfabrication is a processing technique that operates through the addition and subtraction of thin films, these requirements lead the design towards a planar MFC configuration approach. Fig. 4.2 depicts a side-view schematic of the resulting device, and Fig. 4.3 illustrates the fabrication sequence. Taking insight from microfluidic literature, the system consisted of electrodes that were deposited onto a quartz substrate and buried within a dielectric environment, and a PDMS cover structure that provided the 3D features of the system.

The anode and cathode were made of parallel thin film electrodes that were deposited on a quartz wafer and subsequently patterned. The electrodes were indium-tin-oxide (ITO), a n-type semiconductor (band gap = 3.5 to 4.1 eV) that provides a compromise between its electronic conductivity and optical transmissivity. Generally, a 100 nm layer of ITO can provided both 100 Ω/square and 90% transmissivity (in the visible spectrum) from sputtered and annealed films. Next, to mitigate reactions on the bulk of the electrodes, a layer of silicon dioxide was deposited. The passivation layer was subsequently patterned to activate small windows for the bacteria to connect through. These active window areas could be of arbitrary size between 1 μm to 1 mm scale. In this case, windows of 10 to 100 μm were designed to have a broad range of cell densities for the prototype studied.

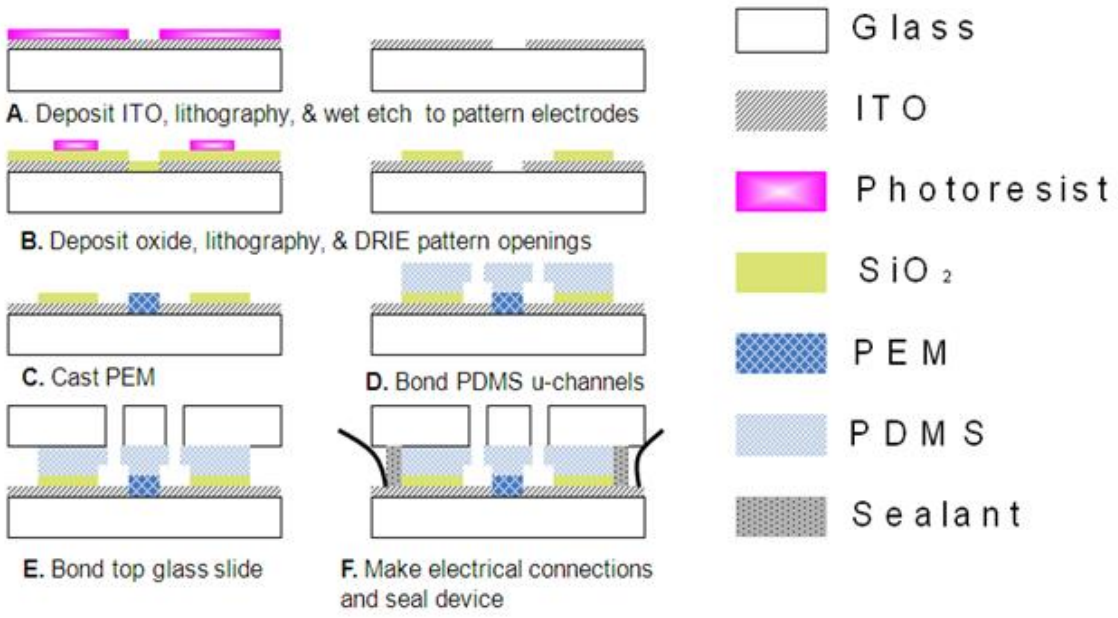

Figure 4.3: Fabrication process for the dual channeled microbial fuel cell. The sequence consisted of a) deposit and pattern ITO, b) deposit and pattern SiO_2, c) cast Nafion ionomer to create the ionic junction, d) irreversibly bond the previously defined PDMS structure with channels, e) irreversibly bond glass cover to mitigate glass diffusion, and f) connect tubing and electrical components.

Once the electrodes were fabricated, a Nafion membrane was casted from ionomer solution on the plane between the electrodes to serve as the junction [56]. To prevent redox mixing, the electrodes were separated by microchannels made of PDMS that were previously delineated through a soft lithography process. The channels were irreversibly bonded to the quartz wafer using an oxygen plasma. As PDMS is conformal, this layer "sealed" and immobilized the casted PEM in place on the processed quartz. To minimize oxygen diffusion to the channels, a second glass slide was covalently bonded to the outer surface of the PDMS to seal the device. Lastly, Upchurch Nanoports were bonded to the top glass slide and electrical connections were attached to the ITO. Appendix A provides the details of the recipes used for microfabrication and assembly.

Figure 4.4 shows an image of the assembled device. The microfluidic chip had an overall dimension of 2 cm wide by 5 cm in length. The large scale was due to the Nanoports that roughly require a centimeter footprint each. The microchannels were 1 mm wide, 200 μm in height, 30 mm long, and 2 mm apart. The PEM spanned along 8 mm between the channels, and was 2 mm wide and 200 nm in height. The catholyte consisted of 50 mM potassium ferricyanide in a 20 mM solution of PIPES buffer with the pH value at 7. The system did not contain a reference electrode. However, it was approximated by the catholyte's redox that was constantly measured and replenished. The impedance of the system with the casted Nafion membrane was measured at 300 kΩ. The resistance of each of the ITO electrodes was measured at 165 Ω using the 4-point probe method.

4.3.2 Results and Discussion: Electrical

To demonstrate the microfluidic microbial fuel cell, we utilized *Geobacter sulfurreducens* that was cultured in anaerobic media with fumarate as a final electron acceptor. The bacteria were injected into the MFC and allowed to settle for 5 hours. Then, the anodic channel was rinsed with 1 mM acetate and allowed to rest for 1 hour. All the measurements were acquired using a Gamry Reference 600 Potentiostat/Galvanostat/ZRA.

The open circuit voltage (V_{OC}) was measured upon inoculation and the initial transient signal is shown in Fig. 4.5. A V_{OC} = 630 mV, that is comparable to previous results [57], was maintained for 2 hours. The response portrays capacitor-like behavior with a characteristic RC constant of 18 sec. As compared with the micro-electrode discussed in the previous Chapter, this system is expected to demonstrate high resistance but lower capacitance (reduced area electrodes).

Figure 4.6 illustrates the current density achieved under ZRA mode six hours after the inoculation of the fuel cell. The catholyte was freshly prepared and provided a redox of +550 mV (vs. SHE) in this case. The total current output of 40 pA was obtained over the total electrode area available for direct bacterial contact.

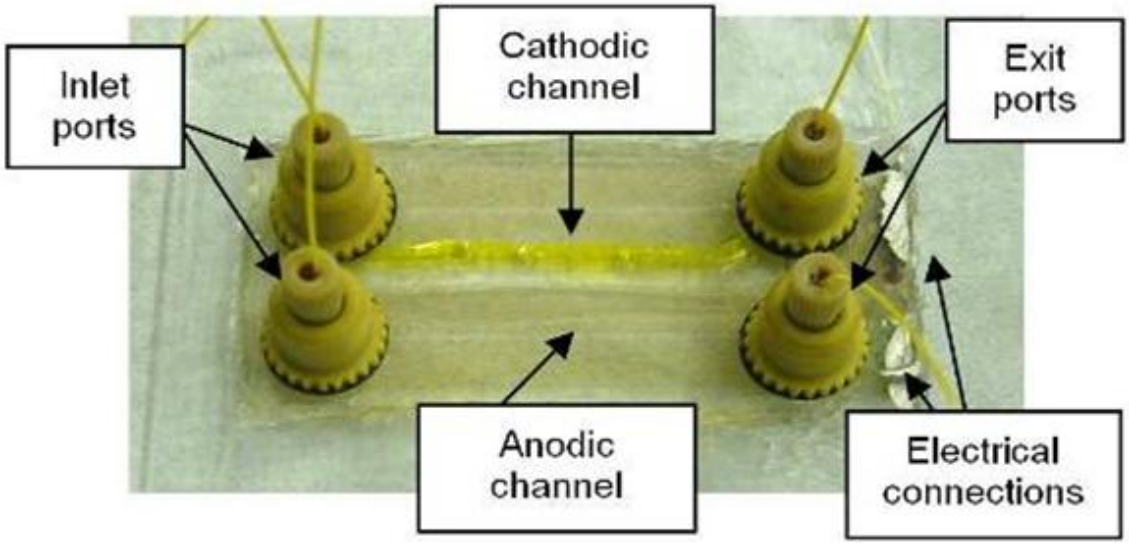

Figure 4.4: Photograph of microfluidic microbial fuel cell (first prototype). The channel geometry was defined by a PDMS structure, and the electrodes were ITO. The anode's electrically active area was defined by patterning windows through a silicon dioxide that served as a passivation layer.

Experimentally, this represents a current density of 4 nA/mm^2 or an order of magnitude lower than what was obtained upon inoculation of the gold micro-electrode. The lower current is likely to stem from the removal of the planktonic biomass during the rinsing step prior to current collection.

Normalizing to Bacterial Loading

The current density can be further normalized by the bacterial count. Fig. 4.7 depicts the anode area available and bacterial loading at the time that the current density in Fig. 4.6 was acquired. With 179 cells counted, only 1.8% of the electrode area had been populated by bacteria after 6 hours assuming a bacterium size of 2 μm x 500 nm. The low population is expected since the organism is unable to complete a cell division cycle during this time [48]. Calculation of the average metabolic rate on an electrode yields 223 fA/bacterium. This calculation, however, does not take into account the contribution to the electrical signal from bacteria on the adjacent oxide, planktonic biomass that is out of the focal plane, or other parameters that could affect the reading. Further characterization and statistical analysis is required to verify this value. However, this preliminary result demonstrates the potential of our microfluidic microbial fuel cell architecture to obtain quantitative metabolic information on a per bacterium basis.

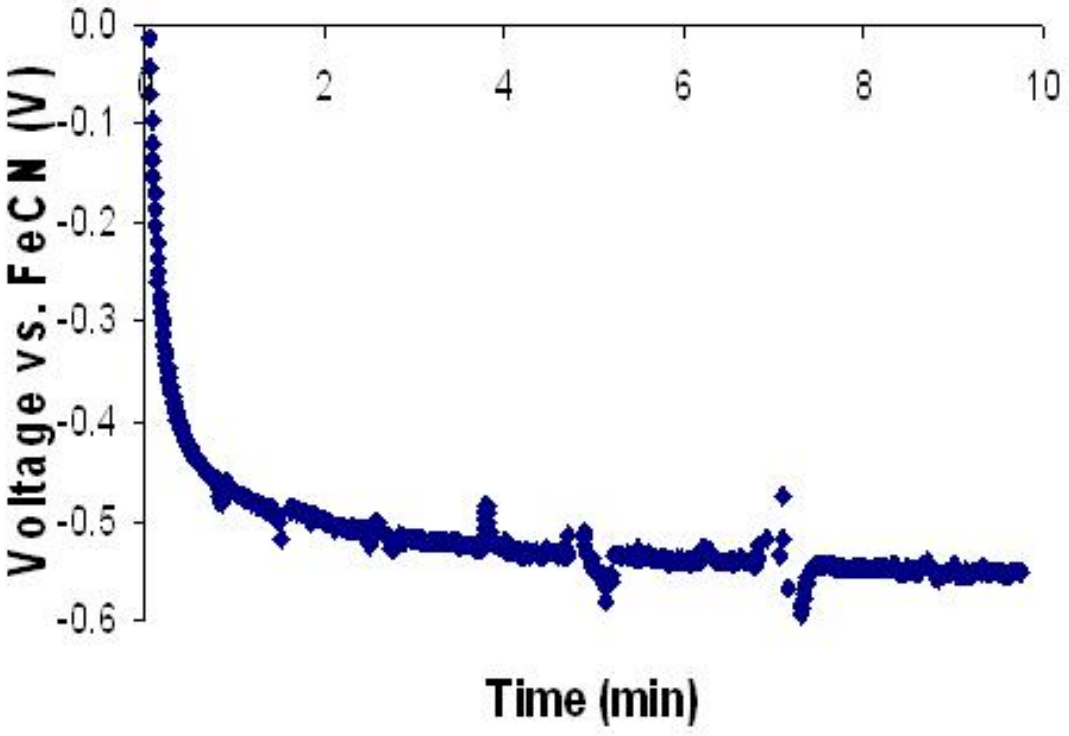

Figure 4.5: Open circuit potential obtained for the microfluidic microbial fuel cell upon inoculation of *G. sulfurreducens*. Catholyte consisted of 50 mM potassium ferricyanide in 20 mM PIPES buffer at pH 7 that provided a redox of roughly +500 mV (vs. SHE). A maximum of 600 mV was reached within 15 minutes after inoculation.

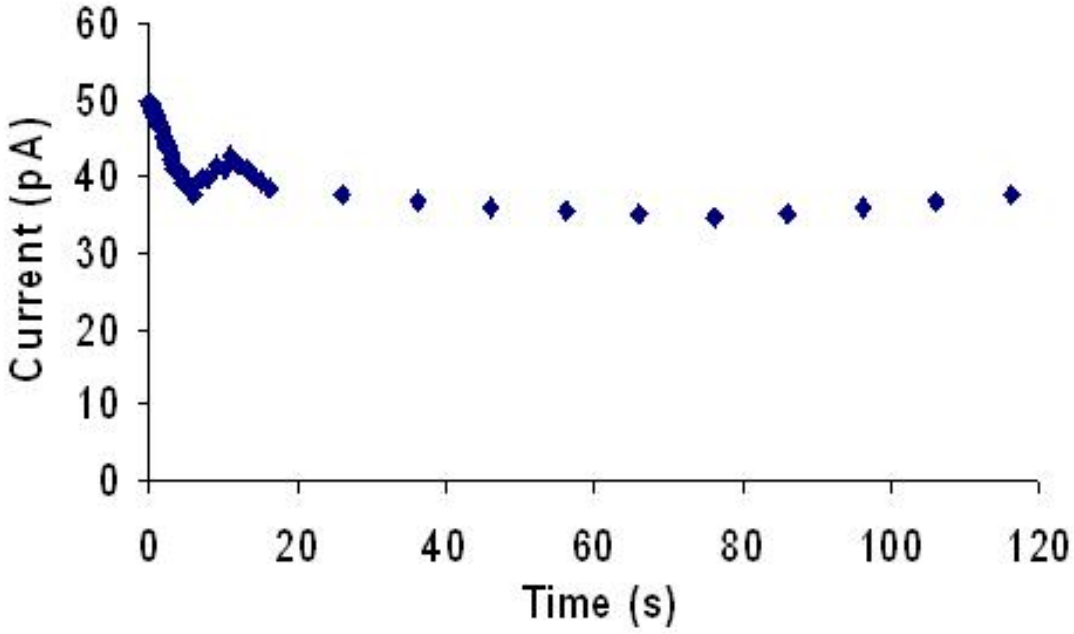

Figure 4.6: From a 100 x 100 μm electrode, a current of 40 pA (4 nA/mm^2) is obtained. This current density is 10x lower than that obtained with the gold micro-electrode upon inoculation. It is hypothesized that the rinsing step prior to current collection washed planktonic biomass which resulted in a lower current generation. Using transmitted light microscopy, 179 cells were counted resulting in 223 fA/cell upon inoculation (6 hours of settling). The signal stabilizes within 20 seconds because of the lower capacitance that stems from the reduced electrode area.

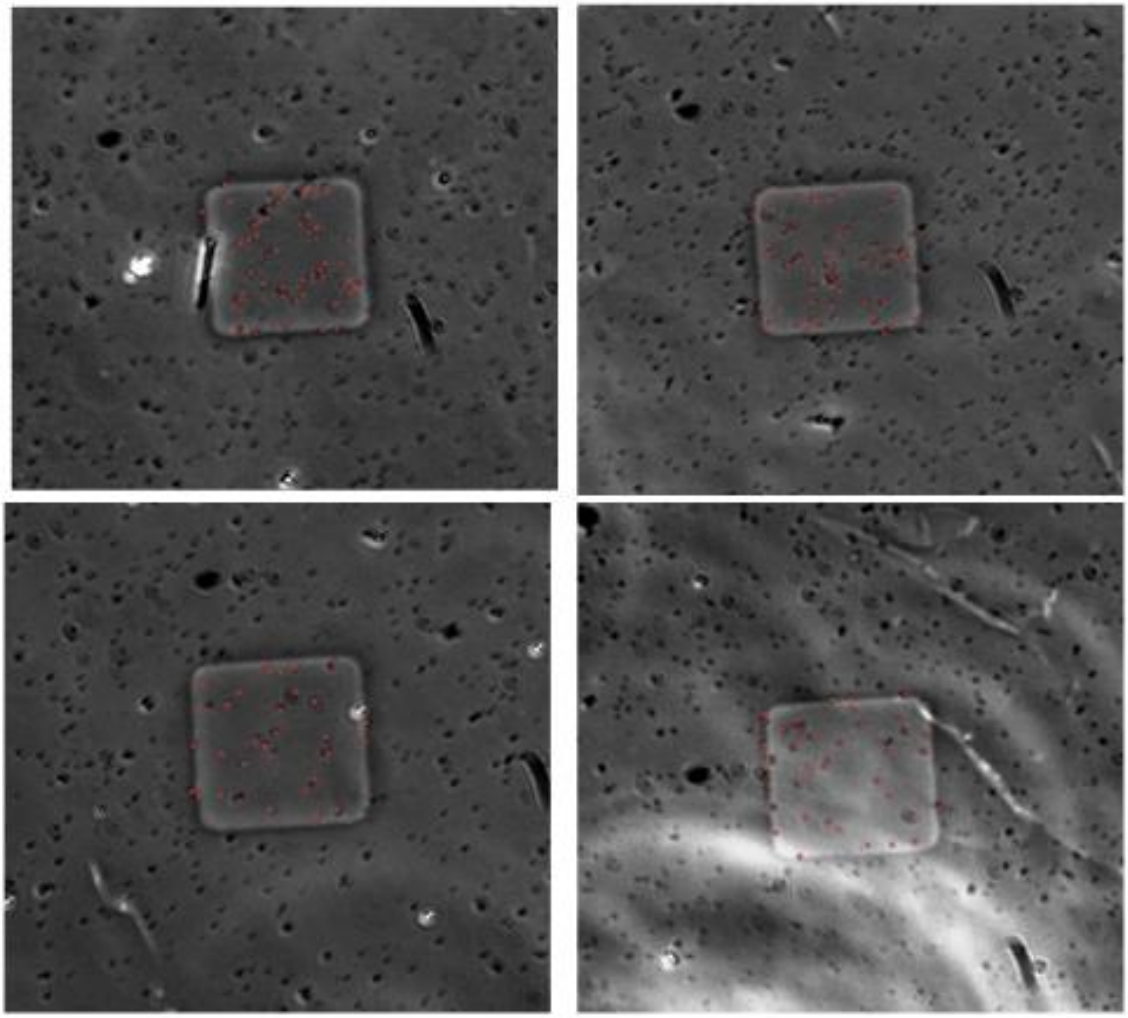

Figure 4.7: Electrode consisted of openings of 4 - 50 μm x 50 μm in area as depicted here at the time that the electrical readings were acquired. Images are phase contrast (at 30X) six hours after inoculation where only 1.8% of the area is populated with 179 cells counted. Bacteria are shown in red.

4.3.3 Results and Discussion: Intrinsic fluorescence

As was previously mentioned, normalizing the current output to a bacterial count obtained through transmitted light microscopy is likely to provide many errors. Viability of the bacteria on the active area is in question, planktonic biomass may be discharging, and bacteria off-electrode may be connected and contributing to the signal. To gain further insight on these issues, this work also involved studying the intrinsic fluorescent properties of *G. sulfurreducens*. As illustrated by Fig. 4.8, it has been demonstrated that membrane cytochromes believed to participate in the transport of electrons to the extracellular environment are fluorescent under UV excitation while in the reduced state [7]. Cytochromes are proteins with multiple metal (iron) centers that provide complex redox properties. As these proteins "shuffle" the electrons from the cytoplasm to the extracellular environment, pinpointing their redox state (ie. through fluorescence) can provide insight on aspects such as redox active areas on the membrane (polarizations), protein density, metabolic rates, and perhaps cell-to-cell electron transfer. However, there are a number of challenges. (1) The specific source of the fluorescence is unknown. It is unclear which protein(s) and where within them the effect stems from. (2) The specific involvement of the fluorescence and quenching behavior with respect to the electron externalization must be determined. Lastly, (3) the intrinsic fluorescence of a single protein is difficult to detect. In order to further develop this work, the development of the microfluidic chip also considered the ability to detect and maximize the intrinsic fluorescence signal from *Geobacter sulfurreducens* on an electrode.

The intrinsic fluorescence that had been previously observed for *Geobacter sulfurreducens* produced a bimodal distribution emission at 402 and 437 nm when excited at 350 nm [7]. Using a mercury lamp that produced a peak at 365 nm and under DAPI filtration, the images on Fig. 4.9 were obtained from bacteria that had been in the microfluidic MFC for 7 days. Although the optics were not optimized, the bacteria provided a strong intrinsic signal as the fluorescence only required 200 ms integration with minimal gain at the lowest setting from the 100 W lamp. However, the robust signal was only observed on quartz areas without the ITO or oxide thin films and after a week of incubating in the system.

A strong fluorescence signal was acquired from bacteria on unprocessed quartz. However, the fluorescence intensity around the ITO electrode was significantly weaker. Figure 4.9 illustrates the fingerprint of the bacteria near an active window area as imaged through ITO and SiO_2. To detect the fluorescence signal, the camera's single photon mode had to be used. Even at the highest lamp setting and 1 second integration, single cells were indistinguishable. The drastic change occurred because of the ITO's optical properties, as the semiconductor has high transmissivity in the visible spectrum but poorer properties in the UV. As the configuration of the microfluidic microbial fuel cell placed the thin film in line between the excitation source and the bacteria, the ITO reflected between 40-60% of the UV. Similarly, 10-20% of the emitted photons from the microorganisms (near-UV) may

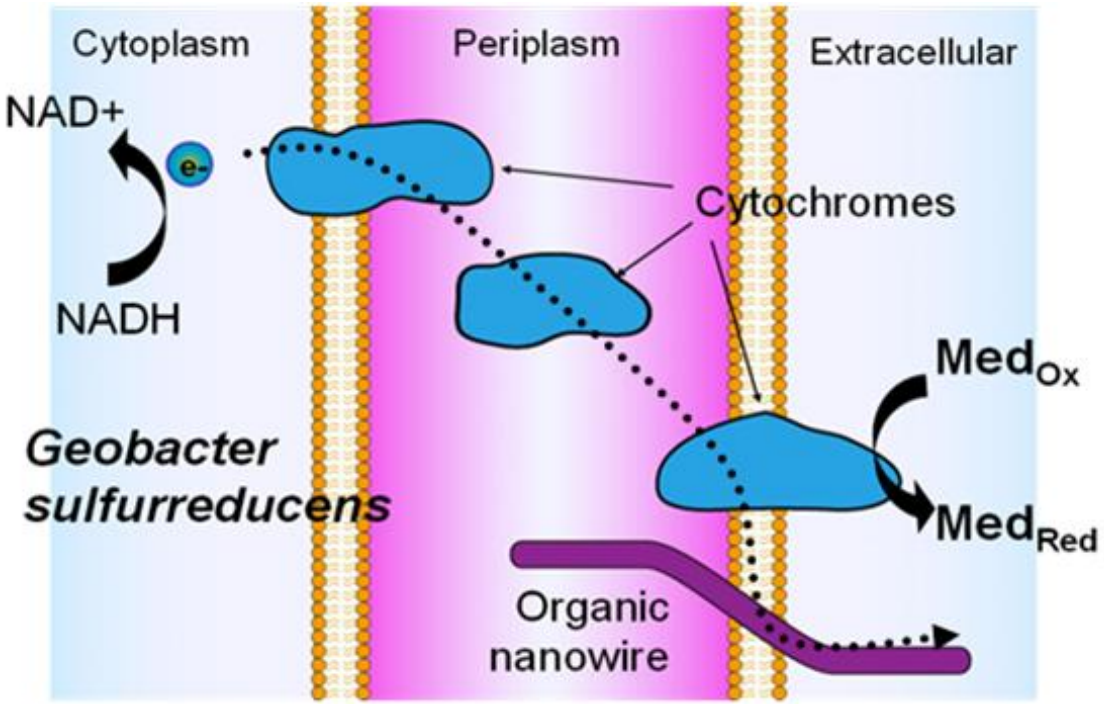

Figure 4.8: Cartoon of *G. sulfurreducens* membrane-bound cytochromes involved in electron shuffling to the extracellular environment. Cytochromes are proteins with 3-10 heme centers that provide complex redox properties. When reduced, these cytochromes have demonstrated fluorescence under UV excitation [7].

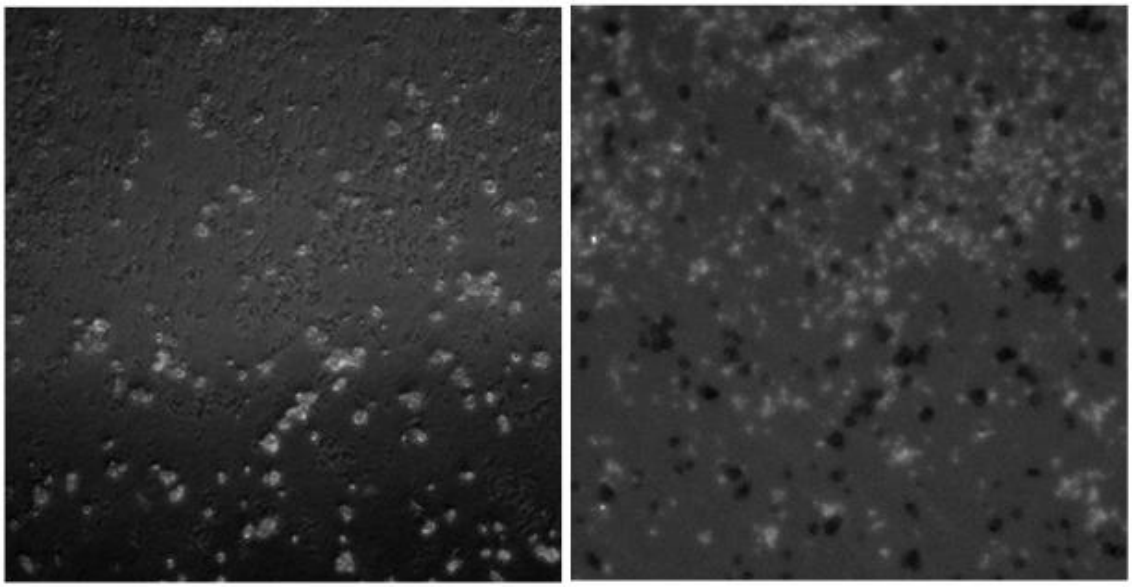

Figure 4.9: Phase contrast image of bacterial growth within a microfluidic microbial fuel cell in an area 4 mm away from the anode on quartz (left). Fluorescent fingerprint of unstained wild-type *G. sulfurreducens* under 365 nm excitation and DAPI collection (right). Images were taken 7 days after inoculation. Fluorescence suggests that bacteria are metabolizing but their contribution to the electrical signal is uncertain as they were millimeters away from the electrode. Single cells are distinguishable within the aqueous (basal media) suspension.

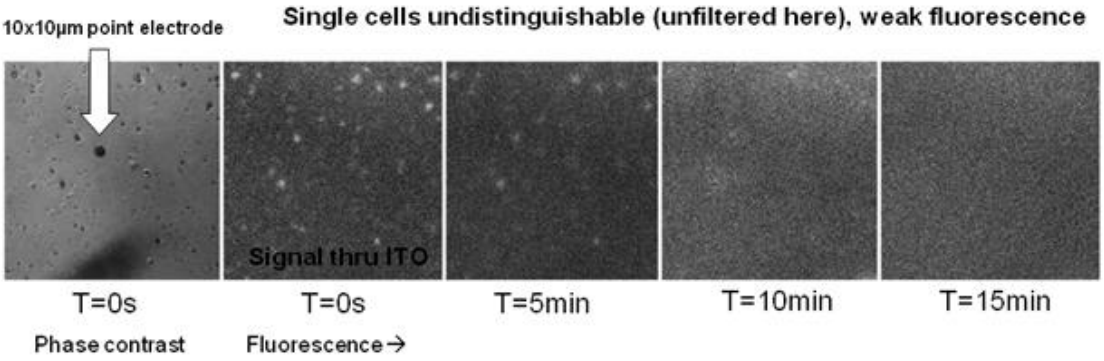

Figure 4.10: Intrinsic fluorescence results of experiment where electrons could have been quenched through electrode. The phase contrast image illustrates the r = 10 μm active area and bacterial distribution in open circuit conditions. The time sequence shows the fluorescence loss over a 15 min period. However, the even fluorescence loss suggests that photobleaching dominated over electrochemical effects.

also have been reflected on the device side away from the collector.

Nevertheless, quenching of the fluorescence through the electrode was attempted, as shown in Figure 4.10. The experiment consisted of poising the electrode to roughly +400 mV (vs. SHE) and capturing the intrinsic fluorescence quenching pattern through a r = 10 μm electrode. The phase contrast image shows the system at open circuit, and subsequent images illustrate the fluorescence dissolution over a 15 minute period of a poised potential. The system was excited at 365 nm by a 100 W mercury lamp at the highest setting and DAPI filters used for collection. However, it is very likely that the fluorescence loss observed was largely due to photobleaching, and not electron quenching through the electrode as was desired, as the signal deteriorated evenly at all radii from the electrode.

Although more experimentation is required to determine the capabilities of intrinsic fluorescence electrochemical quenching as a tool for investigating electron transport in *G. sulfurreducens*, this first device has demonstrated that a strong signal can be attained within a microfluidic device in basal media. However, the system as designed in this iteration was not going to provide the desired results as the fluorescence excitation was detrimentally filtered by the ITO thin film. In addition, the fluorescence signal was not observed for days after inoculation suggesting that oxygen stored within the PDMS matrix may be intervening with the fluorescence and hence the electrical signal. Consequently, the architecture of the microfluidic microbial fuel cell had to be modified to account for these deficiencies.

4.4 System-B: Single-cell ultra-micro-electrode MFC

This section presents the second generation microfluidic MFC. As was just mentioned, this version addressed several of the previous design's shortcomings. Specifically, the system's configuration was modified to overcome the ITO's poor transmissivity in the ultra-violet regime and enhance the microorganisms' intrinsic fluorescence signal. Secondly, as PDMS is highly permeable to gasses, it was eliminated to mitigate losses incurred by gas (oxygen) diffusion that were affecting the fluorescence and current readings. Next, a "low impedance" reference electrode was embedded to probe the redox. And lastly, the anodes were arrayed within the microfluidic device to (1) provide higher throughput, (2) improve the probability of capturing a single cell's on the 7 μm diameter active windows, and (3) further lower the capacitance of the electrodes to provide faster reaction characteristic times.

The electron transfer from *G. sulfurreducens* was measured on the transparent ultra-micro-electrodes in the microfluidic microbial fuel cell. By characterizing the electron transfer at high resolution, the aim is to generate a methodology for species-to-species comparison and formulate a baseline for electrode optimizations. The notion is to mitigate the system effects to the extreme and isolate the biological contribution in this bioelectrochemical process to optimize it. This is critical and fundamental knowledge to be explored within the scope

of MFCs as a power generation device with direct implications to molecular cell biology. Results show that upon inoculation, using *Geobacter sulfurreducens*, the signal to noise ratio (SNR) is dependent on cell seeding density but can reach 4.9 without concentrating the cells. However, sub-unity SNR is obtained for diluted samples suggesting that single cell characterization may prove difficult under standard conditions. Nevertheless, 195 pA are obtained at +200 mV (vs. SHE) using the 50 μm^2 anode from the mature inoculum, which is the equivalent of 3.9 pA/μm^2 (3.9 A/m^2). In addition, integrated Ag/AgCl and Ag_2O reference electrodes demonstrate stability for over 12 hours of operation.

4.4.1 Device Design and Fabrication

In this second iteration, microfluidic MFC was significantly modified. As illustrated by Fig. 4.11, rather than using an aqueous catholyte, the final electron acceptor was changed to a solid-state chemistry. This allowed the two-channel system to simplify into a single one, eliminated the need for PDMS to define the microchannels, and halved the required ports. This was accomplished by an Ag_2O electron sink directly deposited on the cathode, which was buried beneath a casted PEM junction to minimize dissolution of the electron acceptor. Lastly, the planar-electrode single-channel geometry allowed for a low-loss glass cover slip to serve as the "cap" of the device. The device's spacer of arbitrary thickness would provide channel height flexibility to support different types of experiments. Narrow channel heights (less than 10 μm) would provide low Raman scattering for intrinsic fluorescence experiments, and high channels (more than 100 μm) would provide the hemispherical profiles for diffusion studies.

Figure 4.12 is a top-view image that depicts the architecture of the chip. As with the previous prototype, ITO was used as the electrode material and SiO_2 served as the passivation layer. The anodes, shown here as parallel fingers, were arrayed to increase throughput (multiple concurrent characterizations per device) and maximize the probability of capturing a single cell within the active areas. The anodes were 100 μm in width at the tip and widened towards the edge of the chip. As ITO is a semiconductor that results in high resistance through elongated geometries, an additional gold thin film was deposited on non-optical areas to increase the anodes' conductivity.

The reference electrode and cathode were oversized in comparison to the anode electrodes as shown. Structurally, they consisted of a silver thin film that had been processed into either Ag_2O or AgCl chemistries. The reference electrode was 400 x 800 μm, and the cathode was 400 μm x 1.5 mm. Through a stenciling process, a Nafion dispersion was spun on and casted to reach 200 nm dry thickness on both electrodes to mitigate dissolution of the oxides in the aqueous solution.

Each anode "finger" was 100 μm wide, but the active window areas through the oxide layer were limited to either 10 or 20 μm radii, as shown in Figure 4.13. The anodes were

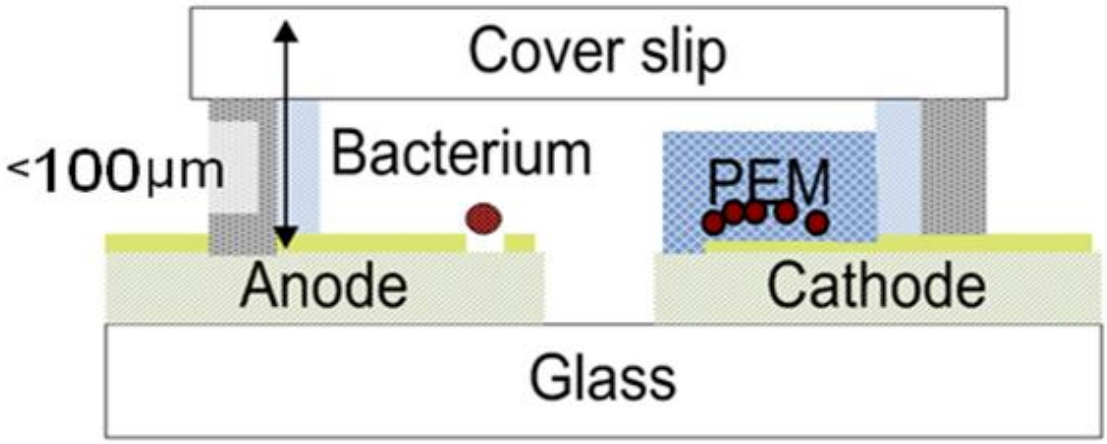

Figure 4.11: Side-view schematic of the second generation single-channel ultra-micro-electrode microfluidic microbial fuel cell. The image illustrates that electrodes lay within the same plane. The cathode and reference electrodes are solid state and buried beneath a casted Nafion membrane. And a low-loss cover slip "caps" the device to be used for microscopy.

spaced at 150, 200, 250, and 300 μm to allow conductance experiments. The reference electrode and cathode consisted of a thin film metal stack. The ITO, in addition to serving as optically transparent anode, it was also utilized as the adhesion layer between Au and the quartz wafer. The gold thin film served to lower the resistance of the semiconductor anodes and provide ohmic contacts to the instrumentation. Next, a silver thin film was evaporated on the gold active area next to the anodes and converted into Ag_2O or AgCl.

Fig. 4.14 shows the assembled device. The overall chip dimensions were 20 x 23 x 1.5 mm. The single channel consisted of a 6 mm long x 4 mm wide, and in the case where the 25 μm spacer was used, a volume of 0.5 μL. The system's ohmic resistance was characterized via the potentiostat and resulted in an impedance of 100 kΩ, which was comparable to the analytical estimation using 5 mS/cm as the electrolyte's conductivity. The capacitance for each of the r = 10 μm electrodes was estimated at 25 pF for the ITO/electrolyte junctions and 3 pF for the SiO_2/electrolyte interface assuming k = 4.2 and as the dielectric constant for PECVD oxide and 0.5 μm passivation layer thickness. Consequently, a 2.8 μs was estimated as the RC constant.

Figure 4.15 shows the fabrication sequence of the device. The process consisted of 5 lithography/film deposition steps, and countless intermediate processing requirements. The major steps of the sequence are summarized here, but the specific recipe can be found in Appendix B.

1. Lithography / sputter ITO (100 nm)

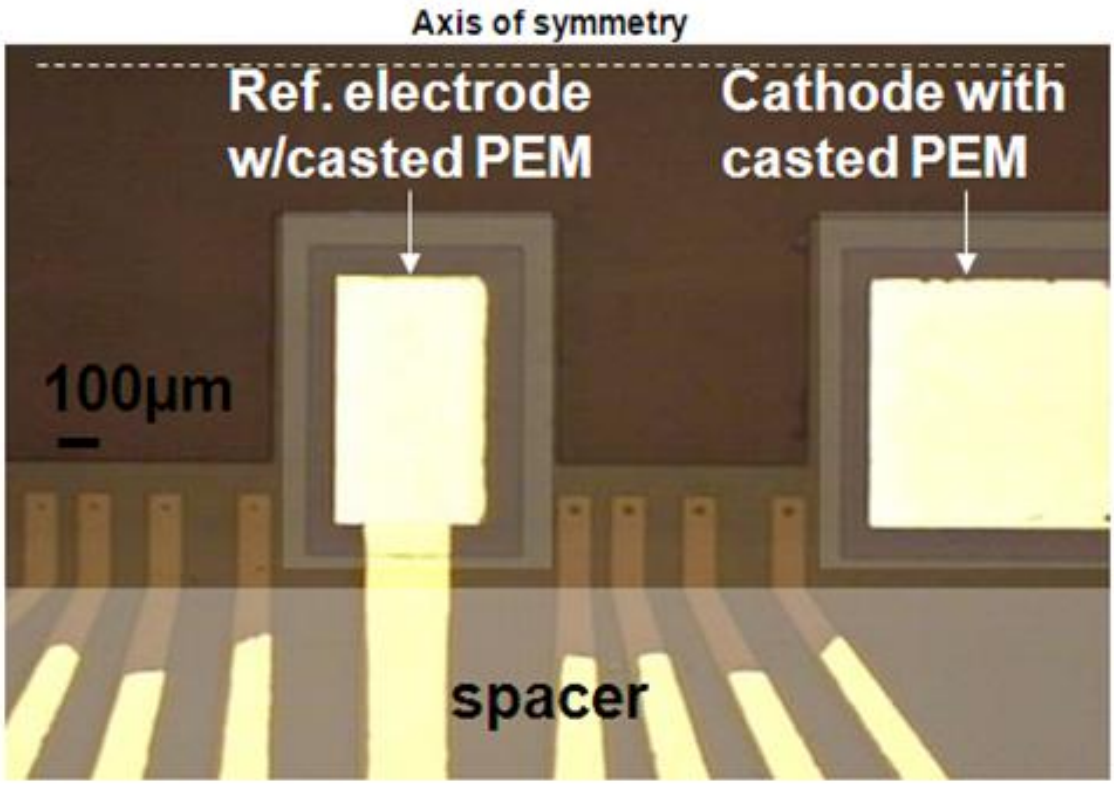

Figure 4.12: Image of ultra-micro-electrodes and embedded reference redox probe and cathode. These were placed in close proximity to mitigate ohmic loss and maximize the potentiostat's stability. The ITO electrodes were arrayed and are shown as the "fingers" in this image. The reference electrode and electron acceptor on the cathode consisted of solid-state silver chemistries. Image actually shows half of the chip as an identical configuration existed across the axis of symmetry shown. Each chip consisted of 16 anodes, 2 reference electrodes, and 2 cathodes.

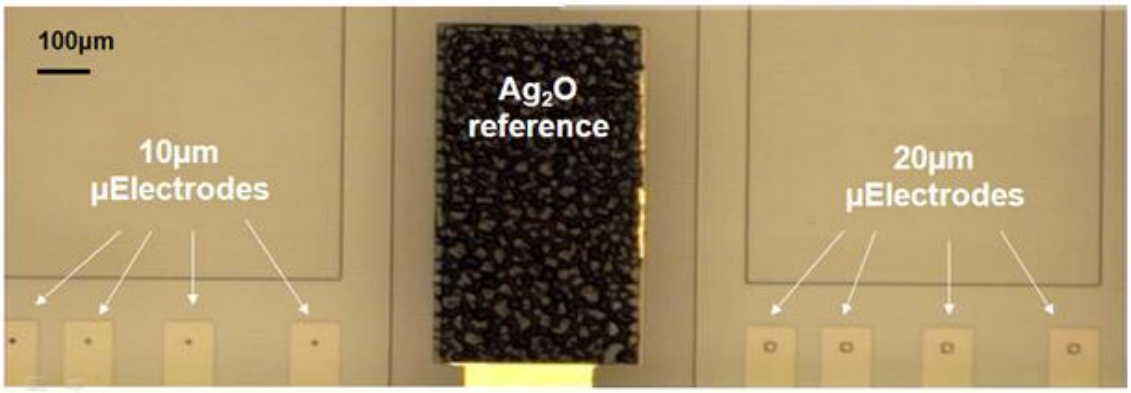

Figure 4.13: Image of ultra-micro-electrodes and embedded reference redox probe and cathode. These were placed in close proximity to mitigate ohmic loss and maximize the potentiostat's stability. The ITO electrodes were arrayed and are shown as the "fingers" in this image. The reference electrode and electron acceptor on the cathode consisted of solid-state silver chemistries. Image actually shows half of the chip as an identical configuration existed across the axis of symmetry shown. Each chip consisted of 16 anodes, 2 reference electrodes, and 2 cathodes.

2. Lithography / evaporate Au (100 nm) / liftoff
3. Anneal metals (350 ^{o}C for 1 hour)
4. Deposit PECVD SiO_2 (500 nm at 350 ^{o}C)
5. Lithography / DRIE through oxide with SF_6
6. Lithography / evaporate Ag (1 μm) / liftoff
7. Use oxygen plasma to generate Ag_2O or $FeCl_3$ solution for AgCl
8. Lithography / cast PEM
9. Dice / drill through glass for ports
10. Oxygen plasma clean
11. Encapsulate with glass cover slip
12. Make electrical connections

4.4.2 Experimental Set Up

Ultra-low currents were expected of the single cell ultra-micro-electrode MFC such that it is important to pay special attention to the experimental set up. Specifically, instrumentation

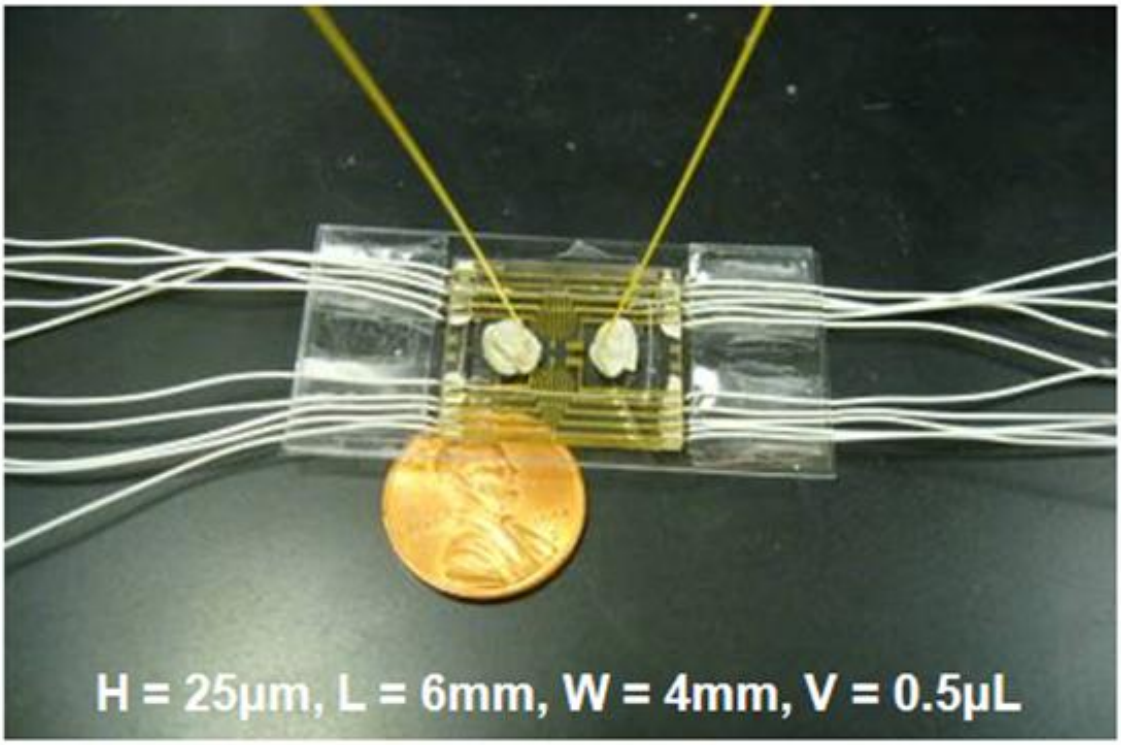

Figure 4.14: Image of assembled single-cell ultra-micro-electrode MFC. The system consisted of 16 anodes, 2 reference electrodes, and 2 cathodes embedded within a single aqueous channel. Each anode contained a single r = 10 or 20 μm active window for bacteria/electrode interactions.

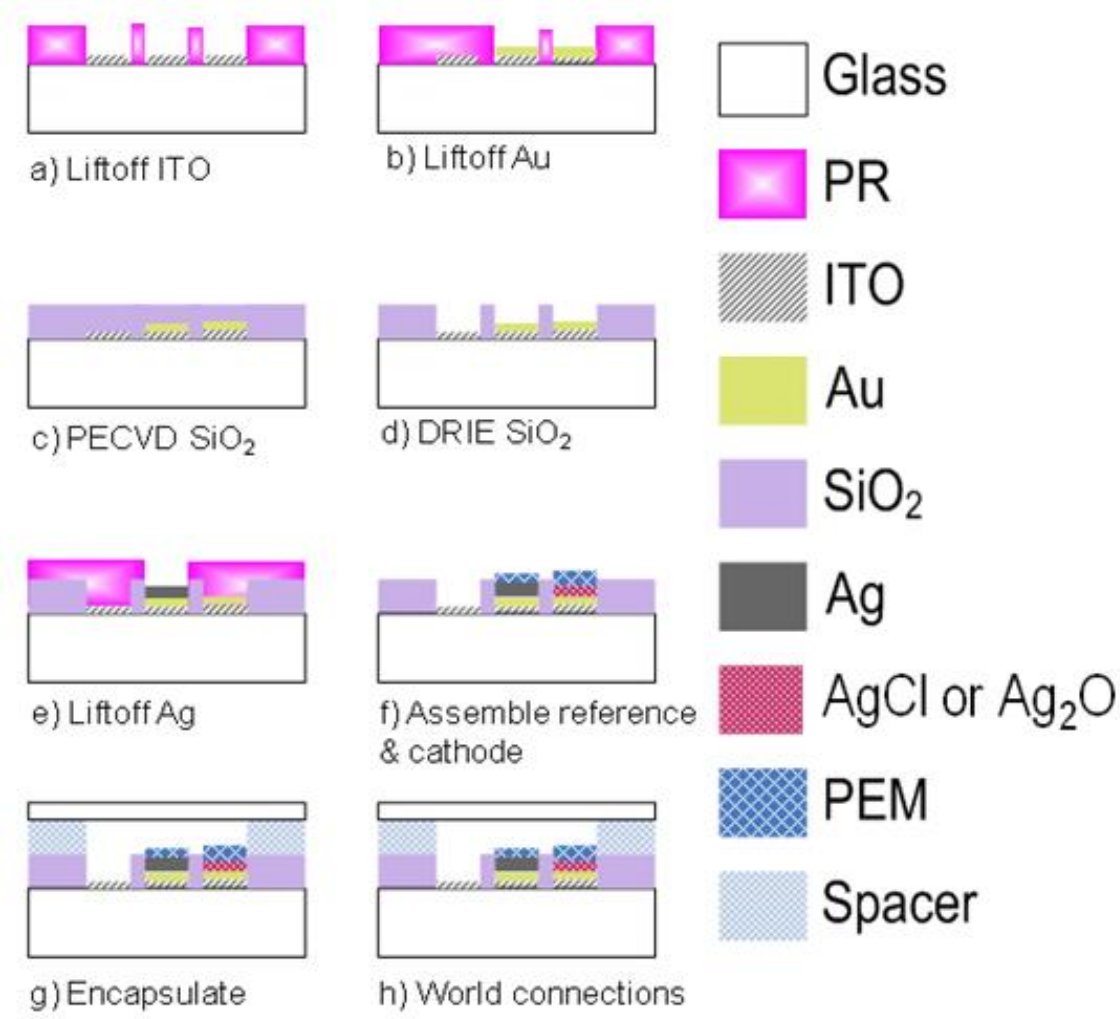

Figure 4.15: Fabrication process for single-cell ultra-micro-electrode MFC. As compared to the simple 2 mask process for the previous prototype, this iteration required 5 masks and countless additional steps. The lithography steps included the definition of the (1) ITO, (2) gold, (3) oxide, (4) silver, (5) PEM layers.

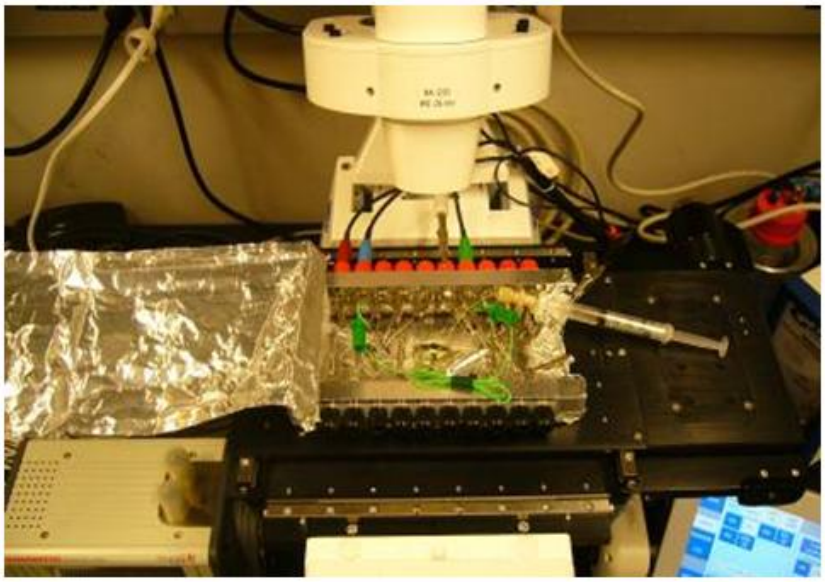

Figure 4.16: Image of experimental set up. Microfluidic 0.5 μL volume system with 16 arrayed anodes required engineering of the electrical connections to world. The chip sat under the microscope a syringe pump was used to pump the solution.

capable of fA electrochemical readings was used in a set up that minimized electromagnetic and other ambient noise as shown in Figure 4.16. Images were acquired using a Zeiss inverted fluorescence microscope equipped with a mercury lamp and a Hamamatsu 9100-13 EMCCD camera. All the measurements were acquired using an unmodified Gamry Reference 600 Potentiostat/Galvanostat/ZRA at the lowest current range setting that was calibrated prior to testing. To mitigate electromagnetic noise, a faradaic cage was incorporated within the microscope tray as shown in Fig. 4.17.

4.4.3 Reference Electrodes and Stability

As the single-cell ultra-micro-electrode MFC was intended to study the bacteria's metabolic kinetics, a reference electrode (RE) was embedded within the system. The RE was micro-fabricated along with and in close proximity of the ultra-micro-electrodes to minimize iR (ohmic) drops to assist the potentiostatic stability. However, micro-reference electrodes require that chemical stability be maintained with small masses in the range of μg. Hence, the stability's longevity was a concern. In this section, two solid-state electrode chemistries, Ag/AgCl and Ag_2O, are discussed. Specifically, their redox potential and stability as microfabricated sensors with minimal mass was investigated for their potential as reference electrodes and final electron sinks in microfluidic microbial fuel cells.

Figure 4.17: Microfluidic chip shown embedded within the faraday cage. Optical window was included to allow microscopy.

Silver Chloride Reference Electrode

Silver chloride (Ag/AgCl) is the most widely used electrode in bioelectrochemistry. It consists of a silver wire where its surface has been oxidized into silver chloride chemically or electrochemically in a salt bath. This RE's potential is dependent on the concentration of chloride ions in the solution adjacent to its surface. Under saturated KCl and standard conditions, its redox potential is +199 mV (vs. SHE). However, dropping the KCl concentration to 0.1M increases the redox to +288.1 mV (vs. SHE). The equilibrium relationship follows

$$\mathrm{Ag}_o(s) + \mathrm{Cl}^- \leftrightarrow \mathrm{AgCl(s)} + e^- \tag{4.1}$$

and E^0 = +199 mV in sat. KCl (vs. SHE). However, the AgCl layer for the purpose of potential stability, is soluble to in aqueous solution to 2 ng/μL. Hence, dissolution of a miniature quasi-electrode's oxide was a concern. Figure 4.18 shows the characterized stability of the microfabricated reference Ag/AgCl electrode. The quasi-RE consisted of a 1 μm thick layer of silver, which was oxidized in a 50 mM solution of $FeCl_3$ for 10 seconds, and passivated with a Nafion membrane that was casted from a 5% ionomer solution. The figure illustrates that the micro-quasi-RE redox drifted from +75 to +0 mV (vs. sat Ag/AgCl) continuously for 10 hours until it catastrophically failed. This behavior can be explained

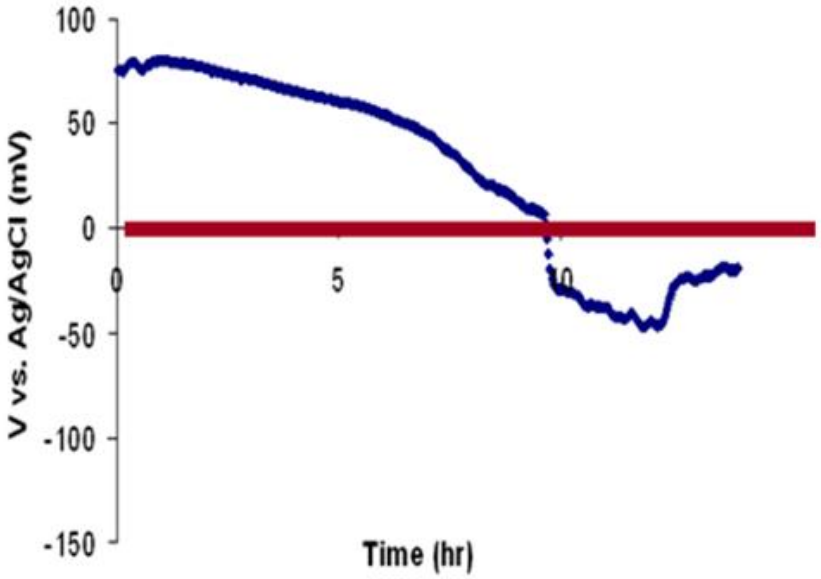

Figure 4.18: Stability characterization of Ag/AgCl microfabricated quasi-reference electrode passivated with a casted Nafion membrane. Potential drift from +75 to + 0 mV (vs. Ag/AgCl) shows the penetration of water molecules through the PEM and slight dissolution of AgCl oxide layer at the membrane/RE interface. With time, the and Cl^- concentration increases and lowers the redox closer to that of the saturated Ag/AgCl.

by the dissolution of AgCl into ions as the PEM hydrated, solvated the reference electrode, and increased the osmotic pressure beneath the Nafion junction. The initial potential was characteristic of a 200 mM KCl solution and reached saturation redox conditions (about 4 M) near 10 hours. At this time, however, the PEM detached and the oxide completely dissolved and unstabilized the potential. These results suggest that the micro-quasi-RE was serving as a redox probe. However, a well attached low-leak junction must be included to maintain stability. Using a casted Nafion membrane that is immobilized purely by van der Waals interactions is insufficient for long term studies. Perhaps utilizing a junction fabricated through sol-gel techniques or mechanically pinning down the membrane would enhance the stability time.

Silver Oxide Reference Electrode

A less common reference electrode consists of the silver oxide chemistry. The Ag/Ag_2O junction provides extremely fast kinetics and is typically found in button "watch" batteries. It provides the advantage that its redox potential does not depend on an ionic concentration of the aqueous solution. However, the oxide phase must be present to maintain stability is,

as the AgCl, oxide, soluble and hence maintaining a layer that is initially in the μg's is a concern in a flow through microfluidic system.

The silver oxide chemistry comes in at least two phases. The more energetic but less stable phase consists of the AgO as follows:

$$2\text{AgO (s)} + \text{H}_2\text{O}(l) + 2e^- \leftrightarrow \text{Ag}_2\text{O(s)} + 2\text{OH}^- \tag{4.2}$$

so that $\text{E}^0 = +0.57$ V (vs. SHE). However, the phase typically found due to its increased stability is:

$$\text{Ag}_2\text{O (s)} + \text{H}_2\text{O (l)} + 2e^- \leftrightarrow 2\text{Ag(s)} + 2\text{OH}^- \tag{4.3}$$

and $\text{E}^0 = +0.35$ V (vs. SHE). The latter was fabricated into a micro-RE and characterized. Figure 4.19 depicts the stability results. This micro-RE initially consisted of a 1 μm Ag evaporated thin film that was oxidized under oxygen in a barrel plasma for 20 minutes to produce the layer shown in Figure 4.13. As Ag_2O is soluble to 25 ng/μL in aqueous solutions, a casted Nafion membrane was also used as a passivation layer to prevent the oxide from dissolving away.

Figure 4.19 shows that Ag_2O provided a redox of +0.15 V (vs. Ag/AgCl) within the first hour of Nafion hydration, as was expected. In contrast to the Ag/AgCl microfabricated electrode, however, the potential demonstrated less of a drift. The redox was stable for 12 hours when it suffered from a 20 mV drop. The exact cause is unknown. However, it could have occurred from a mixed potential with the basal media as the Nafion membrane is expected to have started detaching at this time. The results suggest that the reference electrode catastrophically failed after 17 hours when the PEM detached.

Although more experimentation is needed to deem an electrode chemistry superior, these results suggest that the silver oxide may be simpler to integrate with microfabrication. It does not require an aqueous solution to maintain it and is generally more stable. The casted Nafion membrane also appeared to adhere to the oxide with greater force, perhaps due to the increased surface area generated by the oxidation of the silver in the oxygen plasma or because the silver oxide generated a lower osmotic pressure than the Cl^- when hydrated. However, more studies are still necessary. At 17 hours, the longevity of the microfabricated reference electrode is still insufficient for long term studies. During this period bacteria may barely undergo a division cycle and few physiological changes. Hence, the junction material should be reconsidered. In addition, Ag_2O solubility increases in acidic conditions, which make processing with Nafion ionomer solutions challenging. Lastly, it is unclear whether silver oxides are biocompatible as some literature described that bacterial viability is affected by these compounds [58].

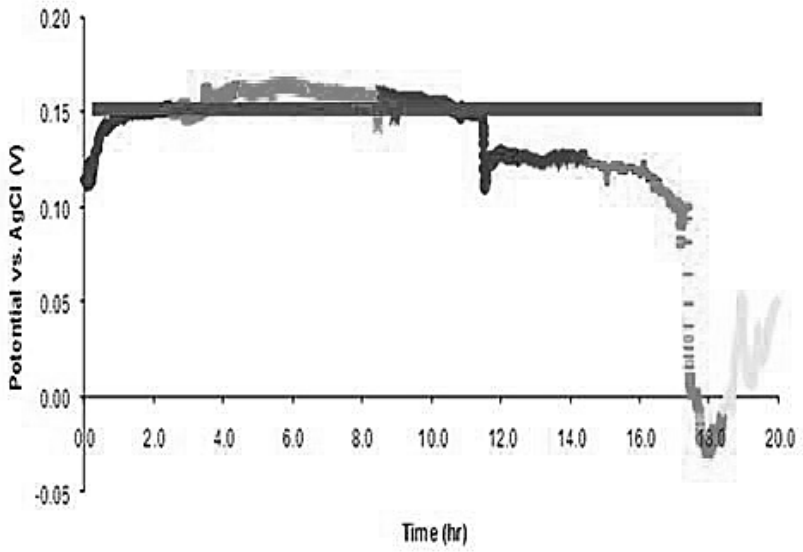

Figure 4.19: Stability characterization of Ag_2O microfabricated reference electrode with a casted Nafion membrane. Potential was stable for 12 hours and drifted slightly between 12-17 hours. This chemistry does not require ionic interactions to remain stable, but the oxide layer is soluble in aqueous solutions.

4.4.4 Results and Discussion: Electron Transfer

Our previous studies have shown that 1.4 μA/mm^2 can be achieved from mature *G. sulfurreducens* biofilms on microfabricated gold electrodes [25, 57] . However, the single-cell ultra-micro-electrode MFC miniaturized the anodes further to study microstructure effects of the biocatalysis with the ultimate objective being to capture a single cell's current output. For this purpose, active areas were patterned on microfabricated electrodes. A sample of the anodes utilized for characterization is depicted in Figure 4.20. The optical image shows the ITO electrode buried underneath a SiO_2 passivation layer with a round "pattern" that served as the window to the ITO. The electrode active areas were drawn as either 10 x 10 μm or 20 x 20 μm squares. However, the smaller active area transferred as a 7 μm round opening with 50 μm^2 surface area. Complete etching through the oxide was secured by doubling the necessary DRIE energy (time) and verifying through impedance testing.

To characterize biocatalysis microstructure effects and determine the signal on a per cell basis, currents in the sub-pA per μm^2 were projected. Hence, background signals from electromagnetic ambient noise and photoinduced currents had to be quantified and minimized. Discerning the biological contribution, or providing a significant signal-to-noise ratio (SNR), was fundamental in understanding the electrodes' sensitivity to biological currents.

The prototype was demonstrated using wild type *Geobacter sulfurreducens* cultured in anaerobic media. The cells were grown with acetate and fumarate as a final electron acceptor and incubated at 30 ^{o}C. Samples were harvested from anaerobic tubes at two different growth conditions. Specifically, one sample was obtained during exponential growth (OD = 0.1 at 24 hours) and the second during stationary phase (OD = 0.6 at 72 hours). The bacteria were filtered prior to being injected into the microfluidic cell and then allowed to rest in the system for 1 hour so that approximately 10^4-10^5 cells were inoculated into the 0.5 μL device.

The metabolic currents were quantified within 2-6 hours after inoculation into the microfluidic device, without rinsing the channel of the soluble electron acceptor, and prior to adaptation to the anode, when the current signal is expected to be at its minimum. As no bacteria were captured in focus, it is believed that these had yet to attach to the electrode, the electrical signal is likely to stem from planktonic biomass intermittently discharging on the electrode.

Abiotic Chronoamperiometric Controls

The ultra-micro-electrode was designed to characterize the metabolic output of microorganisms within their native media, which contains redox active species. Hence, to isolate the bacterial contribution to the current, the background signals had to be characterized. Specifically, the controls consisted of anaerobic basal media without acetate, basal media with 0.2 mM and 10 mM acetate, and the inoculum solution after cell incubation and growth but

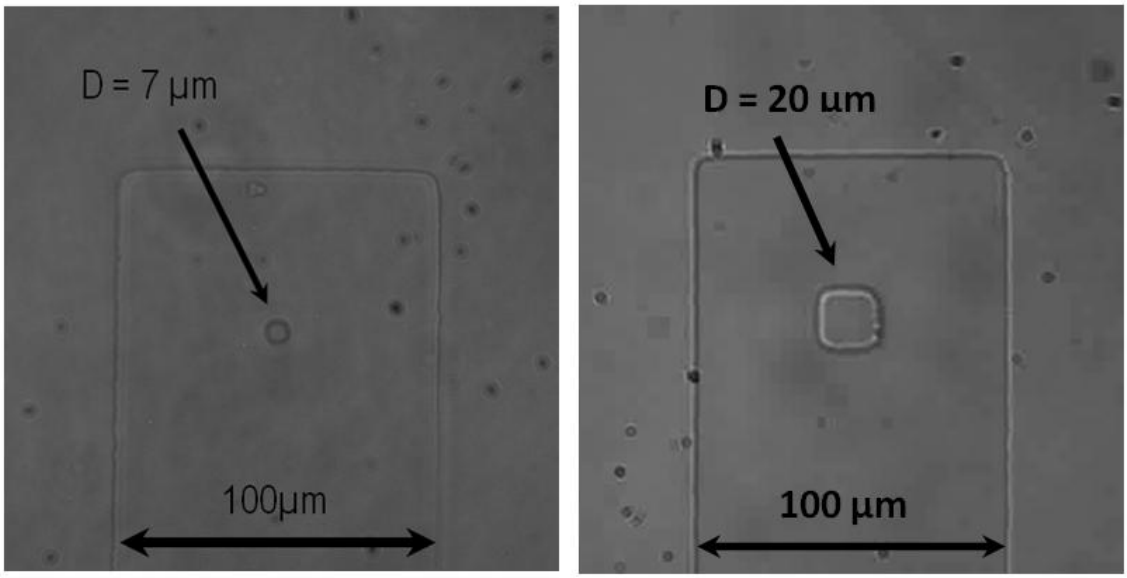

Figure 4.20: Close ups of ultra-micro-electrodes. The 100 μm silhouette depicts the 100 nm ITO layer buried under 1 μm SiO_2. The 7 μm round (a) and 20 x 20 μm square (b) structures are the openings through the oxide layer to the electrode. Due to the limited experimental time scale caused by the unstable reference electrodes, a single cell's current output was not verified. Instead, current measurements from an unknown quantity of planktonic bacteria was characterized prior to attachment.

without cells. In addition, the current was acquired for all these conditions at a two redox potential of -150 mV and +200 mV (vs. SHE) as established by an Ag_2O microfabricated reference electrode. These were to approximate the redox of the SO^{4-}/H_2S (-220 mV) and Fe^{3+}/Fe^{2+} (+200 mV) redox couples that the cells may encounter in nature.

The results of the abiotic controls are shown in Figure 4.21. Various ultra-micro-electrodes under multiple conditions were characterized. Specifically, the testing parameters consisted of redox potential, acetate concentration, and electrode active area size. In addition, the inoculum's media (after anaerobic growth but without cells) was also tested. The gradual increase in current upon closing of the circuit demonstrates the ultra-micro-electrode's minute capacitance as no fast double-layer spike-like currents were obtained from any of the experiments. However, a current of 40 pA was obtained regardless of the testing case. At first sight, the consistency of current output suggests diffusion limited catalytic activity of a redox active species contained within the basal media, and not from acetate electrocatalytic activity on the ITO. If this was a traditional metallic macro-scale electrode, the current should have been proportional to surface area except for the radial diffusion limited case. Similarly, if acetate was the redox active species, a change in redox potential and/or concentration would have provided different currents as well. However, other effects may be at play, as is explained later this chapter that discusses the possible diode-like interactions that ITO may be producing as a semiconductor electrode for bioelectrochemical characterizations.

Biotic Electron Transfer

Understanding the electron transfer rate from the biocatalyst to the electrode to maximize current density is of particular interest in MFCs. An increased metabolic output from bacteria reduces kinetic losses to the electrode and improves fuel cell performance. To determine the signal from the cells, the current from the inoculum and the background were initially measured by poising the anode at +200 mV (vs. SHE). The cells were filtered and injected into a conditioned (previously hydrated) single-cell ultra-micro-electrode MFC. Inocula in exponential (24 hours) and stationary phase (3 days) were characterized with significantly different results.

Figure 4.22 shows the steady state currents with the abiotic contribution subtracted. The sample harvested during exponential growth (10^8 cm^{-3}) provided a steady state current of 21 pA (42 μA/cm^2), which corresponds to a signal-to-noise ratio of 0.5. Although not ideal, such SNR demonstrates that the signal is detectable under these conditions. However, further dilutions may prove to be below the minimal threshold of detection. On the other hand, current output from stationary phase inoculum (10^9 cm^{-3}) demonstrated a current output of 195 pA (392 μA/cm^2) or SNR = 4.9. The increase in current is not surprising as the cell seeding density is also likely to have increased. It is difficult to estimate the quanta of cells injected as the inoculums were filtered in both of these cases. However, assuming that the cell densities were 10^8 and 10^9 cm^{-3} for the exponential and stationary phase, each

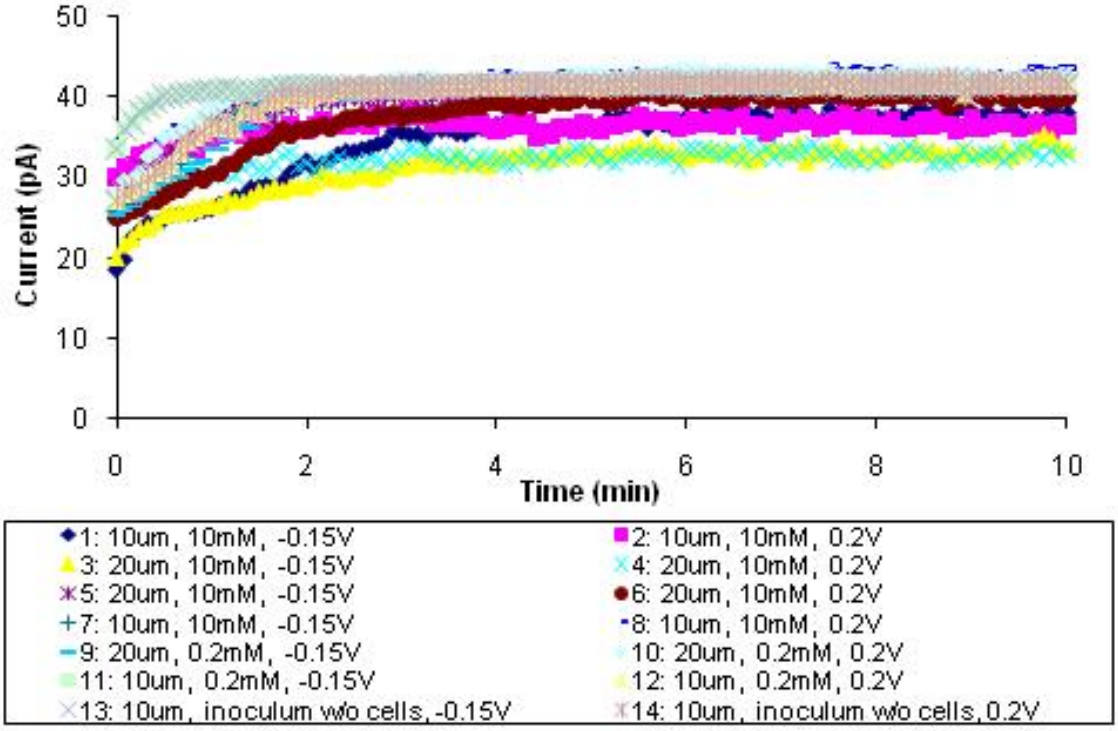

Figure 4.21: Abiotic controls. Several ultra-micro-electrodes were studied under various conditions including acetate concentration, metabolites, and redox potentials. Regardless of the conditions, a current near 40 pA was acquired.

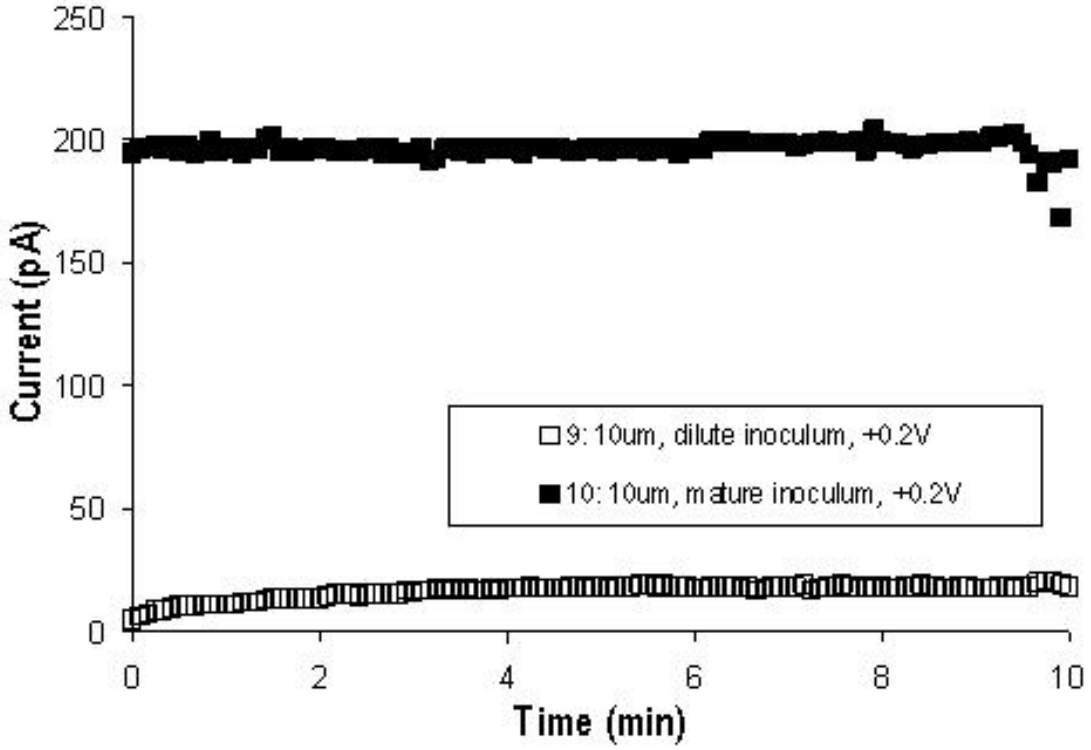

Figure 4.22: Bacterial current signal at +200 mV (vs. SHE) on 50 μm^2 ultra-micro-electrode. Inoculums in exponential and stationary phase were characterized with significantly different results. Roughly, an order of magnitude difference in current output is proportional to the microfluidic cell's seeding densities. The SNR ratios were 4.9 and 0.5 for the mature and exponential phase inoculates, respectively.

of the chambers would have been inoculated with 10^4 to 10^5 cells, respectively. The order-of-magnitude increase corresponds to the 3 additional division cycles that the mature inoculum was expected to have completed. Similarly, the current density also resulted in an order of magnitude increase that appears to be linearly proportional to the inoculation density.

Unfortunately, these experiments did not result with a single-cell's current output on an electrode. Even so, it is questionable whether the corresponding output would have been significant. The sub-unity SNR that resulted from the cells harvested during exponential growth suggests that the single-cell characterization may not be possible from the single-cell ultra-micro-electrode MFC device as designed and fabricated in this section. The background currents will need to be lowered for such experiment to be successful. One option is to reconsider the electrode material, and optimize it to lower its electrocatalytic activity with

the media's redox active species or as a semiconductor electrode. This would mitigate the background currents and accentuate the bacterial contribution. Similarly, determining the background currents' source and either reducing its concentration or eliminating its presence all together (at least during bacterial characterization) could aid the system's sensitivity.

Another important issue during single-cell testing, although less obvious, consists of assuring the removal of microorganisms that are not tallied as "in contact" as a large current density was acquired from the inoculum without visual confirmation of cells on the electrode (in focus). Hence, significant current could be captured from "planktonic" bacteria and uncertainty could be generated during single-cell testing. In this case, fluorescence microscopy could aid visualization of the cells. Unfortunately, the latter was not attempted in time.

Nevertheless, a cell's contribution can be estimated. Assuming a 50 μm^2 electrode area, the current densities for the two cases result in 420 fA/μm^2 and 3.9 pA/μm^2. Assuming that all the bacterium's electrons are forced through the ultra-micro-electrode, transfer can only occur through a monolayer, and a bacterium's footprint is 1 μm^2 (50 bacteria per 50 μm^2 active area), the stationary phase inoculum yields 3.9 pA/cell. Using similar logic, the exponential growth and lower cell density case yields 420 fA/cell. However, these assumptions could be invalid. The per cell current could be underestimated as it is unlikely that the entire electrode area would be loaded simultaneously with bacteria during characterization. On the contrary, it is also possible that planktonic bacteria (not just the monolayer in contact) could contribute to the signal at any given time. In such case, these per cell contributions would be overestimated. Nonetheless, these provide data at the extreme small scale where, currently, estimations can only be concluded from extreme extrapolations.

4.4.5 ITO as a semiconducting ultra-micro-electrode for *Geobacter*

The chronoamperiometry results also bring insight on the ITO-bacteria behavior. As ITO is a semiconductor, it could provide non-intuitive interactions as an electrode to the microorganisms. However, as will be discussed, it is likely to be metallic as an anode for microorganism oxidation but perhaps not to the background redox active species.

ITO is a degenerate n-type semiconductor characterized with a band gap is in the 3.5-4.0 eV that allows the high transmissivity in the visible wavelengths [59]. However, as it is highly doped by O^{2-} carriers, its Fermi energy is near or above the conduction band depending on the processing parameters. It could display diode like behavior if it is insufficiently doped or with a modified surface. Hence the ITO/bacteria contact interface could operate in one of three possible diode I-V regimes. Figure 4.23 illustrates the possible cases. (A) The first consists on the "diode" being in reverse bias where no current would flow. As the ITO here serves anodic reactions, this would occur with a depletion of electrons at the electrode surface through processing or electrode/electrolyte interactions. (B) The second

is the electrode's surface not being depleted of electrons but insufficient doped so that the Fermi level was below the conduction band. Hence, the "diode" would be in forward bias but the experimental conditions could be below the "on-voltage" for ohmic current flow and hence a high "contact resistance" would provide artificially low current results. (C) The third, and ideal for microbial chronoamperiometric oxidation, consists of an interface where the ITO's doping level is high enough to bring the Fermi level near the conduction band so that any or negligible forward bias produces a very low bacteria/ITO contact resistance, which would in turn would allow the bacterial metabolism as the main contributor to the readings.

The experimental conditions as well as the electrode's physical properties dictate in which regime the interface will behave. Theoretically, ITO is highly doped with negative O^{2-} carriers, so generally a negative surface charge is produced. In aqueous solutions, the surface tends to protonate and reduce the electron depletion layer thickness (case B or C) [60]. In the case of a basic solution, however, the electrolyte could "repel" the electrons from the surface, increase the depletion layer, and create a rectifying contact (case A). However, neutral to acidic environments, such as those found in biofilms and basal media, increase in-plane conductivity and reduce the semiconducting effects of ITO (case C). Hence it was expected that the ITO/bacteria interface would produce a forward diode behavior with either a high resistance (case B: below the "on-voltage") or low contact resistance (case C: negligible "on-voltage").

The abiotic controls at first sight suggest that ITO may be functioning within the second regime (case B) or that of a forward bias but below the activation voltage with the redox active species in the media. The sustained positive current output for the various testing cases suggested that the interface is forward biased but demonstrating a very high transfer resistance. In other words, the redox at which the electrode is poised is not providing a sufficiently high voltage difference with the background species to allow electrons to flow freely. Hence, a consistent few electrons are being transferred through.

The biotic currents, however, demonstrate different behavior. The addition of cells to the background electrolyte produces significantly higher current output as shown in Fig. 4.23 . This suggests that the system has shifted and is operating in the forward bias but lower contact resistance regime (case C). As the electrode's poised redox was not changed in comparison to the control studies (also maintained at +0.2 V vs. SHE), the condition that changed the system's behavior must have stemmed from the bacteria. In other words, the electrons that the bacteria are supplying provide a sufficiently large voltage differential with the poised redox on the ITO electrode and allow electrons at the interface to flow more freely. It is difficult to pinpoint the contact resistance and curve specifics from this study, as the Fermi energies of the ITO surfaces as processed were not characterized. However, this illustrates yet another effect that could be studied to fundamentally understand the bacteria/electrode interface. As characterizing where the "on-voltage" or "knee" from case B to case C occurs is intimately related to the material properties and the bacterial "contact

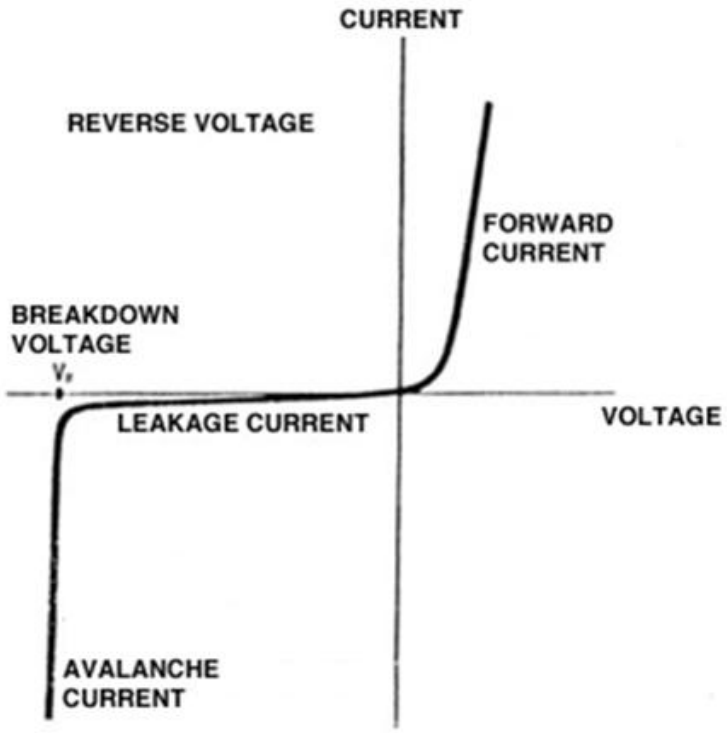

Figure 4.23: Semiconductor/bacteria interface with possible diode behavior in three regions. As ITO is an n-type semiconductor, doping levels and experimental conditions affect the depletion region and current outputs.

resistance".

4.5 Conclusion

Microfluidic and ultra-micro-electrode MFC systems for high resolution characterization of bacterium for energy applications were developed. The chips were microscopy compatible and electrodes were designed in the range of μm in the characteristic length. The system consisted of transparent ITO anodes that utilized SiO_2 as a passivation layer to define active windows for bacterial connection.

The first design consisted of a system with a two parallel chamber configuration with 10's to 100's μm active areas with an aqueous catholyte where potassium ferricyanide was the final electron acceptor. The system did not include a reference electrode. This device produced a low current of 40 pA over a 10^4 μm^2 area. As designed, the microfluidic MFC

provided optical verification of cells on the electrode. The channels were defined through a casted PDMS layer, and the system was redesigned as the system's configuration did not allow intrinsic fluorescence microscopy for single cell identification.

The second device improved upon the first generation. The new configuration eliminated the need for a second channel via a solid-state Ag_2O electron sink. This chemistry was also utilized as an embedded microfabricated reference redox electrode that has been demonstrated as stable for up to 16 hours. Each chip contained an array of 16 micro-scale electrodes with narrow (50-200 μm^2) active window openings to maximize the probability of single-cell characterization. Abiotic controls and experiments with multiple cell seeding densities were performed. With background currents subtracted, the stationary phase inoculum produced 195 pA/50 μm^2, a SNR = 4.9, and the equivalent of 3.9 $\mu A/mm^2$ (at +0.2 V vs. SHE). However, the exponential growth inoculum with 1/10 the seeding density resulted in 21 pA/50 μm^2 and a SNR = 0.5. A single cell experiment showed evasive as the microorganisms did not come into focus during amperiometric characterization. Hence the results are likely due to planktonic biomass intermittently discharging on the electrode. However, the sub-unity SNR for the low seeding density case suggests that single cell characterization would not be detected over the background noises as was performed in this study. The electrical contribution of the background currents must be mitigated first.

The results from the second device also provide insight on the suitability and/or potential of using semiconductors as electrodes in bioelectrochemical systems. As semiconductors can often produce non-ohmic contact or diode behavior, depending on the thin film deposition parameters and experimental conditions, this could be yet another tool to help understand the redox state and microbial interactions with the electrode. Specifically, this study demonstrated a forward bias but below "on-voltage" behavior for the background currents, but above "on-voltage" or "knee" point ohmic contact behavior with the microorganisms. Hence, at least with sputtered 90% In_2O_3, 10% SnO_2 (ITO) at neutral pH, anodic microbial reactions are near an "on" diode threshold level that could be exploited for current/voltage characterizations.

As no other studies at this scale have been performed, these results can only be compared with the electrical outputs of larger systems. Figure 4.24 illustrates the current and power density results from selected publications using small scale systems representing a plethora of testing conditions including: complex and planar electrodes, and consortia to single cultures. This work, which characterized the electrical output through a planar 50 μm^2 ITO electrode, provided a normalized current density of 3.9 $\mu A/mm^2$ using the stationary phase sample upon inoculation into the microfluidic device. These results continue to support the trend that was first discussed in Chapter 2. The energy output is scaling logarithmically with electrode area, but the exact reaction remains to be verified.

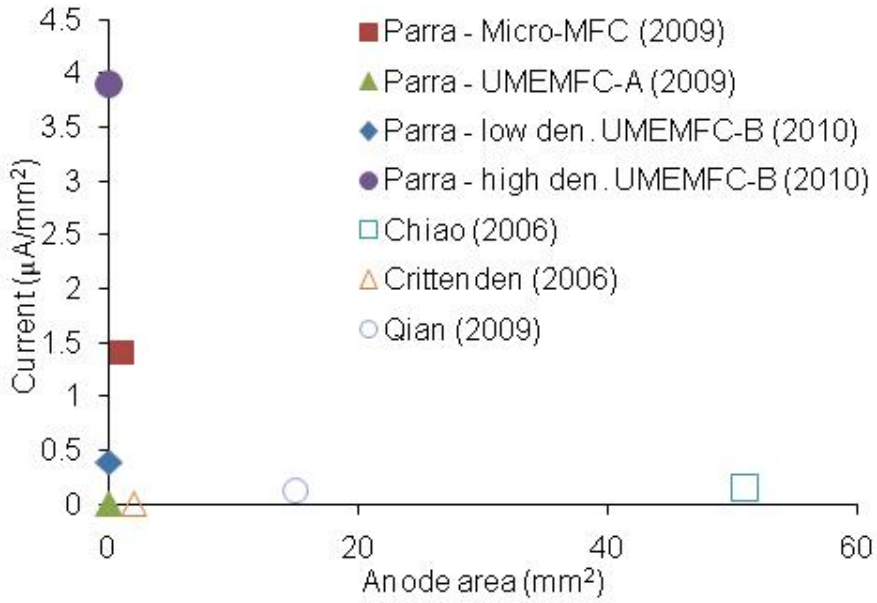

Figure 4.24: Single-cell ultra-micro-electrode MFC results in relation to various other studies. The stationary phase *G. sulfurreducens* in this study provided 3.9 μA/mm^2 (3.9 pA/μm^2) upon inoculation.

Chapter 5

FutureWork

The bioelectrochemistry field, which studies microbial interactions with electrodes, is an emerging discipline with great commercial and humanitarian potential. Microbes, as this work studied, can produce electrical energy from their intrinsic metabolism. However, microbial metabolic diversity extends to a plethora of other applications. Microbes have also been employed in bioremediation and are currently being investigated for biofuel generation. Hence, the microorganisms in these systems could become inexpensive, self-generating, electrically controlled "workers" for the benefit of society.

In this dissertation, the focus was on the development of microfluidic microbial fuel cells (μF-MFC) designed to illuminate the fundamental electrical characteristics of microorganisms capable of extracellular electron transfer (EET). The system, which can also be described as a microbial fuel cell on a microscope slide, offers experimentation at a scale that has not been previously available. The system has single-cell characterization capability, was microscopy compatible, non-invasive, provided complete environmental control, and real-time metabolic characterization on electrodes. Hence, microorganisms could be studied in-situ and at high-resolution allowing metabolic comparisons (physiological adaptations, species-to-species, and within species variability) and revealing their interactions with surfaces as microfabricated electrodes' morphologies and microstructure can also be controlled and characterized.

This work, however, was only the first step on a research agenda that could last decades. In this Chapter, specific improvements on the μF-MFC system are summarized. Also, the future work of μF-MFC is discussed in relation to characterization techniques that take advantage of the high resolution as well as the scaling of the system's parameters. Lastly, commercial applications that take advantage of the high-throughput capabilities of μF-MFC are presented.

5.1 Microfluidic Microbial Fuel Cell Continued Development

The EET microfluidic characterization system that was developed provided initial data. However, a number of improvements could be instilled to provide for a robust platform for single cell studies. Most of these were mentioned throughout the dissertation but are here summarized. In addition, a number of experimental or practical issues are also discussed.

The final ultra-micro-electrode microfluidic platform for single cell characterization consisted of an array of 16 microelectrodes, 2 reference, and 2 cathodes. The system permitted simplification into a single channel configuration because of the conversion of the aqueous catholyte into a solid-state chemistry. However, a couple of issues still remained. Specifically, (1) the microorganisms' position within the chamber could not be controlled and placement of a cell was not verified on the micrometer diameter electrodes. Though many electrodes were designed into the chip to aid the probability of capturing a cell's output, it was not accomplished and a position guidance mechanism is recommended in the next platform design. And (2) the casted Nafion membrane detached from its position within a day, freeing the compounds that equilibrated the redox potential in the reference electrode and liberating micrograms of silver particles that are toxic to microorganisms. The challenges associated with these issues as well as some solutions are discussed below.

5.1.1 Cell placement mechanism

A number of techniques have been developed to place cells at specific locations within microfluidic systems. Lee et al. developed large arrays that used hydrodynamic forces [61]. However, these cannot be easily implemented within a microfluidic microbial fuel cell. In the case of hydrostatic placement, features smaller than the microorganisms are required. As bacteria are micron-sized, features in the nanoscale, outside of typical lithographic techniques, would be needed. To simplify placement, it was suggested to attach the cells to larger silica or polystyrene microspheres. However, that would affect the intrinsic behavior of the cells. In addition, hydrostatic placement requires continuous flow and distortion of diffusion profiles that are intrinsic to fundamental characterization.

Wu el al. have developed optoelectronic tweezers to place cells at specific sites using electromagnetic forces [62]. This technique has demonstrated placement of micron sized structures at specific locations within a microfluidic chamber. Again, this is a powerful tool but it requires special media that would not permit kinetic studies in microfluidic MFCs.

Yet another cell placing technique consists of covalently bonding the cells to the electrodes. Anodes could be functionalized via SAMs or other surface modifications. However, as the system was to study the intrinsic EET from the cells, artificially attaching the microorganisms is likely to alter the results.

Hence, controlling the position of the micrometer sized microorganisms is not a trivial undertaking. However, a technique that shows potential is currently being developed by Buie et al. [52]. It consists of using dielectrophoresis (DEP) to manipulate the position of the cells in the channel. As it uses electrical potential, it can function in quiescent flow and necessitates only embedded electrodes. The cell's electrical properties (membrane resistance and capacitance) need first be understood, but the technique shows promise as a non-intrusive method for bacterial placement.

5.1.2 Reference and counter electrode electrolyte membrane

The ultra-micro-electrode system as presented in this dissertation had a limited experimental time scale, which is unideal for physiological characterization of the microorganisms. The longevity issue occurred because the casted Nafion junction that separated the silver oxide compounds from the microorganisms would detach from the electrodes causing the chip to fail. The electrolyte junction was needed to keep the silver oxide from dissolving into the aqueous media, as direct contact would cause the reference electrode to lose the equilibrium potential, the counter electrode to lose the electron sink, and the dissolved silver particles would sacrifice cell viability.

A potential solution to the PEM stability dilemma may be to utilize sol-gel techniques in conjunction or instead the polymeric electrolyte membrane. Sol-gel techniques that utilize biocompatible silica nanospheres (sub 20 nm) have been developed to covalently attach nonplanar glass structures [63]. Such a technique is an attractive alternative for bonding the chip as well as creating a low-leak junction.

5.2 Fundamental Work for Microfluidic Microbial Fuel Cells

As this dissertation is the first attempt to study EET in the per cell regime, an infinite number of fundamental experiments can be envisioned. This section summarizes the most impactful investigations that derive directly from the work discussed in the previous chapters.

5.2.1 Metabolic Kinetics and Redox Optimality

A fuel cell's electrical signal is the macroscopic manifestation of a system fundamentally dependent on microscopic effects. In the case of microbial catalysis, the heterogeneous nature of the system is not only limited to the microstructure of the electrode and reactant chemistry, but also to the biocatalyst loading and state of the microorganisms at the time of testing.

Hence, the electrical behavior of MFCs is contingent on many temporal factors. Microscopy compatible electrodes, as developed in the μF-MFC, offer the advantage of simultaneously monitoring the biomass, the electrical characteristics (metabolism) of the system, as well as controlling the nutrient concentrations. Consequently, poised electrode's redox effects on metabolism kinetics (electrical current), viability, as well as cell division (optically verifiable) can be studied concurrently. Although it appears incremental, a very powerful study consists of quantifying the Monod kinetics, the model that relates biomass division rates with nutrient concentrations as a lumped approximation of metabolic enzyme kinetics, under both nutrient limited and poised electron acceptor conditions. Such a study would provide insight on the energy gain and metabolic kinetics relationship that has not been quantified as currently these can only be performed under acceptor saturation. A good reference that discusses the implications can be found in [64].

5.2.2 Estimation of Biocatalyst Loading and Biofilm on Electrode through Electrochemical Spectroscopy

In addition to the biotic microstructure characterization capability, micro-scale electrochemical devices offer the scaling advantage of a fast response time. Miniature MFC's characteristic time, or RC constant, is generally in the order of seconds to minutes. Hence, steady state is reached quickly and the transient behavior of the system, specifically the microorganisms' capacitance and faradaic (charge transfer) resistance, can be analyzed with high temporal resolution. Consequently, through empirical characterization of the biofilm discharge characteristics along with its physical structure (as permitted through optical microscopy), a model that estimates biocatalyst loading and biofilm thickness could be developed. Such a technique would be a priceless tool for the bioelectrochemical community that currently has few if any methods to accurately and non-invasively estimate biomass on electrodes. This technique could be extended to quantify redox active proteins involved in EET and/or shuttling flavin compounds in systems not involved with direct electron transfer.

5.2.3 System Scaling for Performance

A literature survey of the MFC publications demonstrated that electrical performance is not proportional to system size. Dewan et al. explored this concept by testing systems of various scales using *Shewanella oneidensis* (MR-1) and reported that the power density of systems was in fact scaling with the logarithm of electrode area [20]. Hence a strong dependence of a scaling parameter(s) affects MFC power densities. Intuitively, the miniaturization advantage consists of greater environmental controllability and homogeneous/absolute biofilm coverage of the electrode. However, other scaling properties may be at play. Logan el al. had previously reported that the high resistivity of the electrolyte (media) causes ohmic

losses to dominate MFC systems [34]. One hypothesis that has not been explored consists in that the reduced electrical currents in miniature devices mitigate the potential loss due to electrolyte resistance and allows the system to increase its specific performance. In addition, small scale systems have the advantage of non-planar diffusion profiles, particularly at the sub-millimeter regime. Through parametric modeling of miniature systems that explore electrochemical, thermo-chemical, and biocatalytic scaling characteristics, a micro- and ultra-micro-electrode MFC could also investigate the optimum scale of bioelectrochemical systems for various objectives.

5.2.4 Intrinsic Fluorescence - Cell and Biofilm Level

As was previously discussed, bacteria that demonstrate direct EET also contain high densities of c-type cytochromes [65]. These cytochromes have shown to fluoresce when reduced [7]. Hence, theoretically, the "state" (reduced vs. oxidized) of the protein could be detected via fluorescence spectroscopy. At the most basic level, this technique should provide information on the location of reduced proteins on the bacterial membrane and their density (protein polarization). However, it could also provide information on how the bacteria discharge on the electrode (electrochemical fluorescence quenching) at the cell level, as well as the biofilm level. If successful, the technique could illuminate the biofilm electron discharge patterns through an electrode. However, many challenges exist for such a technique to become a reality. First, intrinsic protein fluorescence is difficult to detect. The emission intensity is several orders of magnitude lower than commercially available fluorophores. The presence of any molecular oxygen quenches the signal. And the emission spectra overlaps with that of NADH and Raman scattering that create background noise. Second, at least for cytochromes, excitation occurs at UV wavelengths, which are in general toxic to microorganisms. Third, there will be many technical issues identifying where the fluorescence comes from and what it means. In addition to the unwanted sources of noise, the protein movement may affect the fluorescence emission if the emission is directional, which may be misconstrued as a redox change. Nevertheless, it could be a powerful technique if developed.

5.2.5 Semiconductor/material Interactions

Directly stemming from this work is the consideration of microbial interactions with semiconductors. As the many of the minerals that the EET capable microorganisms come in contact with in nature are intrinsic semiconductors rather than metallic conductors, it is of interest to study the effects of the various material properties. The parameters that could be investigated consist of the positive versus negative carrier materials (p-type or n-type), band gaps, doping effects (Fermi energy), surface energy, lattice structure or phase, crystallinity,

etc. Although not comprehensive, this is an entry level list of bioelectrochemical/electrode material interactions that could be explored through microscale systems as these provide highly controlled deposition and environmental parameters. In this dissertation, ITO was utilized as the electrode material. The results indicate that the bacteria did not exhibit diode like behavior. However, the background currents were insufficient to "activate" the junction. It would be very interesting to pursue this topic further and create a protocol that could select the biological contribution over the background during characterization using this phenomenon.

5.3 Commercial Applications of Microscale Microbial Fuel Cell Systems

In addition to fundamental studies, microfluidic and/or micro-electrode microbial fuel cells could contribute to other fields than that of energy generation. The ultra-high resolution and high-throughput capabilities also have applications in the pharmaceutical and environmental industries. A few are discussed below.

A very simple yet powerful advantage of EET capable bacteria is that their metabolic rate can be instantly and quantitatively measured electrically. This unique characteristic allows the detection of metabolic changes independently from other studies. If the metabolism of EET bacteria could be robustly understood on a per cell basis, deviations of such due to environmental factors could be directly detected to determine causality for systems biology. As it has been discussed previously by Collins [66, 67], few techniques to determine toxicity of compounds in cells exist. Live/dead staining is a destructive technique that can only indicate when the cells' membrane has been compromised, and can only identify the very "dead" end of the spectrum. In this case, assuming a comparable physiology between EET bacteria and cells that would be of interest, a high-throughput microbial fuel cell platform could be utilized to test the effects of chemicals in the pharmaceutical and industrial products market.

Another area that could benefit from the use of microscale microbial fuel cells is that of environmental sensing. As bioremediation sites and wastewater plants must sense the progress of the process, miniature systems offer the advantage of a fast response time and sensitivity. In the case of perchlorate bioremediation, micro-scale MFCs could be utilized to determine the redox state within a narrow band as to not over reduce the site. Wastewater plants, on the other hand, could utilize the system to detect organics concentration and biofouling of membranes and components.

Bibliography

[1] L. De Schamphelaire, K. Rabaey, P. Boeckx, N. Boon, and W. Verstraete, "Outlook for benefits of sediment microbial fuel cells with two bio-electrodes," *Microbial Biotechnology*, vol. 1, pp. 446–462, 2008. 10.1111/j.1751-7915.2008.00042.x.

[2] G. D. Hitchens, "Electrode surface microstructures in studies of biological electron transfer," *Trends in Biochemical Sciences*, vol. 14, no. 4, pp. 152 – 155, 1989.

[3] K. A. Weber, L. A. Achenbach, and J. D. Coates, "Microorganisms pumping iron: anaerobic microbial iron oxidation and reduction," *Nat Rev Micro*, vol. 4, no. 10, pp. 752–764, 2006.

[4] E. A. Parra, T. Liu, C. R. Buie, J. D. Coates, and L. Lin, "Microfabricated microbial fuel cell for real-time biocatalyst optical monitoring and electrical signal coupling," in *Proceedings of the 2nd Microbial Fuel Cell Conference*, pp. 191–194, 2009.

[5] J. S. McLean, G. Wanger, Y. A. Gorby, M. Wainstein, J. McQuaid, S. i. Ishii, O. Bretschger, H. Beyenal, and K. H. Nealson, "Quantification of electron transfer rates to a solid phase electron acceptor through the stages of biofilm formation from single cells to multicellular communities," *Environmental Science and Technology*, vol. 44, no. 7, pp. 2721–2727, 2010. PMID: 20199066.

[6] R. O'Hayre and F. B. Prinz, "The air/platinum/nafion triple-phase boundary: Characteristics, scaling, and implications for fuel cells," *Journal of The Electrochemical Society*, vol. 151, no. 5, pp. A756–A762, 2004.

[7] A. Esteve-N*úñez*, J. Sosnik, P. Visconti, and D. R. Lovley, "Fluorescent properties of c-type cytochromes reveal their potential role as an extracytoplasmic electron sink in geobacter sulfurreducens," *Environmental Microbiology*, vol. 10, no. 2.

[8] D. of Energy, "International energy outlook 2010," tech. rep., 2010.

[9] H. Heyer and W. E. Krumbein, "Excretion of fermentation products in dark and anaerobically incubated cyanobacteria," *Archives of Microbiology*, vol. 155, pp. 284–287, 1991. 10.1007/BF00252213.

[10] D. R. Bond and D. R. Lovley, "Electricity production by geobacter sulfurreducens attached to electrodes," *Appl. Environ. Microbiol.*, vol. 69, no. 3, pp. 1548–1555, 2003.

[11] A. P., R. K., C. P., and V. W., "Microbial fuel cells for wastewater treatment," *Water Sci Technol.*, vol. 54, no. 8, pp. 9–15, 2006.

[12] B. Logan, "Scaling up microbial fuel cells and other bioelectrochemical systems," *Applied Microbiology and Biotechnology*, vol. 85, pp. 1665–1671, 2010. 10.1007/s00253-009-2378-9.

[13] C. Melhuish, I. Ieropoulos, J. Greenman, and I. Horsfield, "Energetically autonomous robots: Food for thought," *Autonomous Robots*, vol. 21, pp. 187–198, 2006. 10.1007/s10514-006-6574-5.

[14] I. Ieropoulos, I. A. Anderson, T. Gisby, C.-H. Wang, and J. Rossiter, "Microbial-powered artificial muscles for autonomous robots," in *Proceedings of the Electroactive Polymer Actuators and Devices (EAPAD) 2009* (Y. Bar-Cohen and T. Wallmersperger, eds.), vol. 7287, p. 728708, SPIE, 2009.

[15] I. Ieropoulos, C. Melhuish, and J. Greenman, "Artificial gills for robots: Mfc behaviour in water," *Bioinspiration and Biomimetics*, vol. 2, no. 3, p. S83, 2007.

[16] C.-P.-B. Siu and M. Chiao, "A microfabricated pdms microbial fuel cell," *Microelectromechanical Systems, Journal of*, vol. 17, pp. 1329 –1341, dec. 2008.

[17] M. Chiao, K. B. Lam, and L. Lin, "Micromachined microbial and photosynthetic fuel cells," *Journal of Micromechanics and Microengineering*, vol. 16, no. 12, p. 2547, 2006.

[18] Y. Han, C. Yu, and H. Liu, "A microbial fuel cell as power supply for implantable medical devices," *Biosensors and Bioelectronics*, vol. 25, no. 9, pp. 2156 – 2160, 2010.

[19] H. I. Park, D. Sanchez, S. K. Cho, and M. Yun, "Bacterial communities on electron-beam pt-deposited electrodes in a mediator-less microbial fuel cell," *Environmental Science and Technology*, vol. 42, no. 16, pp. 6243–6249, 2008. PMID: 18767694.

[20] A. Dewan, H. Beyenal, and Z. Lewandowski, "Scaling up microbial fuel cells," *Environmental Science and Technology*, vol. 42, no. 20, pp. 7643–7648, 2008. PMID: 18983087.

[21] F. Qian, M. Baum, Q. Gu, and D. E. Morse, "A 1.5 μl microbial fuel cell for on-chip bioelectricity generation," *Lab on a Chip*, vol. 9, no. 21, pp. 3076–3081, 2009.

[22] H. Hou, L. Li, Y. Cho, P. de Figueiredo, and A. Han, "Microfabricated microbial fuel cell arrays reveal electrochemically active microbes," *PLoS ONE*, vol. 4, p. e6570, 08 2009.

[23] S. R. Crittenden, C. J. Sund, and J. J. Sumner, "Mediating electron transfer from bacteria to a gold electrode via a self-assembled monolayer," *Langmuir*, vol. 22, no. 23, pp. 9473–9476, 2006.

[24] A. Dumitru, A. Morozan, M. Ghiurea, K. Scott, and S. Vulpe, "Biofilm growth from wastewater on mwnts and carbon aerogels," *physica status solidi (a)*, vol. 205, no. 6, pp. 1484–1487.

[25] H. Richter, K. McCarthy, K. P. Nevin, J. P. Johnson, V. M. Rotello, and D. R. Lovley, "Electricity generation by geobacter sulfurreducens attached to gold electrodes," *Langmuir*, vol. 24, no. 8, pp. 4376–4379, 2008. PMID: 18303924.

[26] M. Sun, F. Zhang, Z.-H. Tong, G.-P. Sheng, Y.-Z. Chen, Y. Zhao, Y.-P. Chen, S.-Y. Zhou, G. Liu, Y.-C. Tian, and H.-Q. Yu, "A gold-sputtered carbon paper as an anode for improved electricity generation from a microbial fuel cell inoculated with shewanella oneidensis mr-1," *Biosensors and Bioelectronics*, vol. In Press, Corrected Proof, pp. –, 2010.

[27] S. Cheng and B. E. Logan, "Ammonia treatment of carbon cloth anodes to enhance power generation of microbial fuel cells," *Electrochemistry Communications*, vol. 9, no. 3, pp. 492 – 496, 2007.

[28] E. Ostuni, R. G. Chapman, M. N. Liang, G. Meluleni, G. Pier, D. E. Ingber, and G. M. Whitesides, "Self-assembled monolayers that resist the adsorption of proteins and the adhesion of bacterial and mammalian cells," *Langmuir*, vol. 17, no. 20, pp. 6336–6343, 2001.

[29] X. Jiang, R. Ferrigno, M. Mrksich, and G. M. Whitesides, "Electrochemical desorption of self-assembled monolayers noninvasively releases patterned cells from geometrical confinements," *Journal of the American Chemical Society*, vol. 125, no. 9, pp. 2366–2367, 2003.

[30] U. Schrder, J. Niessen, and F. Scholz, "A generation of microbial fuel cells with current outputs boosted by more than one order of magnitude," *Angewandte Chemie), volume = 115, number = 25, issn = 1521-3757, url = http://dx.doi.org/10.1002/ange.200350918, pages = 2986-2989 year = 2003.*

[31] Y. Zou, C. Xiang, L. Yang, L.-X. Sun, F. Xu, and Z. Cao, "A mediatorless microbial fuel cell using polypyrrole coated carbon nanotubes composite as anode material," *International Journal of Hydrogen Energy*, vol. 33, no. 18, pp. 4856 – 4862, 2008.

[32] M. Adachi, T. Shimomura, M. Komatsu, H. Yakuwa, and A. Miya, "A novel mediator-polymer-modified anode for microbial fuel cells," *Chemical Communications*, no. 17, pp. 2055–2057, 2008.

[33] Z. He, Y. Huang, A. K. Manohar, and F. Mansfeld, "Effect of electrolyte ph on the rate of the anodic and cathodic reactions in an air-cathode microbial fuel cell," *Bioelectrochemistry*, vol. 74, no. 1, pp. 78 – 82, 2008. Special Issue: Cellular Electrochemistry, Proceedings of the XIXth International Symposium on Bioelectrochemistry and Bioenergetics.

[34] H. Liu, S. Cheng, and B. E. Logan, "Power generation in fed-batch microbial fuel cells as a function of ionic strength, temperature, and reactor configuration," *Environmental Science and Technology*, vol. 39, no. 14, pp. 5488–5493, 2005.

[35] U. Schroder, "Anodic electron transfer mechanisms in microbial fuel cells and their energy efficiency," *Physical Chemistry Chemical Physics*, vol. 9, no. 21, pp. 2619–2629, 2007.

[36] G. Reguera, K. D. McCarthy, T. Mehta, J. S. Nicoll, M. T. Tuominen, and D. R. Lovley, "Extracellular electron transfer via microbial nanowires," *Nature*, vol. 435, no. 7045, pp. 1098–1101.

[37] W. C. Lin, M. V. Coppi, and D. R. Lovley, "Geobacter sulfurreducens Can Grow with Oxygen as a Terminal Electron Acceptor," *Appl. Environ. Microbiol.*, vol. 70, no. 4, pp. 2525–2528, 2004.

[38] J. C. Biffinger, J. Pietron, R. Ray, B. Little, and B. R. Ringeisen, "A biofilm enhanced miniature microbial fuel cell using shewanella oneidensis dsp10 and oxygen reduction cathodes," *Biosensors and Bioelectronics*, vol. 22, no. 8, pp. 1672 – 1679, 2007.

[39] J. C. Biffinger, J. N. Byrd, B. L. Dudley, and B. R. Ringeisen, "Oxygen exposure promotes fuel diversity for shewanella oneidensis microbial fuel cells," *Biosensors and Bioelectronics*, vol. 23, no. 6, pp. 820 – 826, 2008.

[40] J. Coates, E. Phillips, D. Lonergan, H. Jenter, and D. Lovley, "Isolation of Geobacter species from diverse sedimentary environments," *Appl. Environ. Microbiol.*, vol. 62, no. 5, pp. 1531–1536, 1996.

[41] M. Driscoll, M. Romine, F. Juhn, M. Serres, L. McCue, A. Beliaev, J. Fredrickson, and T. Gardner, "Identification of diverse carbon utilization pathways in shewanella oneidensis mr-1 via expression profiling," vol. 18, pp. 287–298.

[42] K. C. Wrighton, P. Agbo, F. Warnecke, K. A. Weber, E. L. Brodie, T. Z. DeSantis, P. Hugenholtz, G. L. Andersen, and J. D. Coates, "A novel ecological role of the firmicutes identified in thermophilic microbial fuel cells," *ISME*, vol. 2, no. 11, pp. 1146–1156, 2008.

[43] B. C. Jong, B. H. Kim, I. S. Chang, P. W. Y. Liew, Y. F. Choo, and G. S. Kang, "Enrichment, performance, and microbial diversity of a thermophilic mediatorless microbial fuel cell," *Environmental Science and Technology*, vol. 40, no. 20, pp. 6449–6454, 2006.

[44] C. G. Zoski, *Handbook of electrochemistry*. Elsevier Science, 2009.

[45] R. O'Hayre, *Micro-scale electrochemistry: Application to Fuel Cells*. PhD thesis, Stanford University, 2004.

[46] E. Marsili, D. B. Baron, I. D. Shikhare, D. Coursolle, J. A. Gralnick, and D. R. Bond, "Shewanella secretes flavins that mediate extracellular electron transfer," *Proceedings of the National Academy of Sciences*, vol. 105, no. 10, pp. 3968–3973, 2008.

[47] H. Richter, K. P. Nevin, H. Jia, D. A. Lowy, D. R. Lovley, and L. M. Tender, "Cyclic voltammetry of biofilms of wild type and mutant geobacter sulfurreducens on fuel cell anodes indicates possible roles of omcb, omcz, type iv pili, and protons in extracellular electron transfer.," vol. 2, no. 5, pp. 506–516, 2009.

[48] A. Esteve-N*úñez*, M. Rothermich, M. Sharma, and D. Lovley, "Growth of geobacter sulfurreducens under nutrient-limiting conditions in continuous culture," vol. 7, no. 5, pp. 641–648, 2005.

[49] M. Izallalen, R. Mahadevan, A. Burgard, B. Postier, R. D. Jr., J. Sun, C. H. Schilling, and D. R. Lovley, "Geobacter sulfurreducens strain engineered for increased rates of respiration," *Metabolic Engineering*, vol. 10, no. 5, pp. 267 – 275, 2008.

[50] I. Giaever and C. R. Keese, "A morphological biosensor for mammalian cells," *Nature*, vol. 366, pp. 591–592, 1993.

[51] J. Wegener, C. R. Keese, and I. Giaever, "Electric cell-substrate impedance sensing (ecis) as a noninvasive means to monitor the kinetics of cell spreading to artificial surfaces," *Experimental Cell Research*, vol. 259, no. 1, pp. 158 – 166, 2000.

[52] C. Buie, E. A. Parra, R. Sochol, J. D. Coates, and L. Lin, "Characterization of bacteria for microbial fuel cell applications using dielectrophoresis," in *Proceedings of MicroTAS*, 2009.

[53] V. Berry, S. Rangaswamy, and R. F. Saraf, "Highly selective, electrically conductive monolayer of nanoparticles on live bacteria," *Nano Letters*, vol. 4, no. 5, pp. 939–942, 2004.

[54] D. B. Weibel, W. R. DiLuzio, and G. M. Whitesides, "Microfabrication meets microbiology," *Nat Rev Micro*, vol. 5, no. 3, pp. 209–218, 2007.

[55] H. Liu, S. Cheng, L. Huang, and B. E. Logan, "Scale-up of membrane-free single-chamber microbial fuel cells," *Journal of Power Sources*, vol. 179, no. 1, pp. 274 – 279, 2008.

[56] Y.-A. Song, C. Batista, R. Sarpeshkar, and J. Han, "Rapid fabrication of microfluidic polymer electrolyte membrane fuel cell in pdms by surface patterning of perfluorinated ion-exchange resin," *Journal of Power Sources*, vol. 183, no. 2, pp. 674 – 677, 2008.

[57] E. Parra and L. Lin, "Microbial fuel cell based on electrode-exoelectrogenic bacterial interface," in *Proceedings of 22th IEEE Micro Electro Mechanical Systems Conference*, pp. 31–34, 2009.

[58] D. G. Ahearn, L. L. May, and M. M. Gabriel, "Adherence of organisms to silver-coated surfaces," *Journal of Industrial Microbiology and Biotechnology*, vol. 15, pp. 372–376, 1995. 10.1007/BF01569993.

[59] C. G. Granqvist, "Transparent conductive electrodes for electrochromic devices: A review," *Applied Physics A: Materials Science and Processing*, vol. 57, pp. 19–24, 1993. 10.1007/BF00331211.

[60] A. L. Swint and P. W. Bohn, "Effect of acidic and basic surface dipoles on the depletion layer of indium tin oxide as measured by in-plane conductance," *Applied Physics Letters*, vol. 84, pp. 61 –63, jan. 2004.

[61] D. D. Carlo and L. P. Lee, "Dynamic single-cell analysis for quantitative biology," *Analytical Chemistry*, vol. 78, no. 23, pp. 7918–7925, 2006.

[62] P. Y. Chiou, A. T. Ohta, and M. C. Wu, "Massively parallel manipulation of single cells and microparticles using optical images," *Nature*, vol. 436, no. 7049, pp. 370–372, 2005.

[63] S. Sivasankar and S. Chu, "Optical bonding using silica nanoparticle sol-gel chemistry," *Nano Letters*, vol. 7, no. 10, pp. 3031–3034, 2007. PMID: 17854226.

[64] C. Y. Hoh and R. Cord-Ruwisch, "A practical kinetic model that considers endproduct inhibition in anaerobic digestion processes by including the equiiibrium constant," *Biotechnology and Bioengineering*, vol. 51, pp. 597–604, 1996.

[65] J. Butler, N. Young, and D. Lovley, "Evolution of electron transfer out of the cell: comparative genomics of six geobacter genomes," *BMC Genomics*, vol. 11, no. 1, p. 40, 2010.

[66] A. S. Khalil and J. J. Collins, "Synthetic biology: applications come of age," *Nat Rev Genet*, vol. 11, no. 5, pp. 367–379.

[67] M. P. Brynildsen and J. J. Collins, "Systems biology makes it personal," vol. 34, no. 2, pp. 137–138, 2009.

[68] E. A. Parra, A. Higa, C. R. Buie, J. D. Coates, and L. Lin, "Real-time biocatalyst loading and electron transfer via microfabricated transparent electrode," in *Proceedings of 23th IEEE Micro Electro Mechanical Systems Conference*, pp. 1183–1186, 2010.

[69] H.-Y. Wang, A. Bernarda, C.-Y. Huang, D.-J. Lee, and J.-S. Chang, "Micro-sized microbial fuel cell: A mini-review," *Bioresource Technology*, vol. In Press, Corrected Proof, pp. –, 2010.

[70] C. Leang, X. Qian, T. Mester, and D. R. Lovley, "Alignment of the c-Type Cytochrome OmcS Along Pili of Geobacter sulfurreducens," *Appl. Environ. Microbiol.*, pp. AEM.00023–10, 2010.

Appendices

Appendix A

System-A: Micro-electrode MFC Fabrication

Step	Electrode microfabrication: Description
A.	Clean quartz wafer in piranha bath - 10 min and cycle with DI 4 times
B.	Dehydrate at 120 ^{o}C for 30 minutes.
C.	Sputter ITO. RF at 20 mTorr and 50 W for 20 min. Get roughly 100 nm.
D.	Anneal ITO in air for 1 hour at 350 ^{o}C.
E.	Spin 1 m g-line PR (4000 rpm for 30 sec). Softbake at 90 ^{o}C for 2 minutes.
F.	Using mask aligner, pattern PR. Use 2X the recommended dose to account for substrate effects.
G.	Hardbake PR on hotplate. 120 ^{o}C for 2 minutes.
H.	Define electrodes by etching ITO. Immerse wafer in a 16% solution of HCl for X minutes at 25 ^{o}C.
I.	Strip PR thoroughly.
J.	Deposit 1 μm SiO_2 at 350 ^{o}C using PECVD.
K.	Spin 1 μm g-line PR (4000 rpm for 30 sec). Softbake at 90 ^{o}C for 2 minutes. Repeat.
L.	Using mask aligner, pattern PR. Use 4X the recommended dose to account for substrate effects and increased thickness.
M.	Using a plasma etcher, generate active windows. Etch oxide with SF_6/O_2 at 150 W/12 inch diameter chamber for 20 min.
N.	Strip photoresist if any is left.

Step	Microchannel mold for PDMS casting: Description
A.	Clean silicon wafer in piranha bath - 10 min and cycle with DI 4 times.
B.	Dehydrate at 120 ^{o}C for 30 min.
C.	Activate surface with oxygen plasma at 50 W for 2 minutes.
D.	Deposit HMDS adhesion layer.
E.	Spin on 200 μm SU8. Softbake according to instructions. Assure PR looses "stickiness".
F.	Using mask aligner, pattern SU8. May want to run multiple exposures to complete dose as to minimize substrate heating.
G.	Follow post-exposure sequence according to manufacturer's guidelines: post-exposure bake and development.
H.	Pour 10:1 mixture of PDMS precursor and crosslinker to provide 1 mm thickness of epoxy. Heat on hotplate at 70 ^{o}C for 1 hour. Peel, wrap in syran wrap, and cut to specifications.

Appendix B

System-B: Single-cell ultra-micro-electrode MFC

Step	Process	Substep	Description
1	cleaning		Clean wafers in piranha, dehydrate in 120 ^{o}C oven for 30 min
2	ITO layer	PR dep.	PR dep: Spin 1 μm i-line, softbake, and flood expose. Spin 1 μm g-line and softbake.
3		lithography	Use mask aligner to expose mask 1 (ITO layer). Time should be 2x that of recommended single coat to account for substrate effects.
4		definition	Develop, rinse, and dry with N2 gun. Descum with O_2 plasma, and hardbake.
5		deposition	Deposit ITO in sputterer. DC sputter at 1 W/cm^2 at 5 mT in Ar for 20min for about 100 nm film.
6		liftoff	Lift off in acetone. May need PRS300 for 20 min. Clean in metal bath.
7	Au layer	PR dep.	Repeat PR deposition as above STEP 2.
8		lithography	Repeat lithography as above STEP 3. Use mask2.
9		definition	Repeat development (definition) as in STEP 4.
10		deposition	Evaporate 50 nm of elemental gold at 2 nm/s and sub mTorr
11		liftoff	As STEP 6.
12		cleaning	Clean in pre-furnace cleaning bath + QDR + spin dry. Dehydrate wafers in 120 ^{o}C oven for 30 min.
13	SiO_2		In PECVD deposit 500 nm oxide at 350 ^{o}C.
14	Active area def	PR dep.	Spin on 1 m g-line and softbake. Repeat.
15		lithography	Use mask aligner to expose mask 3 (SiO_2). Time should be 4x that of recommended single coat to account for substrate effects and double PR layer. Develop.

Step	Process	Substep	Description
16		etch	Use DRIE to open active areas. SF_6/O_2 @1W/cm^2 for 2min.
17		clean	Strip leftover PR. Clean in metal bath. QDR+spin dry. Dehydrate wafers in 120 ^{o}C oven for 30min
18	Ag	layer PR dep.	Repeat PR deposition as above (STEP 3).
19		lithography	Repeat lithography as above STEP 3. Use mask4.
20		definition	Repeat development (definition) as in STEP 4.
21		deposition	In evaporator deposit 1m elemental Ag at 5nm/s and sub mTorr.
22		liftoff	As STEP 6.
23	Ag_2O layer		In plasma tool, at ultra-low power density, oxidize Ag in oxygen for 20 min.
24	PEM layer	PR dep.	Spin-on single g-line coat. Softbake.
25		lithography	Use mask aligner to expose mask 5 (PEM). Time should be 2x that of recommended single coat to account for substrate effects.
26		definition	Develop, descum, and softbake.
27		deposition	On PEM areas, manually deposit a drop of 5% Nafion ionomer. Spin to acquire desired thinkness. Cast polymer at 60 ^{o}C for 1minute and 90 ^{o}C for 10min.
28		clean	Remove PR in acetone.
29	Dice		Spin a layer of PR for protection. Hardbake. Dice chips in saw.
30	Drill ports		Drill press.
31	Clean		Remove PR and dry.
32	Assemble		Using piranha cleaned coverslips, assemble with Teflon adhesive tape. Make fluidic and electrical contacts.